Aus der Neurologischen Universitätsklinik Tübingen
Abteilung Neurologie mit Schwerpunkt Neurodegenerative Erkrankungen

Functional MRI for the early detection of Parkinson's disease: ROI analysis of the putamen in a population at risk of developing Parkinson's disease

Inaugural-Dissertation
zur Erlangung des Doktorgrades
der Medizin

der Medizinischen Fakultät
der Eberhard Karls Universität
zu Tübingen

vorgelegt von
Binder, Tobias
2022

Dekan:	Professor Dr. B. Pichler
1. Berichterstatter:	Professor Dr. D. Berg
2. Berichterstatter:	Professor Dr. A. Gharabaghi
Tag der Disputation:	26.08.2021

Dedication

To all participants of this study, whose selfless commitment for a better future care for Parkinson's disease patients I admire.

To our research team, whose support I could always count on, and who inspired me to specialize in neurology.

To my family, who encouraged me to try to become a physician in the first place.

Index

List of abbreviations

ANOVA	Analysis of Variance
AWMF	Arbeitsgemeinschaft der Wissenschaftlichen Medizinischen Fachgesellschaften
BOLD (signal)	Blood Oxygenation Level Dependent (signal)
DMN	Default Mode Network
EPI	Echo Planar Imaging
fMRI	functional Magnetic Resonance Imaging
FWE	Family-wise Error Correction
FWHM	Full Width at Half Maximum
ICA	Independent Component Analysis
MNI	Montreal Neurological Institute
MRI	Magnetic Resonance Imaging
PD	Parkinson's Disease
RBD	Rapid eye movement sleep Behavior Disorder
ReHo (analysis)	Regional Homogeneity (analysis)
REM (sleep)	Rapid Eye Movement (sleep)
ROI	Region of Interest
rs-fMRI	resting-state functional Magnetic Resonance Imaging
RSN	Resting-state Network
UPDRS	Unified Parkinson's Disease Rating Scale
SMA	Supplementary Motor Area
STS	Scan to Scan

List of figures

List of tables

1. Introduction

1.1 Parkinson's disease

Worldwide, Parkinson's disease (PD) is the second most common neurodegenerative disorder among older adults, only surpassed by Alzheimer's (de Lau & Breteler, 2006). Its pathologic hallmark is a loss of dopaminergic cells in the substantia nigra pars compacta, a region of the midbrain (Fearnley & Lees, 1991), and the development of neuronal Lewy bodies (Gibb & Lees, 1988). Its principal symptom is a general slowdown of movement (bradykinesia) paired with either a slow tremor of the extremities while resting with a frequency of 4-6 Hz, or a stiffening of the extremities due to hypertension of the muscles (rigor). The disease is named after James Parkinson, who first described its symptoms in his "Essay on the Shaking Palsy" in 1817 (Parkinson, 2002).

The onset of disease typically lies in between 40 to 60 years of age. An onset of disease before 40 years of age indicates a strong genetic disposition. Worldwide its prevalence rises with age: from 41 per 100 000 in individuals from 40 to 49 years of age, up to 1903 per 100 000 in individuals over the age of 80. There is an insignificant effect of sex in the prevalence of PD, with men being slightly more affected then women (Pringsheim et al., 2014).

While the ultimate cause of PD is still unknown, there is an increasing understanding of the mechanisms leading to Parkinsonian symptoms. At the core of the pathophysiology of PD is the death of the dopaminergic neurons of the substantia nigra. The substantia nigra is part of a network of different brain regions summed up as the basal ganglia, which regulate and enable movement of the body. Normally, the basal ganglia release the neurotransmitter dopamine to allow the body to perform a motion. In PD, dopaminergic cells of the substantia nigra die due to so far unknown reasons. Consequently, they can no longer allow motion, which leads to the principal symptom of PD, bradykinesia (Trepel, 2008).

Diagnosis of PD takes several steps. First, a patient must exhibit symptoms as defined by the UK Parkinson's Disease Society Brain Bank diagnostic criteria (Hughes et al., 1992) and updated by the clinical criteria of the Movement Disorders Society (Postuma, 2015): bradykinesia, accompanied by at least one of the cardinal symptoms, rigidity and tremor. Second, when treated with a drug for PD the patient must show an improvement of symptoms. Third, red flags and absolute exclusion criteria need to be checked to discern differential diagnoses as listed in the guideline of the "Arbeitsgemeinschaft der Wissenschaftlichen Medizinischen Fachgesellschaften" (AWMF) released in 2012 (Eggert et al., 2012).

The differential diagnosis of sporadic PD can be divided in three subgroups: Secondary Parkinson syndromes, atypical Parkinson syndromes and familial PD. Secondary Parkinson syndromes are caused by any other than primary neurodegenerative process that damages the basal ganglia network and its connections, e.g. trauma, tumor, hematoma, hydrocephalus, drug or toxin induced damage and M. Wilson - among many others. Atypical Parkinson syndrome is the umbrella term for parkinsonian symptoms in the context of neurodegenerative diseases other than PD, of which the most common are multisystem atrophy, corticobasal degeneration, progressive supranuclear palsy and Lewy body dementia (Ahlskog, 2000; Tolosa et al., 2006). Familial PD is caused by genetic mutations, which anticipate with varying penetrance rates the parkinsonian pathophysiology. Up to this date 16 risk loci have been identified. One example are mutations in the *SNCA* gene (protein: alpha-synuclein) that lead to an early accumulation of high amounts of Lewy bodies in the brain. Other important mutated genes are *LRRK2, Parkin, PINK1, and ATP13A2* (Singleton et al., 2013).

1.2 Prodromal stage

In PD there is a delay between the start of the degeneration of dopaminergic cells and the development of its cardinal symptoms - not until around 60% of the dopaminergic neurons of the substantia nigra have died, cardinal symptoms start to become evident (Pakkenberg et al., 1991). Thus, early PD can be divided into preclinical, prodromal and clinical stages (see fig. 1, p. 6). In the preclinical stage, neuronal loss has started but is fully compensated, which allows the body to function normally. For now, this stage is undetectable due to a lack of clinical and biological markers. With continuing neuronal loss, the compensating mechanisms begin to fail and non-motor symptoms and slight motor symptoms start to occur. (Gaenslen, 2014; Postuma & Berg, 2016). These non-motor and slight motor symptoms are referred to as prodromal markers. On the basis of current diagnostic criteria, these prodromal markers do not allow diagnosis, but are associated with an increased risk of developing PD (Postuma, 2009; Postuma, Lang, Gagnon, Pelletier, & Montplaisir, 2012). The markers with the highest association with an increased risk of developing PD are rapid eye movement sleep behavior disorder (RBD), impaired olfaction and lifetime depression. The duration of the prodromal stage is still unclear and may vary intraindividually. In general it is supposed to last more than a decade (Fearnley & Lees, 1991; Marek & Jennings, 2009; Postuma & Berg, 2016).

RBD is a condition which lacks the normal loss of muscle tone in the dreaming phase of sleep. Thus, the often lively dreams or nightmares are encountered with defending movements, resulting in kicking, punching or jumping out of bed (Schenck et al., 1986). Epidemiological studies have shown that in the course of 12 years the risk of RBD patients to develop PD is more than 80%, which is why RBD is considered to be the strongest prodromal marker of PD (Postuma, Gagnon, Bertrand, Marchand & Montplaisir, 2015). The olfactory bulb, which houses the neurons responsible for the olfactory sense, is known to be one of the first affected brain regions in PD, and therefore impaired olfaction is a prodromal marker and one of the first symptoms that develop in the course of

the disease. Overall, 85% of PD patients suffer from impaired olfaction (Goedert & Spillantini, 2012; Siderowf, 2012).

Also, experiencing a depression is accompanied with a two- to threefold risk of developing PD (Ishihara & Brayne, 2006). Already in the early 20th century a specific, depressed, personality type was observed in PD patients (Camp, 1913).

Further symptoms associated with an increased risk of developing PD are constipation (Abbott, 2001), orthostatic hypotension, hyperhidrosis, urinary urge (Müller et al., 2011), cognitive impairment, pain and disturbance of color vision (Gaenslen, 2014), slow reaction time, excessive day time sleepiness and impaired executive function (Ross et al., 2012).

In addition to these features of early PD, studies based on interviews revealed, that also subtle changes in movement occur prior to full blown PD. These studies either retrospectively asked PD patients whether they experienced symptoms prior to their diagnosis or they asked healthy subjects whether they experienced any symptoms and then followed them prospectively until they were diagnosed with PD. Among these motor features of prodromal PD are slowing of fine hand movement, reduced arm swing and changes in movement patterns (Alexandra Gaenslen et al., 2011), stiffness, tremor and imbalance (De Lau et al., 2006). However, with a prevalence of up to 40% in people in between 70 and 80 years of age, these features are common in the elderly and of low specificity and low positive predictive value, meaning that the likelihood of somebody showing one of these features actually having PD is very small. A rather new but promising way to detect subtle motor markers is the identification of changes in movement patterns with wearable sensors, e.g. gyroscopes and/or accelerometers. These sensors help evaluate several aspects of motor control that are generally impaired in PD, such as transferring from sitting to standing, walking and turning, gait initiation and speed of movement. The advantage of these sensors over a clinical “snapshot” assessment is that they

allow the collection of objective data over a long period of time and thus might be superior in detecting changes in movement hinting at PD in its prodromal state (Maetzler & Hausdorff, 2012; Maetzler, 2012).

On its own, each one of these prodromal markers is an insufficient indicator of PD. Nonetheless, there is evidence that a higher specificity can be achieved by combining multiple prodromal markers. For example, Ross ea showed that screening their study population with a combination of the prodromal markers excessive daytime sleepiness and impaired olfaction results in a ten-fold increase of the incidence of PD (Ross, 2012). Therefore, it is plausible that combining multiple motor and non-motor markers might allow us to designate individuals in the prodromal phase of PD. Lately, Berg ea established a mathematical model to estimate the likelihood of prodromal PD being present using a multiplication of different diagnostic information expressed as likelihood ratios. Diagnostic information included background information such as clinical motor (Unified Parkinson's disease rating scale, short UPDRS) and non-motor markers (risk factors), genetic findings and neuroimaging (DAT-Scan). A likelihood of > 80% was defined as prodromal PD being present. This definition is intended to help delineate the prodromal phase from early PD, thus establishing a common baseline for further studies (Berg, 2015).

Figure 1: The stages of Parkinson's disease and their markers

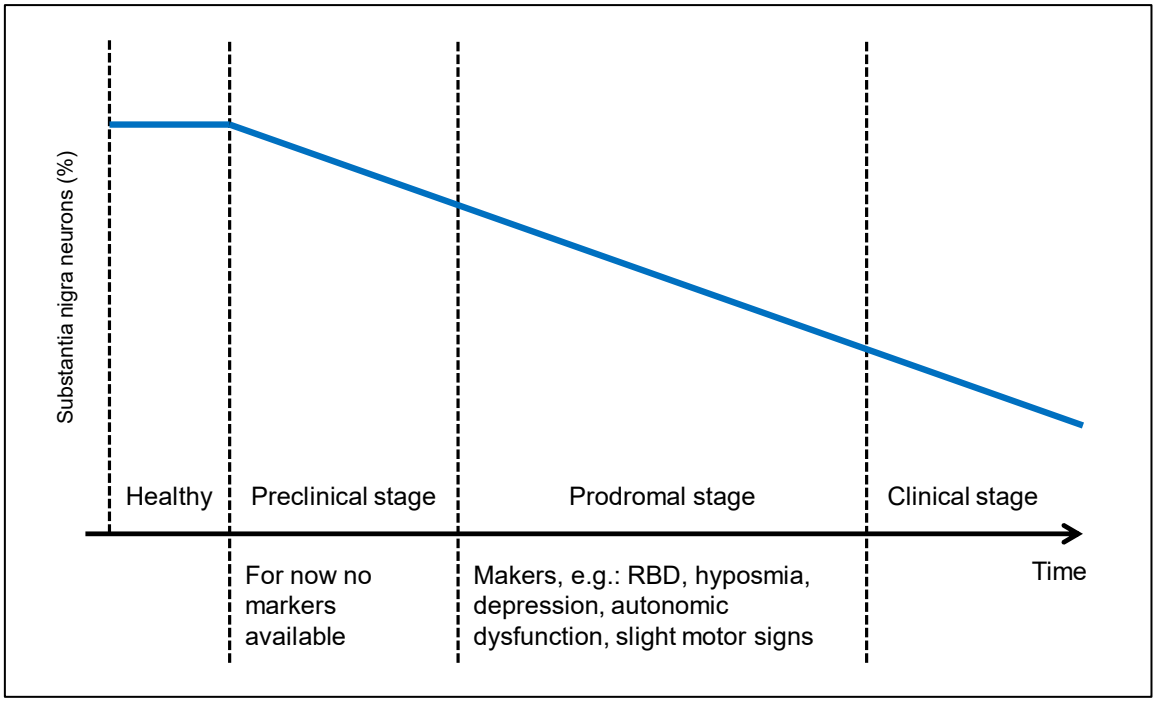

Symbolic illustration of the loss of dopaminergic cells in the substantia nigra over the course of Parkinson's disease and the chronology of onset of some of the established prodromal markers. The loss of cells depicted as linear is a simplification and most likely not true.

1.3 Introduction to Magnetic Resonance Imaging and functional Magnetic Resonance Imaging

Magnetic Resonance Imaging (MRI) is an imaging technique during which a subject is put into a strong magnetic field, in which it itself becomes magnetic. This is due to the fact, that the protons, which make up the core of every atom, represent spinning positive charges and are consequently surrounded by their own magnetic field. On its own, this magnetic field is not measurable. But when put in a strong external magnetic field, the spin of all protons aligns in the same direction, their magnetic fields add up and become measurable. The problem to overcome is that the proton's magnetic field points in the same direction as the magnetic field of the scanner and both are indistinguishable. Therefore, the protons are hit with an electromagnetic pulse. When the pulse is applied in the right frequency, it transfers energy to the protons – they resonate to it – and they change direction. The sum of the magnetic fields of all protons can be

differentiated from the field of the scanner and is picked up by the antenna of the MRI scanner, a coil, which picks up the native MRI signal. When the electromagnetic pulse is switched off, the protons stop resonating and relax back into their alignment with the strong external magnetic field. The speed of this process is described by the time constant T1. When the pulse is switched of, the protons go back to their relaxed state with different speed, which is described by the time constant T2. T1 and T2 depend on properties of the microscopic magnetic fields of the protons, which are influenced by the neighboring nuclei and inhomogeneities of the strong magnetic field of the scanner. Therefore, they are specific to a certain position in the scanner and to tissue characteristics, which is utilized when creating an image from the signal (Schild, 1990).

In functional MRI (fMRI), the sequence of magnetic pulse application and the gradation of magnetic field force is tailored to portray the oxygenation level of the blood – this is possible as magnetic properties of the blood change according to its oxygenation status: deoxygenated blood is more magnetic (paramagnetic) than oxygenated blood (diamagnetic) and creates microscopic magnetic distortions in and around blood vessels leading to a hyperintense MRI signal wherever blood is deoxygenated (Pauling, 1935). Thus, the name of the recorded signal is: Blood Oxygenation Level Dependent signal, abbreviated BOLD signal (Ogawa et al., 1990). The oxygenation level of the blood and therefore the BOLD signal physiologically correlates with brain activity via a mechanism named the hemodynamic response: in active brain regions blood perfusion increases. This phenomenon was first described by Charles Scott Roy in 1890, who measured brain volume and pulse rates during stimulation of different peripheral nerves in dogs (Roy & Sherrington, 1890). He observed that under stimulation brain volume and pulse rate increased, hypothesizing that brain activity leads to an increase of its perfusion with blood. This increased blood flow is the physiological reaction to an increased demand for energy (oxygen and glucose) of the activated neurons. It is important to understand, and somewhat counter intuitive, that in active brain areas BOLD signal intensity

actually decreases. This is due to the fact that in activated brain areas perfusion increases by around 30 to 50%, while actual oxygen utilization only increases by around 5% and as a result the fraction of deoxygenated hemoglobin decreases in activated brain areas leading to a slight decrease in BOLD signal intensity (Fox & Raichle, 1986). The exact relation between the BOLD signal and neuronal activity was further defined by Logothetis ea in 2001, who measured simultaneously BOLD signal intensity and intracortical activity around a microelectrode in the visual cortex of monkeys. He showed that the BOLD signal mainly correlates with synaptic activity and afferences to a certain brain region, not so much with its efferences or activity of the nerve cell (Logothetis et al., 2001). The MRI scanner measures the BOLD signal with a mode of data collection called Echo Planar Imaging (EPI). With this acquisition mode it is possible to capture one slice of an image in one electromagnetic pulse and its subsequent echo resulting in fast acquisition times of around 20-30 ms for one slice. As the depiction of a whole brain consists of around 30 slices, a whole brain can be captured in less than two seconds – compared to other MRI measurements this is lightning fast and crucial for distinguishing the timing of activation between different brain regions.

The BOLD signal and its interpretation underlie certain limitations: first, the BOLD signal only portrays the sum of neuronal activation. The BOLD signal of a few high spiking neurons and the signal of a big group of neurons, that increase their activity only a bit, look exactly the same. Thus, the signal intensity does not allow inferences on the number of active neurons as well as the degree of activity. Second, the signal intensity is also influenced by different factors that are not due to changes of the oxygenation status of hemoglobin and therefore not the result of neuronal activity. Shortly, these factors produce unwanted signal referred to as noise. Some sources of noise arise from the MRI setup and cannot be changed when measuring subjects like the inhomogeneity of the magnetic field of the scanner or thermal influences to the signal at room temperature. Others arise from physiological processes like pulse, respiration and the subject’s movement, which blur the image and complicate the correct

localization of signal increase. In extreme situations up to 90% of signal intensity must be attributed to noise (Friston, Williams, Howard, Frackowiak & Turner, 1996). Consequently, when making inferences based on functional MRI data it is vital to correct for the effects of physiological noise in the data (Faro, Scott & Mohamed, 2006). Third, the BOLD signal itself has a suboptimal spatial resolution. Focal brain activation is accompanied by oxygenation and perfusion changes that (at three tesla) spread about 3.5mm around the actual center of activation (Engel, Glover & Wandell, 1997). Furthermore, if a voxel (a voxel is a value in a three-dimensional space, which is the equivalent of one pixel in an MRI image) picks up the signal from a large vessel draining an activated brain region, the signals intensity is stronger than in the activated area itself, temporally delayed and also distant to the true origin of activation. And lastly, although EPI significantly reduces the capture time for a whole brain, the time needed to visualize the activation is still magnitudes higher than the time of the actual activation itself (Bandettini, 2009).

1.4 Resting-state and functional connectivity

Functional MRI measurements can be conducted in two ways: with the participant completing a task or with the participant at rest. One simple example for a task could be the administration of an auditory stimulus e.g. a beep at fixed intervals during a measurement, and then the analysis of the areas where changes in the BOLD signal occur in time with the stimulus – thus connecting the brain function “hearing” to its topography, the auditory cortex. In addition to these task-induced changes of the BOLD signal, there are also spontaneous low frequency (< 0.1 Hz) fluctuation of the BOLD signal. They occur in the absence of any tasks or stimulus all over the brain, which is called the resting-state. Most interestingly these fluctuations appear temporally correlated across brain areas that are modulated by the same tasks implying a deeper physiological meaning. This was first described by Biswal ea in 1995, who measured subjects during rest as well as when performing a finger tapping task (Biswal et al., 1995). He observed, that the BOLD signal fluctuations of the

bilateral sensorimotor cortices, which he had identified using the finger tapping task, are highly temporally correlated during resting-state fMRI (rs-fMRI). Until the publication date of this thesis, multiple networks have been described, that show a synchronous activity while the brain is resting, which are called resting-state networks (RSN). Among them the most important being the visual, auditory, sensorimotor, language, dorsal and ventral attention networks and the default mode network (DMN). Although the origin and the exact interpretation of these low frequency fluctuations are still unknown, the hypothesis is that they could carry information about brain architecture and brain organization, that the narrow paradigm of task based fMRI cannot portray (Fox & Raichle, 2007; Rosazza & Minati, 2011; Sala-Llonch et al., 2015).

Analyzing rs-fMRI means searching for brain regions, which show a synchronous change in the slow frequency fluctuations of the BOLD signal, indicating that they are activated and deactivated at the same time. Therefore, the different techniques for analyzing rs-fMRI are summed up with the term functional connectivity analysis. Rs-fMRI can not only be used to investigate the above mentioned RSNs, but also to precisely investigate the connection of one or more specifically selected regions to the rest of the brain. One approach to analyzing fMRI is the seed-based analysis. When performing a seed-based analysis, a region of interest (abbr. ROI, also referred to as seed region or just seed) is defined and its mean BOLD signal for every scan taken during the MRI measurement is calculated. The result is called a time course, a graph with the BOLD signal intensity on the y-axis and the number of scans on the x-axis. This time course is then correlated with the time course of every other voxel in the brain (voxel-wise correlation), revealing those that are activated and deactivated at the same time as the seed region (Biswal et al., 1995; Friston, 2011).

Other popular approaches to functional connectivity analysis are hierarchical clustering, graph theory, independent component analysis (ICA) and regional homogeneity analysis (ReHo). When using hierarchical clustering multiple seed regions are defined and their time course is extracted. Then a clustering

algorithm is used to determine which regions are more closely related and which are more distantly related, allowing a visualization of the degree of synchronous activation between regions with a hierarchical tree. In a graph theory approach, multiple ROIs are chosen and the functional connectivity of each ROI to every other ROI is calculated. In this case, ROIs are referred to as nodes and the functional connections to other nodes are referred to as links. For each node all its links are summed up in one value called the total connectivity degree, which depicts the amount of information the nodes receive and how well they are connected within the network of chosen ROIs (Jiang et al., 2004). ICA does not need the a priori definition of seed regions. Instead a mathematical algorithm is used to decompose the BOLD signal of the entire data set into statistically maximal independent components. Each component is represented by a spatial map showing maximal dependent components, which are mostly activated simultaneously during the measurement. The benefit of this technique is that some spatial maps represent noise, while others represent actual functional networks, which can be used to differentiate noise from neuronal activity. A possible approach is to use an ICA to determine and eliminate patterns of noise and continue with a seed-based analysis (Fox & Raichle, 2007; Prodoehl et al., 2014). In ReHo the time course of each voxel is compared to the time course of its neighboring voxels, thus the focus lies on short distance functional connectivity. A decrease in ReHo is interpreted as locally desynchronized blood flow due to reduced gray matter concentration (Choe et al., 2013).

1.5 Resting-state functional MRI in Parkinson's disease

Several studies have used one or more of the above-mentioned methodologies to compare rs-fMRI in PD with healthy controls. Based on the well documented pathophysiology of the motor impairments in PD, the focus of most of the studies lay on functional connectivity of the striatum (Helmich et al., 2010; Kwak et al., 2010; Luo et al., 2014; Yu et al., 2013) or other regions that are part of the basal ganglia like the subthalamic nucleus (Baudrexel et al., 2011). A few

studies investigated further regions involved in execution of motion like the cerebellum (Liu et al., 2013) and the motor cortex (Wu et al., 2011; Yu et al., 2013). Other studies investigated changes in RSNs, e.g. the DMN (Krajcovicova et al., 2012; Tessitore et al., 2012) or the sensorimotor network (Esposito et al., 2013). Other studies used graph theory or the simultaneous evaluation of multiple ROIs (Sharman et al., 2013; Wu et al., 2009). Two studies used ReHo to further define pathologically altered regions in PD (Choe et al., 2013; Yang et al., 2013). The findings of the above-mentioned studies are described below and listed in detail in table 1, p. 14 to 15.

Hacker ea described an increase in functional connectivity of the striatum to the cerebellum and brainstem, which is consistent with findings of Wu ea who identified an increase of the functional connections of the cerebellum using a graph theory approach (Hacker et al., 2012; Wu et al., 2011). Baudrexel ea and Liu ea chose to investigate functional connectivity of the subthalamic nucleus and the dentate nucleus, revealing increased connectivity of the subthalamic nucleus to the motoric and sensory cortex and increased functional connectivity within the cerebellum (Baudrexel et al., 2011; Liu et al., 2013). Sharman ea found an overall decrease in functional connectivity within the striatum using a seed-based approach consistent with findings of Szewczyk-Krolikowski ea using ICA to analyze connections within the basal ganglia network, which consists of the putamen, the caudate nucleus and the anterior thalamus (Sharman et al., 2013; Szewczyk-Krolikowski et al., 2014). Krajcovicova ea and Tessitore ea investigated changes of the DMN in PD. The DMN is an RSN consisting of the medial temporal, medial prefrontal and cingulate cortex. It is thought to be important for the planning of cognitive processes while resting. DMN alterations have been identified in other neurodegenerative disorders like Alzheimer's disease, multiple sclerosis and frontotemporal dementia (Bonavita et al., 2017; Grieder et al., 2018). Krajcovicova ea found no significant differences in DMN connectivity in PD patients, however Tessitore ea described reduced connectivity in the medial temporal lobe and the inferior parietal lobe (Krajcovicova et al., 2012; Tessitore et al., 2013).

Esposito ea investigated changes in the sensorimotor network (primary and secondary sensory and motor cortex) and found a decrease in functional connectivity in the supplementary motor area (SMA), while the functional connectivity of other sensory and motoric areas remained unchanged (Esposito et al., 2013). Choe ea and Yang ea both conducted a ReHo analysis and while the description of the results differs in the details both studies share multiple observations. Both found increased regional homogeneity in the inferior parietal lobe and the middle occipital lobe. They had adverse results regarding regional homogeneity in an area around the hippocampus and the sensory and motor cortices (Choe et al., 2013; Yang et al., 2013).

Some studies also investigated the influence of anti-parkinsonian medication on functional connectivity by directly comparing rs-fMRI of PD patients on medication and after 12 hours off medication. As an effect of levodopa administration in PD patients an increase of functional connectivity was described for the basal ganglia network (Szewczyk-Krolikowski et al., 2014), the SMA, the thalamus (Esposito et al., 2013) and the dorsolateral prefrontal cortex (Wu et al., 2009). A decrease of functional connectivity was described for the right parietal cortex, left cerebellum and primary motor cortex (Wu et al., 2009) as well as for the cortico-striatal loop (Kwak et al., 2010). While the findings were diverse (which can be attributed to the different experimental foci that were chosen), each study reported that the levodopa administration returned functional connectivity in PD patients to a healthy state.

The majority of the above-mentioned studies are not directly comparable due to differences in methodology, e.g. type of analysis and targeted brain areas, and differences in study population, e.g. handedness, disease stage, dominant symptoms and medication of the patients. Nonetheless the most common (and therefore presumably robust) finding is an increase in functional connectivity of the striatum to different cortical brain regions (Hacker et al., 2012; Helmich et al., 2010; Kwak et al., 2010; Yu et al., 2013) and a decrease of functional connectivity within the basal ganglia (Hacker et al., 2012; Sharman et al., 2013;

Szewczyk-Krolikowski et al., 2014; Yang et al., 2013; Yu et al., 2013) in PD patients. In an attempt to further define this finding, several studies investigated the connection of the anterior and posterior putamen separately, as dopamine depletion spreads from the anterior to the posterior putamen in PD patients (Hacker et al., 2012; Helmich et al., 2010; Luo et al., 2014). Hacker ea and Helmich ea found an increase in functional connectivity of the anterior putamen to the motor and sensory cortex and a decrease of functional connectivity of the posterior putamen, which corresponds to the chronology of dopamine depletion of the putamen (Kish et al., 1988). However, Luo ea had adverse findings showing an overall decrease of functional connectivity of the cortico-striatal loop in PD.

Table 1: Literature review of resting-state fMRI in Parkinson's disease

Author	**Method**	**Number of individuals**	**Disease (y)**	**UPDRS III**	**Functional connectivity changes in PD vs controls**	
					Functional connectivity ↑	**Functional connectivity ↓**
Yu ea 2013	Seed-based analysis of SMA, CN, PU	19 PD* 20 HC rh	2.7	27	Bilateral PU to bilateral SMA, SMA to AM	Bilateral CN
Helmich ea 2010	Seed-based analysis of ant. and post. PU (AP/PP), CN	41 PD* 36 HC	6	28	AP to S2 and SMG	PP to S1, SMG, CC, S2, IPC
Kwak ea 2010	Seed-based analysis of six striatal seeds	25 PD** 24 HC	5.2	17	TH, PFC, inferior temporal gyrus, CC, superior frontal gyrus (off)	M1, SMA, PFC (on)
Hacker ea 2012	Seed-based analysis of AP, PP, CN	13 PD 19 HC	12.9	22	Sensorimotor and visual regions	TH, midbrain, CE and brainstem
Wu ea 2011	Seed-based analysis of rostral SMA and M1	18 PD* 18 HC rh	4.2	22	SMA to M1, bilateral M1	SMA to PU, insula, PMC and inferior parietal lobe
Liu ea 2013	Seed-based analysis of dentate nucleus	18 PD 18 HC rh	10.9	16	Ipsilateral CPL	Contralateral parietal lobe

Luo ea 2014	Seed-based analysis of AP, PP, CN	52 PD*** 52 HC rh	2	25	AP to AM, HI, OA, PP to S1, AP/PP to contralateral PU	-
Baudrexel ea 2011	Seed-based analysis of subthalamic nucleus	PD: 31* HC: 44	4.9	16	SMA, M1, S1	-
Sharman ea 2013	ROI to ROI analysis of striatum, TH, SN, associative, sensorimotor and lymbic cortical areas	PD: 36 HC: 45	5	18	Putamen to DLPFC, VLPFC, TH and limbic cortex areas	Thalamus to SMC, Sensorimotor cortex to TH, GP to PU and TH, SN to GP, PU and TH
Choe ea 2013	Reho	PD: 22* HC: 25 rh	3.2	10	Inferior parietal lobe, angular gyrus, SMG, middle occipital gyrus, PHG	M1, S1, SMA
Yang ea 2013	Reho	PD: 17 HC: 17 rh	1.6	21	CE, parietal lobe, temporal lobe, precuneus, frontal gyrus, STN	PU, inferior frontal gyrus, HI, anterior cingulum and bilateral lingual gyrus
Krajcovicova ea 2012	Investigation of DMN with ICA, seed-based analysis and a task	PD: 18 HC: 18 rh	4.4	14	-	-
Tessitore ea 2013	ICA, DMN	PD: 16 HC: 16 rh	5.4	12	-	Medial temporal and bilateral inferior parietal lobe
Szewczyk-Krolowski ea 2014	ICA, BGN	PD: 19** HC: 19	2.6	30	-	PU, CN, midbrain, superior temporal gyrus, DLPFC, precuneus
Esposito ea 2013	ICA	PD: 20*** HC: 18	1.6	20	-	SMA
Wu ea 2009	Graph theory with M1, CE, SMA, PMC, cingulate motor area, PU, Striatum, TH, DLPFC, parietal cortex	PD: 22** HC: 22 rh	4.1	12	Parietal cortex, CE (on) and CE, M1, parietal cortex (off)	SMA, PU (on) and SMA, DLPFC, PU (off)

**measured after 12h off medication; **measured on and off medication; ***drug-naive; AM, amygdala; AP, anterior putamen; BG, basal ganglia; BGN, basal ganglia network; CC, cingulate cortex; CE, cerebellum; CN, caudate nucleus; CPL, cerebellar posterior lobe; DLPFC, dorsolateral prefrontal cortex; DMN, default mode network; GP, globus pallidus; HI, hippocampus; ICA, independent component analysis; IPC, inferior parietal*

cortex; l, left; lh, left handed; M1, primary motor cortex; OA, olfactory area; PD, Parkinson's disease; PFC, prefrontal cortex; PHG, parahippocampal gyrus; PMC, premotor cortex; PP, posterior putamen; PU, putamen; r, right; rh, right-handed; SMA, supplementary motor area; SMG, supramarginal gyrus; SMN, sensorimotor network; S1, primary somatosensory cortex; S2, secondary somatosensory cortex; VLPFC, ventrolateral prefrontal cortex.

1.6 Resting-state functional MRI in the prodromal stage of Parkinson's disease

So far (2020) only three studies have been published using fMRI as a mean to detect differences in brain activity in a group of participants with risk factors for developing PD (see table 2, p. 17). Ellmore ea investigated functional connectivity in the resting-state in a group of ten patients with RBD, age and gender matched with eleven PD patients and ten healthy controls using a seed-based approach with the substantia nigra as ROI. Compared to healthy controls the PD group showed increased functional connectivity of the right substantia nigra to the right superior occipital gyrus, decreased functional connectivity of the right substantia nigra to the right precuneus and of the left substantia nigra to the putamen. In all except one cluster the functional connectivity of the RBD group took a middle position between healthy controls and PD patients, portraying RBD as an attenuated version of PD (Ellmore et al., 2013). Rolinski ea performed rs-fMRI and functional connectivity analyses on a group of 26 patients with RBD, comparing them to 23 healthy control and 48 PD patients using ICA. They found reduced functional connectivity within the basal ganglia network as well as in the cingulate, the paracingulate and the orbital, inferior and middle frontal gyrus when comparing patients with PD and RBD to healthy controls. Again the findings in the RBD group mirrored the changes in functional connectivity found in the PD group (Rolinski et al., 2016). Dayan and Browner did a ROI to ROI analysis within the basal ganglia network as well as a seed-based analysis with the left and the right putamen as seed region comparing 15 participants suffering from RBD and/or hyposmia to 17 healthy controls. Their ROI to ROI analysis showed a decrease within the basal ganglia network in

their prodromal group that mirrored the findings of Rolinski ea. In the seed-based analysis with both putamina as ROI they found decreased functional connectivity of the right putamen to the left putamen and of the left putamen to the bilateral striatum in the prodromal group (Dayan & Browner, 2017).

Table 2: Literature review of resting-state fMRI in the prodromal stage of Parkinson's disease

Author	Method	Number of individuals	Disease (y)	UPDRS III	Functional connectivity changes in PD vs Controls	
					Functional connectivity ↑	Functional connectivity ↓
Ellmore ea 2013	Seed-based analysis of RSN and LSN	PD: 11* HC: 10 RBD: 10 rh + lh	-	33	RSN to r. superior occipital gyrus PD > RBD > control	LSN to left PU Control > RBD > PD, RSN to right precuneus RBD > Controls > PD
Rolinski ea 2016	ICA	PD: 48* HC: 23 RBD: 26	1.8	26	-	BGN, cingulate and paracingulate cortices, frontal orbital gyri, middle and inferior frontal gyri
Dayan and Browner 2017	Seed-based analysis of PU, ROI to ROI within the basal ganglia	RBD or HYP: 15 HC: 17	-	-	-	Within the striato-thalamo-pallidal network, left PU to bilateral striatum, right PU to left PU

**measured 12h of medication; BGN, basal ganglia network; HC, healthy controls; HYP, hyposmia; ICA, independent component analysis; lh, left-handed; LSN, left substantia nigra; PD, Parkinson's disease; PU, putamen; RBD, REM sleep behavior disorder; rh, right-handed; ROI, region of interest; RSN, right substantia nigra; UPDRS, Unified Parkinson's disease Rating Scale Motor part III.*

1.7 Aims and hypothesis

This study aimed to compare the functional connectivity of both putamina to the rest of the brain in the resting-state of PD patients, healthy controls and a highly preselected, unique group of participants with an increased risk of developing PD (prodromal group) using rs-fMRI. All participants in the prodromal group had at least two risk factors for PD. We wanted to determine the place the prodromal group takes in comparison to healthy controls and patients in our functional connectivity analysis and especially whether there are differences between healthy controls and the prodromal group that might allow the use of fMRI to detect PD in its prodromal stage.

2. Materials and Methods

2.1 Description of the study population

The study population consists of participants from the TREND study and of PD patients from the ward and the outpatient clinic of the Neurodegenerative Department of the Center of Neurology, University Hospital of Tuebingen. The abbreviation TREND stands for **T**uebinger evaluation of **R**isk factors for **E**arly detection of **N**euro**D**egeneration. In the TREND study 1200 participants who exhibit prodromal markers of PD as well as healthy controls without specific prodromal markers undergo a battery of examinations, among others a quantitative motor assessment battery every two years (for details concerning the TREND study visit: www.trend-studie.de). For this study, the TREND database was prescreened for suited participants using the study requirements as well as the in- and exclusion criteria described below. The study was approved by the Ethics committee of the Medical Faculty of the University of Tuebingen (approval-no.: 370/2013BO2).

2.1.1 Groups and baseline criteria

The study population consisted of three groups: A high risk (prodromal) group, a low risk group (negative controls) and PD patients (positive controls).

Group 1 – Prodromal group: individuals at risk for PD

The prodromal group was defined by the occurrence of at least two out of three non-motor risk factors for PD (hyposmia, depression and RBD).

Group 2 – Healthy controls

A low-risk group from the same experimental protocol as group 1 without any of the three non-motor risk factors for PD.

Group 3 – PD patients

PD patients in an early state of the disease that were age matched to the other groups.

2.1.2 Inclusion and exclusion criteria

The following criteria were applied for in- and exclusion to our functional MRI study:

Inclusion criteria

- Male or female between 50 – 85 years of age.
- For groups 1-2: Participants of the TREND study, no diagnosis of PD.
- For group 1: At least two of the non-motor risk factors hyposmia, depression and RBD for PD.
- For group 2: Absence of any of the three non-motor risk factors hyposmia, depression and RBD for PD.
- For group 3: Diagnosis of PD according to the UK Brain-Bank criteria, Hoehn & Yahr stage I or II, i.e. without obvious balance deficit or a relevant gait disorder. Treatment with oral medication, but not with deep brain stimulation.
- No contraindication of the MRI scan, e.g. absence of metal implants, pacemakers, claustrophobia (for details, refer to the informed consent form for participation in the fMRI experiments, p. 85-88).
- Able to communicate well with the investigator, to understand and comply with the requirements of the study.
- Provide written informed consent to participate in the study and understand the right to withdraw consent at any time without prejudice to participate in the TREND study and to future medical care.

Exclusion criteria

- Any disability that may prevent the subject from completing the informed consent form or other study requirements.
- Any disease which renders the subject unable to communicate well with the investigator or to understand and comply with the requirements of the study.
- Fulfilling the criteria for dementia according to ICD-10.

- Participation in any clinical investigation of a new investigational compound or therapy within four weeks prior to baseline visit, or any other limitation of participation based on local regulations.
- Alcohol, medication or drug dependency or abuse (except for nicotine).
- Contraindications for the MRI scan.
- Disagreement to the study rule of getting informed about incidental findings and being counselled by a neuroradiologist.

2.1.3 Screening and recruitment process

The whole TREND database containing 1200 participants was prescreened on the basis of our baseline criteria. For matched PD patients, records of the outpatient clinic were screened. In a second step, a telephone interview was conducted informing the possible participants about the study, and if interested checking for in- and exclusion criteria using a checklist. Only participants who were interested in the study and fulfilled all in- and exclusion criteria were considered for the assessment and received a letter containing a fact sheet explaining the study in detail (see appendix, p. 79-84). After two weeks of time for consideration purposes, we contacted the potential participants again by phone to answer questions and, in the case of the ongoing wish to partake in our study, made an appointment for clinical and fMRI assessment. In the course of the recruitment process 231 potential participants were contacted and informed about the study. 126 potential participants had to be excluded as they did not meet the studies inclusion criteria, leaving 105 participants who were invited to clinical assessment and scanning: 55 prodromal participants, 25 healthy controls, and 25 patients. All subjects provided written informed consent and understood their right to withdraw their consent at any time without consequence regarding participation in the TREND study or future medical care.

2.2. Assessments

All assessments were identical for all participants. They were performed in an ambulatory setting and needed the participants to be present at the Neurological outpatient clinic of the University Hospital Tuebingen and the Max Planck institute for Biological Cybernetics for a duration of overall six hours. These six hours consisted of around four hours of clinical assessment and preparation for the MRI measurements followed by one hour of measurements in the scanner with an hour lunch break in between. The subjects were able to choose whether they wanted to perform the measurements on one day or on two consecutive days.

2.2.1 Clinical assessment

The clinical data collection began with an interview investigating clinical history as well as current medication and double-checking exclusion criteria of the MRI assessment. Motor disabilities were examined using the Unified Parkinson's Disease Rating Scale (MDS-UPDRS part III). Further clinical assessments were made, which were used for other studies.

2.2.2 Functional MRI assessment

In the scanner room, participants were equipped with silicone ear protection and then placed on the scanner tray. Utmost care was taken for the most comfortable position using multiple cushions. To minimize head movement the space between head and coil was stuffed with different upholstery. PD patients were measured on medication to prevent unwanted movements and to minimize subject burden. Additionally, all participants were instructed to lie as still as possible during the measurement. First, a localizer was performed to ensure the correct positioning of the brain volume. Then, a high-resolution anatomical scan (MPRAGE: magnetization prepared rapid acquisition gradient echo sequence) was acquired. For the resting-state measurement the

participants were told to focus on a black cross on gray background presented on an overhead display, to think of nothing in particular and to stay awake. We measured for the duration of ten minutes, capturing whole brain images every two seconds, resulting in over all 300 whole brain images per participant. During this measurement the participants' pulse was sampled using an MRI safe pulsometer. Acquisition of the resting-state data failed in overall four cases, once due to technical issues, once due to the subject falling asleep, and two times due to the participant suffering from claustrophobia.

After the rs-fMRI measurement altogether five more measurements were performed as part of the "imagination" study conducted in cooperation with the University Hospital of Nijmegen. Lying in the scanner the participants had to visualize two motor tasks concerning gait and balance they had trained beforehand. Then, they had to imagine to watch the task being done, while remaining passive. Lastly, a diffusion tensor imaging sequence was acquired for future fibre tracking studies. For an overview of all measurements, see table 3 below.

Table 3: List of all MRI measurements conducted

measurement		**duration (min)**
Imaginary task	MI of gait	10
	VI control of gait	10
	MI of balance	10
	VI control of balance	10
Resting-state		10
Structural imaging		5-6
Diffusion tension imaging		7-8

MI, motor imagination; MPRAGE, magnetization prepared rapid acquisition gradient echo; VI, visual imagination.

2.2.3 Technical data of the MRI measurements

All participants were imaged on the same 3 tesla MR-scanner equipped with a standard 20 channel head coil (Siemens Prismafit syngo MR D13D). First, anatomical images were acquired using T1-weighted magnetization-prepared rapid acquisition gradient echo (MP-RAGE) with TR/TE = 2300/4.18 ms, TI = 900 ms and a voxel size of 1x1x1 mm^3. To correct for image distortion later on, a field map was acquired with TE1 = 4.92 ms, TE2 = 7.38 ms, TR = 400 ms, gap 0.8 mm and a voxel size of 3x3x3.2 mm^3. Then, using echo planar imaging (EPI) with TR/TE = 2000/31 ms 300 volumes were acquired, each consisting of thirty-six slices with a 64x64 matrix, yielding 3x3x3.2 mm^3 voxels. An MRI save pulsometer was used to sample the pulse wave during measurements.

2.3. Data preparation and selection

2.3.1 Challenge of functional MRI data analysis

When analyzing fMRI datasets an inference is made from the BOLD signal intensity of a voxel or a group of voxels to a region of the brain. Therefore, it is vital, that every voxel always represents exactly the same spot in the brain. Already within a single participant's dataset this is never the case, because the participant himself as well as the vibration of the machine moves the head in the coil, shifting different brain regions through the rigid voxel frameset. Additionally, when comparing different participant's datasets, the unique anatomy makes a direct comparison impossible. To make the data comparable allowing for any kind of inference a sequence of image editing steps commonly referred to as data preprocessing is applied to each participant's data set. In this study we kept to well established preprocessing steps, which are listed and explained down below. All preprocessing steps were automated using the SPM12 software package (Penny, Friston, Ashburner, Kiebel, & Nichols, 2006; download: www.fil.ion.ucl.ac.uk/spm/software/spm12). If not explicitly named the recommended default settings for fMRI preprocessing were used.

2.3.2 Data preprocessing

Prior to the automated preprocessing steps, the origin of each scan (which is the reference point for all changes applied to the images) was manually set to the anterior commissure in the anatomical and the functional images.

Step 1: Calculating a voxel displacement map

When acquiring EPI images, the native images show a geometric distortion caused by static magnetic field inhomogeneities inherent to the scanner. This results in pixel shifts and signal loss (drop out) especially at tissue borders. In this first preprocessing step magnetic field inhomogeneities around the participant's head in the scanner are captured and written in a so called voxel displacement map (VDM), which is later used to unwarp the EPI images (Jezzard & Balaban, 1995).

Step 2: Realignment and unwarping

The 300 images of a participant's data set can be thought of as a shuffled deck of cards that are in disarray due to the head movement in between scans. In the realignment step all cards are brought into alignment with the top card. This is achieved using an approach called rigid body transformation. For each image six motion parameters are calculated describing its translation and rotation in relation to a reference scan using a least square approach. By means of these parameters all scans are then brought into alignment with the reference scan. The realigned images were unwarped using the VDM calculated earlier (Ashburner & Friston, 2003).

Step 3: Slice timing

Statistical models that analyze EPI images assume that an image is taken at one point in time. In reality, this is not the case, as one image consists of many slices taken over a period of time. In our case a scan consisted of 36 slices acquired in two seconds. Also, slice acquisition happened interleaved, which means that first all the odd number slices were scanned (1, 3, 5…), followed by

the even number slices (2, 4, 6…). As a consequence, neighboring slices are acquired as much as one second apart from each other. During slice timing correction voxel values of every slice are corrected for this shift in time, resulting in an image in which each slice corresponds to the same point in time.

Step 4: Anatomical coregistration

Functional images have a worse spatial resolution than structural images. Therefore, the functional images are brought into alignment with a high resolution anatomical scan, resulting in functional images that are more similar to an individual's actual anatomy than the native scans (Collignon et al., 1995).

Step 5: Spatial normalization

The scans of each participant are warped into the same, standardized anatomical space. This ensures that across participants each voxel represents the same brain region. Every participant's anatomical scan is warped into the space of a tissue probability map (TPM) in standard space. A TPM contains the probability of the tissue classes gray matter, white matter and cerebrospinal fluid, which are detected at each location of the image. Using the TPM, each voxel is classified as being one out of three tissue classes. The estimated warping parameters are applied to the functional scans. In our study, the scans were warped into the space of the templates of the Montreal Neurological Institute (MNI), which were implemented in SPM12 (Ashburner & Friston, 2005).

Step 6: Smoothing

Smoothing is the intentional blurring of the functional scans. Each voxel's value is spread across the neighboring voxel values by means of a Gaussian filter, averaging the voxel values. This has different effects: It reduces the impact of noise in the functional data. It enlarges clusters of active voxels making them easier to detect. It puts neighboring voxels into a dependency, thereby reducing the degrees of freedom and the amount of correction needed for multiple testing when analyzing the data. For this study the data sets were smoothed with a Gaussian filter of 8 mm full width at half maximum (FWHM).

2.3.3 Exclusion of data sets due to motion of the participants

Motion of the participants is a substantial generator of noise in fMRI data sets. This is especially an issue in rs-fMRI, in which the baseline signal of the brain and not specific task evoked activation is investigated. Here, already minimal movements can be detrimental (Power et al., 2012). Therefore, thorough analyses of the participants' movements were performed using the "motion fingerprint" and "analyze motion" scripts written and kindly provided by Marko Wilke (Wilke, 2012). These two scripts evaluate the six motion parameters obtained during the rigid body transformation of the realignment procedure. Among other motion measures they calculate the participants' motion in between two consecutive scans, also referred to as scan to scan motion (STS). Because STS is more difficult to regress out of the data than large continuous motion throughout the whole measurement (Lemieux et al., 2007), every dataset with an STS displacement of more than 0.5 mm in more than 20% of the data (60 scans out of 300) was excluded from the analysis. For the remaining data sets with a number of STS displacement of 0.5 mm in less or equal 20% of the data, all the motion influenced images were discarded and replaced by a mean image of the two neighboring scans. This process was automated using a proprietary script kindly provided by Marko Wilke. Also, the first five images of every participant's dataset were discarded due to T1 saturation effects. Altogether 15 datasets had to be excluded from analysis. One data set was deficient and could not be preprocessed, six datasets had incomplete or partially missing pulse samples and eight datasets were excluded due to motion. In the end, 86 data-sets were included in the study (see fig. 5, p. 36).

2.4 Statistical analysis: seed-based analysis

The remaining preprocessed functional scans were entered into a seed-based analysis. In this type of analysis, a region of interest (ROI, also referred to as seed) is chosen and its mean signal intensity over the time of the measurement,

also referred to as time course, is extracted. The time course is a graph with the time on the x-axis and the mean signal intensity of the ROI on the y-axis. Then, the time course of the ROI is correlated to the time course of every other voxel in the brain. This results in a correlation map for each subject, in which every voxel represents the correlation to the chosen ROI. Voxels or clusters of voxels with a high resemblance of their time course to the time course of the ROI have high correlation values, marking them as regions that were synchronously active with the ROI – and are therefore thought to be functionally connected. For this study the left and right putamen were chosen as ROI and two separate seed-based analyses were performed, one for each seed. The putamen was chosen as its functional connectivity, precisely a decrease within the basal ganglia and an increase to other brain regions i.e. cerebellum, precentral gyrus and supplementary motor area is well documented in PD patients (Hacker et al., 2012; Helmich et al., 2010; Kwak et al., 2010; Liu et al., 2013; Luo et al., 2014; Tessitore et al., 2012). Additionally, the putamen was a practical choice, as its volume is big enough to serve as seed. Smaller regions are difficult to measure reliably due to the bad spatial resolution of the BOLD signal (Boubela et al., 2015). The seed-based analysis was calculated using the REST toolbox V.1.8 (Song et al., 2011; download: www.rfmri.org/REST). First, the linear trend was removed from each participant's dataset to focus the analysis on fluctuations around the trend. Then, assuming that the signal of interest and noise are present at separable frequencies, the detrended scans were temporally filtered only retaining frequencies of BOLD fluctuation between 0.01-0.08 Hz.

When conducting a seed-based analysis masks are needed. A mask is a binary image, consisting of zeroes and ones, that is laid over the functional scans during the analysis. Only where the mask has the value one, the underlying functional scan is visible and correlation analysis can be performed. One mask hides the whole brain except the ROI. With this mask overlaid, the mean time course of all voxels of the ROI is extracted and averaged, resulting in one mean time course for the region of interest. Before this mean time course of the region of interest is correlated to every voxel of the scan, a second binary mask is

overlaid over the image, called the brain mask. The brain mask covers all the space outside of the brain, so that only correlation of actual brain volume and not the space around the brain is calculated. The resulting correlation values are corrected for noise in the data using a table of covariates. For this study the data was corrected for noise due to motion of the subject and pulse. The creation of the brain mask, the seed mask as well as the table of covariates is described in further detail below. Lastly, the R-values of the correlation maps were Fisher's z-transformed. This is a necessary step when doing statistical analysis to determine if two correlating values are significantly different. In Fisher's z-transformation, a confidence interval is calculated for each R-value. If the confidence intervals of two z-scores do not overlap, then there is a significant difference.

2.4.1 Creation of a brain mask and a ROI mask

The masks for the ROI as well as the whole brain mask were derived from the Hammersmith atlas n30r83 kindly provided by A. Hammers (© Copyright Imperial College of Science, Technology and Medicine 2007, all rights reserved, atlas source: www.brain-development.org). This atlas is an adult maximum probability brain map based on 83 manually delineated regions drawn on MR images of 30 healthy adult participants (Hammers et al., 2003). The Hammersmith atlas was chosen over more common tools for mask creation like Automated Anatomic Labeling (AAL) as it is based on the anatomy of multiple participants and therefore takes anatomical variations into account (Tzourio-Mazoyer et al., 2002). Also, the mean age of the individuals on whom the Hammersmith atlas is based (31 years) is closer to the mean age of our participants than the age of the single male template (a student) used in AAL.

The Hammersmith atlas defines the putamen as the region bordered anteriorly by the frontal lobe, the internal capsule and the insula, posteriorly by the internal capsule, medially by the internal capsule, the lamina medullaris lateralis and the substantia perforata anterior, laterally by the frontal lobe, the parietal lobe and

the insula, superiorly by the most superior slice where the putamen is seen and inferiorly by the frontal lobe. The ROI masks of the left and right putamen were reduced in their volume via four iterations of smoothing with a Gaussian kernel with 4 mm FWHM and thresholding (60%) to account for brain atrophy due to aging (Galluzzi et al., 2008) and to increase specificity of the analysis. This process was automated using a proprietary script by M. Wilke. Original and reduced volumes of the masks as well as MNI coordinates of their center of mass are listed in Table 4 below. The center of mass was calculated using the MARSBAR toolbox (Brett et al., 2002; download: marsbar.sourceforge.net).

Table 4: ROI coordinates and its volume prior and post reduction

ROI	Original volume	Reduced volume	MNI coordinates
Left putamen	7028 mm^3	790 mm^3	-24 4 -0.3
Right putamen	6719 mm^3	720 mm^3	25 6 -0.5

MNI, Montreal Neurological Institute; ROI, region of interest.

Figure 2: Creation of brain mask using iterations of smoothing and thresholding

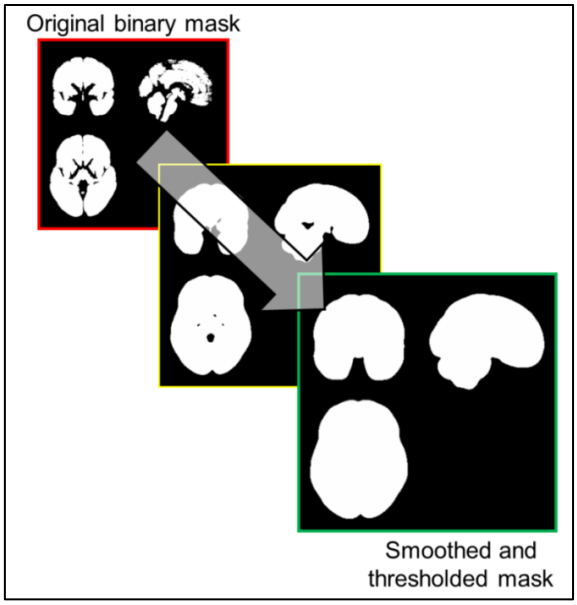

The red outlined image shows the original hammersmith atlas, the yellow outlined image an intermediate state after two iterations of smoothing and thresholding and the green outlined image the final brain mask.

For the brain mask, the Hammersmith atlas was converted into a binary mask using the Image Calculator in SPM8 (download: fil.ion.ucl.ac.uk/spm/software). This mask was then smoothed with a Gaussian Kernel with 8mm FWHM and the resulting image was binarized with a threshold of 5% (all voxels with a likelihood of belonging to the brain of five percent were included). This resulted in a mask that was more inclusive than the original one as gaps that were left by areas not defined in the Hammersmith atlas were closed (see fig. 2, p. 30).

Finally, the masks (dimension: 181x217x181 voxels) were resliced using the "coregister: reslice" function of SPM12 to match the dimension of the functional images (53x63x53 voxels). Correct topography of all masks was visually inspected by overlaying them on a mean anatomical image of all participants in MRIcron (Chris Rorden, download: people.cas.sc.edu/rorden/mricro, see fig. 3 below).

Figure 3: ROI masks overlaid over a normalized mean anatomical image of all participants

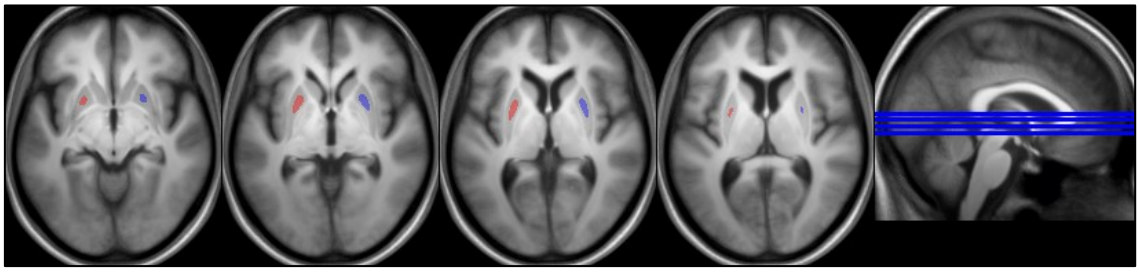

This image shows the ROI masks overlaid over a mean anatomical image of all participants. The four images on the left are axial scans through the seed regions. Their exact location is represented by the blue lines over the single sagittal scan on the right. The red volume is the left putamen ROI, the blue volume is the right putamen ROI.

2.4.2 Implementation of covariates for pulse and motion

Covariates for pulse and motion of the participants were regressed out of the correlation maps. Pulse wave samples were obtained using an MRI safe pulsometer fixed on the participants' index finger during the MRI measurement. The recorded pulse samples were stored in physio files and were later converted into covariates using the RETROICOR toolbox (Glover et al., 2000), which is part of the PhysIO toolbox (Kasper et al., 2017; download: nitrc.org/projects/physio). The RETROICOR toolbox was adapted to the studies scanner and sensor setup by Michael Erb. RETROICOR transformed the sample wave of the pulse to a single value for every time point (which means every single scan) of the measurement which later was subtracted from the activation signal while calculating the correlation maps with the REST toolbox.

The six motion parameters obtained through the rigid body transformation during the realignment procedure were used as motion estimates, a 24-parameter Volterra expansion was applied to them and used as covariate in the seed-based analysis to compensate for noise through motion of the participants. For each scan 24 movement regressors were calculated, that consisted of the six original movement parameters, the exponentiation of the 6 movement parameters (R^2), a shift of the 6 movement parameters to the next time point (R_{t-1}), and again the exponentiation of the shifted parameters (R_{t-1}^2): R $R^2 R_{t-1} R_{t-1}^2$. Shifting of the movement parameters means applying the movement parameter estimated of a scan to the consecutive scan. This procedure accounts for the fact that the current position of a participant in the scanner results from multiple movements that happened in the past that still influence the signal intensity. The exponentiation of the original and shifted motion parameters represents the exponential effect motion has on the noise level in functional scans (Friston et al., 1996). The 24-parameter Volterra expansion and the combination of the motion regressor and pulse regressor into one file (requirement of the REST toolbox) were achieved with a proprietary script provided by Marko Wilke.

2.5 Statistical analysis

Using SPM12, two one-way between subject analysis of variance (ANOVA) were performed with the z-transformed correlation maps, one for each seed region. Differences in demographics and clinical characteristics were evaluated using ANOVA with post-hoc t-tests or Chi-squared test, where appropriate.

2.5.1 Analysis of differences in demographic and clinical data

Differences in age, movement in the scanner defined by STS movement and UPDRS III scores were analyzed using one-way between subject ANOVAs in JMP (JMP®, Version 13. SAS Institute Inc., Cary, NC, 1989-2007; download: www.jmp.com/en_us/home). If significant, directionality was investigated using post-hoc two-sample t-tests. Significance of distribution of gender in the study population was analyzed with Chi-squared test.

2.5.2 One-way between-subject ANOVA

Any differences in correlation with the left and right putamen among the three groups – PD patients, healthy controls and participants at risk for developing PD (prodromal group) – were assessed by calculating two one-way between-subject ANOVAs in SPM12 over the whole brain: the first ANOVA was computed using the correlation maps of the left putamen and the second ANOVA using the correlation maps of the right putamen. Both age at MRI assessment and gender were added as covariates of no interest. To detect any significant difference in correlation to the putamen six different t-contrasts were used (see fig. 4, p. 34). The resulting maps were inspected using a threshold of $p < 0.001$ uncorrected for multiple comparisons and a deliberately chosen minimum cluster size of 60 voxels (results with at least 60 coherent voxels were regarded as significant) was applied. Significant clusters were saved and further evaluated. The anatomical regions part of the significant clusters were identified

using AAL toolbox implemented in SPM12, and then visually reviewed overlaid on a mean anatomical image of all participants (Tzourio-Mazoyer et al., 2002).

Figure 4: T-contrasts used in the ANOVA

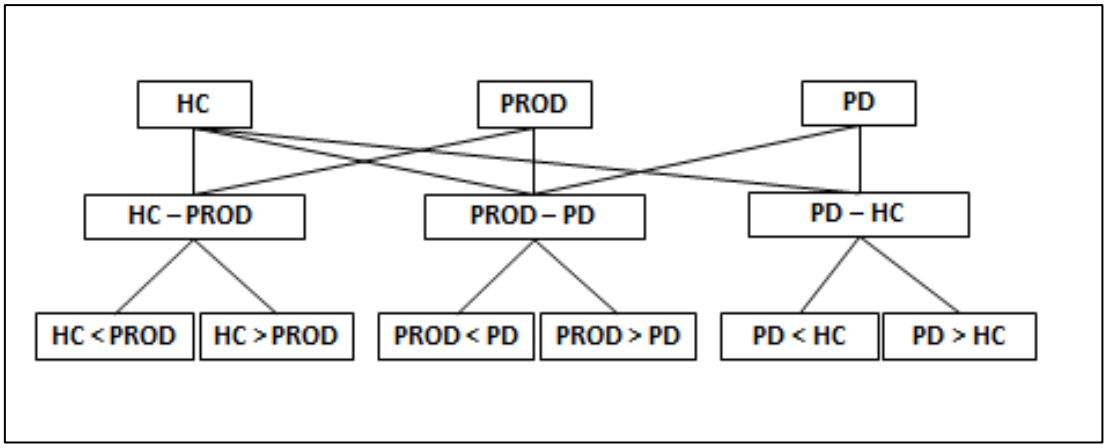

The top row shows all three groups and the middle row all options of pairing them. The bottom row depicts all possible ways to contrast them. HC, healthy controls; PD, Parkinson's disease patients; PROD, prodromal group.

2.5.3 Extraction of mean z-scores in significant clusters

To determine the hierarchy of the functional connectivity in the three groups, the average correlation in all significant clusters was extracted from each participant's correlation maps for the left and the right putamen using a proprietary script provided by Marko Wilke. The extracted z-scores were entered into a spreadsheet in JMP, and their distribution graphically plotted to illustrate the order of the groups.

2.6 New classification of groups based on number of risk factors at the follow-up closest to the functional MRI assessment

The first data analysis conducted as described above did not yield any significant results. Searching for an explanation it became obvious that a probable reason was the selection of participants based on the risk factors they displayed at the baseline assessment of their inclusion into TREND. For some participants, this assessment dated back as much as six years before the fMRI assessment. Participants suffering from RBD and depression were treated, and therefore their number of risk factors changed over time. Also, participants affected with hyposmia at the baseline assessment surprisingly regained their sense of smell at later follow-ups. Furthermore, participants who did not display risk factors at the baseline assessment and were counted as healthy controls developed one or multiple risk factors over time. Therefore, it was decided to reclassify the groups based on the prodromal markers assessed at the follow-up closest to our fMRI measurement to truly portray the actual number of risk factors present during our study. Finally, the study population comprised of 21 patients, 24 healthy controls and 22 participants in the prodromal group. In the prodromal group eleven participants suffered from depression and hyposmia, nine participants from depression and RBD, one participant from hyposmia and RBD and one participant from all three risk factors (see fig. 5, p. 36).

Figure 5: Flowchart of the recruitment process

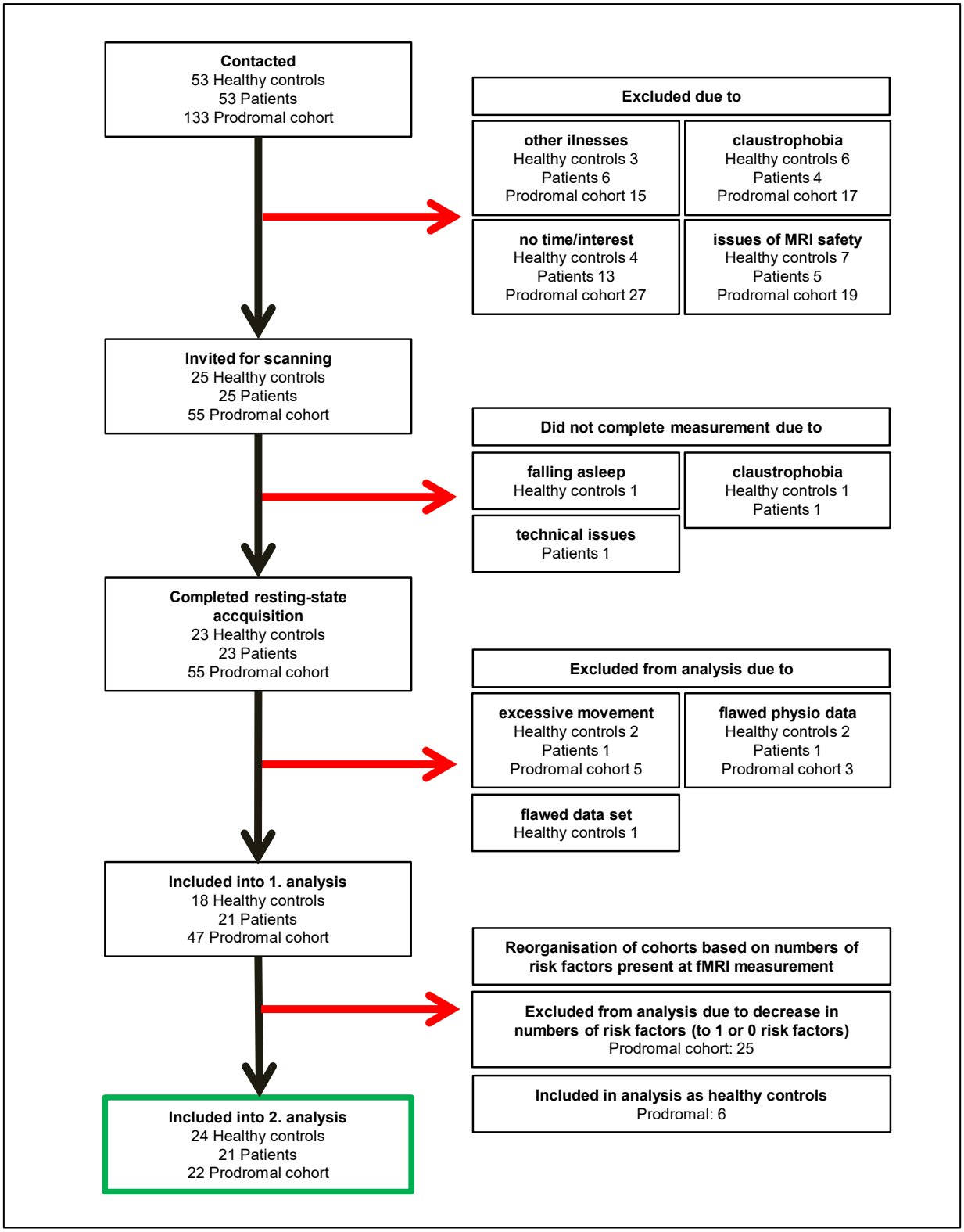

This flowchart depicts in detail the recruitment process as well as the exclusion of participants. The green outlined box at the bottom shows all participants included in the study.

2.7 Subgroup analysis based on handedness and Parkinson's disease subtype

While drafting the summary for this thesis it became evident that the original study layout missed two exclusion criteria, that are important for reliable results in functional imaging: handedness of the participants and PD subtype. Differences in handedness determine different brain morphology and activation patterns in functional imaging (Amunts et al., 1996; Hammond, 2002). The same applies to different PD subtypes: Tremor-dominant disease subtype shows different activation patterns in ReHo than the akinetic-rigid subtype (Zhang et al., 2015). For these reasons, a subgroup analysis was done excluding all left-handed participants and all PD patients of the tremor-dominant subtype. While checking the clinical data of all patients for disease subtypes, it was discovered that three participants of the patient cohort were later diagnosed with atypical PD. Additionally, two patients were excluded due to disease subtype. Four participants of the healthy control group and two participants of the prodromal group were excluded due to handedness. Then, the subgroups consisted of 20 healthy controls, 16 patients and 20 participants of the prodromal cohort (see fig. 6, p. 38). The same statistics as described above were used in the subgroup analysis. The results will be discussed after the main discussion, which is fashioned according to the original study layout.

Figure 6: Flowchart of the exclusion process for the subgroup analysis

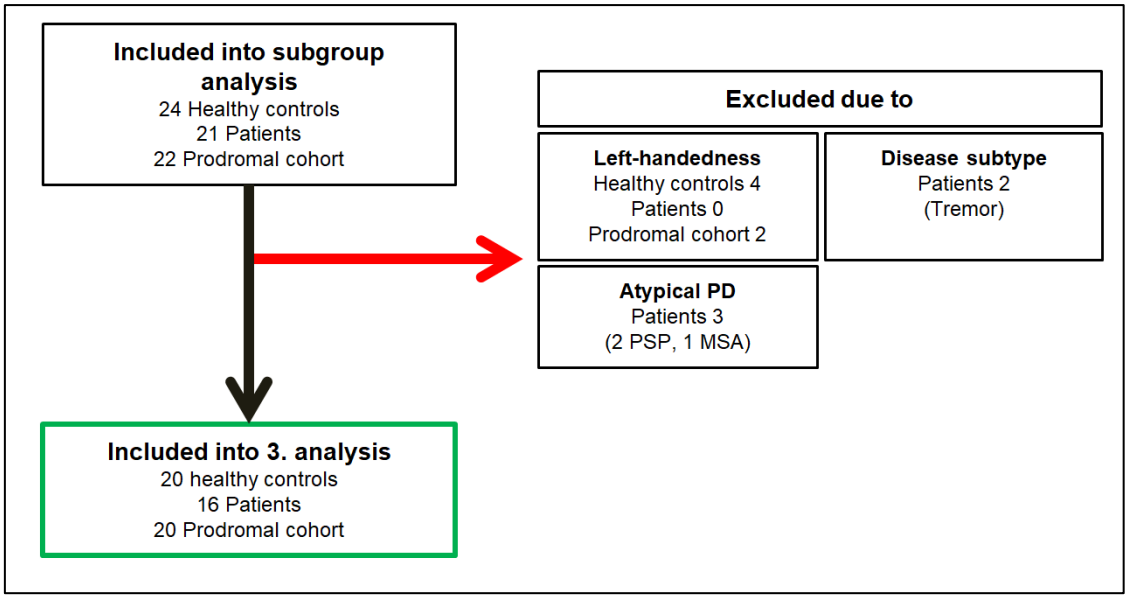

This flowchart accounts for all the datasets excluded for the subgroup analysis. Datasets were excluded due to handedness, disease subtype and diagnosis of atypical PD. MSA, multisystem atrophy; PD, Parkinson's disease; PSP, progressive supranuclear palsy.

3. Results

3.1 Differences in demographic and clinical characteristics of the groups

There were no significant differences regarding age, gender and movement in the scanner between the healthy controls, the prodromal group and PD patients. Movement in the scanner was defined by the count of STS movement > 0.5 mm. A significant difference could be found in the MDS-UPDRS III scores. As expected, scores of the patients' group were significantly higher compared to controls ($p < 0.0001$) as well as compared to the prodromal group ($p < 0.0001$). Mean disease duration in the patients' group calculated from the time point of first manifestation of symptoms was 2.3 years with a range from one year to six years. Mean Hoehn & Yahr stage was 1.8 with a range from 1 to 2.5. In eleven patients the side more severely affected by PD was the left side, in seven patients the right side. In two patients the more prominently affected side could not be determined (see table 5, below).

Table 5: Demographic and clinical data of the groups

	HC (n=24)	PROD (n=22)	PD (n=21)	Statistics
Age (years)	67.7 ± 6	65.8 ± 7.0	66.2 ± 7.7	0.6025
Men/Women (female%)	12/12 (50)	8/14 (63.6)	14/7 (33.3)	0.1384
STS > 0.5	8.0 ± 11.4	5.8 ± 10.3	8.4 ± 9.2	0.667
MDS-UPDRS III (0-132)	2 ± 3	4 ± 4	24 ± 10	< 0.0001
Disease duration (years)	-	-	2.3 ± 1.1 (1-6)	-
H&Y (0-5)	-	-	1.8 ± 0.5 (1-2.5)	-
Most effected side (l/r) *	-	-	11/7	-
Levodopa equivalent dose (mg)	-	-	321.1 (30-640)	-

** most affected side of two patients unknown; HC = healthy controls; PD = Parkinson's disease patients; PROD = prodromal group.*

3.2 Results of the one-way ANOVAs of the correlation maps

As described above, two one-way between subject ANOVAs were calculated and contrasted for the main effect of groups to detect any significant differences in functional connectivity to the left and the right putamen between the groups.

3.2.1 One-way between-subject ANOVA with the correlation maps of the left putamen

The left putamen showed increased functional connectivity in five clusters in the prodromal group, when compared to patients. One cluster of 170 voxels was mainly located in in the right middle frontal gyrus (MNI coordinate 30 38 38, $p = 0.025$). A right hemispheric cluster of 251 voxels comprised of parts of the precuneus, the superior parietal lobule, the postcentral gyrus and the cingulate gyrus (MNI coordinate 21 -40 44, $p = 0.006$). A third cluster of 257 voxels was located in the right middle and inferior temporal gyrus (MNI coordinate 39 2 -49, $p = 0.005$). A fourth cluster of 975 voxels encompassed parts of the right SMA, the left and right cingulate gyrus and the left middle and superior frontal gyrus. (MNI coordinate -3 5 29, $p < 0.001$). The last cluster of 5522 voxels was located in both cerebellar hemispheres and the vermis, the right precuneus and the right cuneus, the right occipital and fusiform gyrus, the left hippocampus and the left middle and inferior temporal gyrus (MNI coordinate -42 -82 -13, $p < 0.001$).

The left putamen also showed increased functional connectivity in two clusters in the prodromal group, when compared to healthy controls. One cluster of 372 voxels was located in the left and the right pre- and postcentral gyrus and the right cingulate gyrus (MNI coordinate -6 -37 74, $p = 0.001$). A second mostly symmetric cluster of 633 voxels comprised of parts of the cingulate gyrus, the superior frontal gyrus and the right SMA (MNI coordinate 0 35 23, $p < 0.001$). For a detailed overview over all clusters see table 6 and 7, p. 42 as well as fig. 7 p. 43.

The analysis yielded no significant clusters when comparing healthy controls to PD patients.

Table 6: Clusters with increased functional connectivity of the left putamen in the prodromal group compared to patients

Cluster	p-value	MNI coordinates (mm)	Anatomical area
170	0.025	30 38 38	r. middle frontal gyrus
251	0.006	21 -40 44	r. precuneus r. superior parietal lobule r. postcentral gyrus r. cingulate gyrus
257	0.005	39 2 -49	r. middle temporal gyrus r. inferior temporal gyrus
975	< 0.001	-3 5 29	r. SMA l. and r. cingulate gyrus l. superior frontal gyrus l. middle frontal gyrus
5522	< 0.001	-42 -82 -13	l. and r. cerebellar hemisphere vermis r. precuneus r. cuneus r. occipital gyrus r. fusiform gyrus l. hippocampus l. middle temporal gyrus l. inferior temporal gyrus

MNI coordinates, Montreal neurological institute coordinates; SMA, supplementary motor area.

Table 7: Clusters with increased functional connectivity of the left putamen in the prodromal group compared to healthy controls

Cluster	p-value	MNI coordinates (mm)	Anatomical area
372	0.001	-6 -37 74	l. and r. postcentral gyrus l. and r. precentral gyrus r. cingulate gyrus
633	< 0.001	0 35 23	l. and r. cingulate gyrus l. and r. superior frontal gyrus r. SMA

MNI coordinates, Montreal neurological institute coordinates; SMA, supplementary motor area.

Figure 7: All clusters with the left putamen as ROI

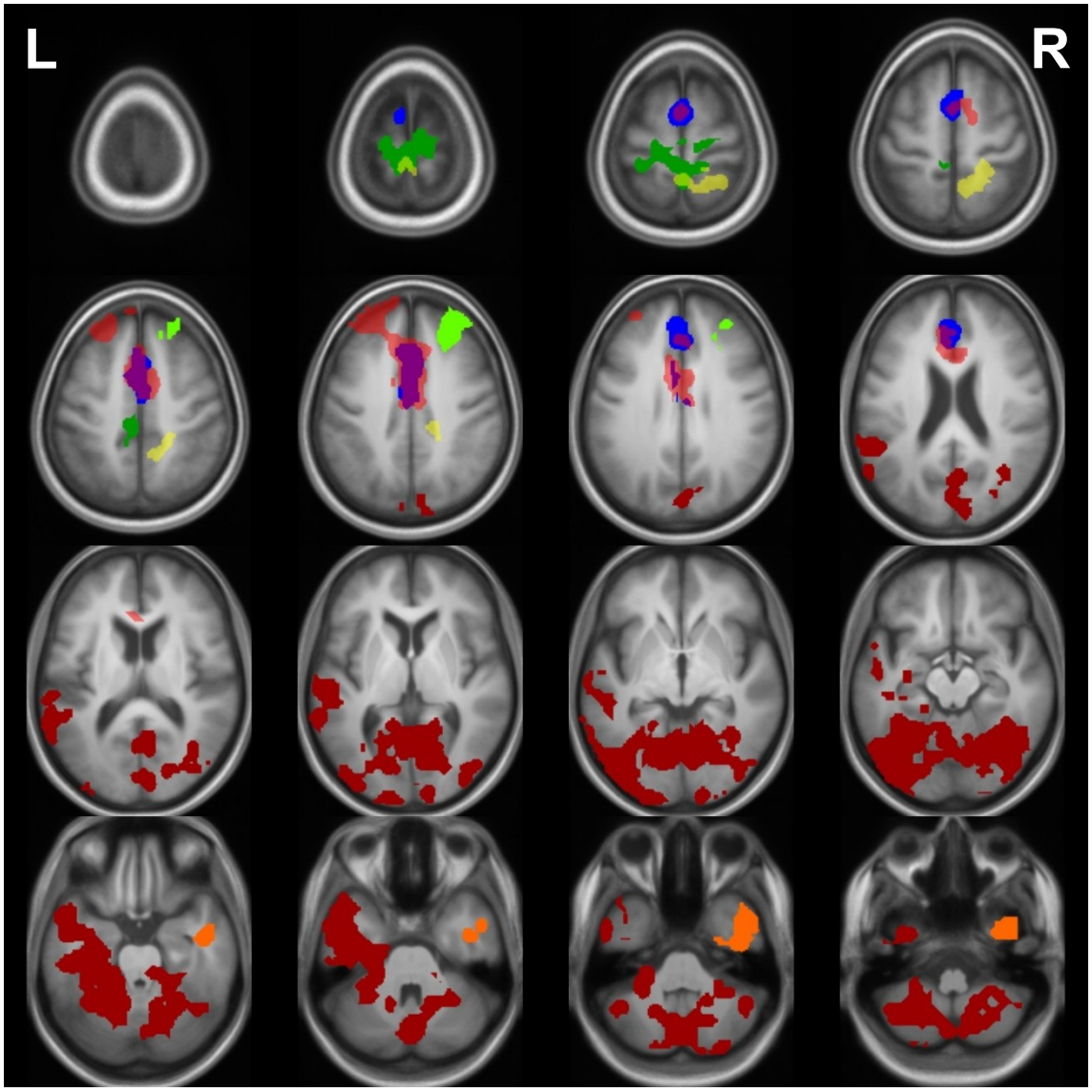

The clusters are overlaid on a mean anatomical image of all participants. All clusters shown indicate increased functional connectivity in the prodromal group. Clusters with increased functional connectivity compared to PD patients are displayed in warm colors. Clusters with increased functional connectivity compared to healthy controls are shown in cold colors. Color mapping for each cluster: 5522 voxels, dark red; 975 voxels, red; 257 voxels, orange; 251 voxels, yellow, 170 voxels bright green; 633 voxels, blue; 372 voxels, dark green. L, left side; R, right side.

3.2.2 One-way between-subject ANOVA with the correlation maps of the right putamen

The right putamen showed increased functional connectivity in four clusters in the prodromal group, when compared to patients. One cluster of 177 voxels was located in left middle and superior frontal gyrus (MNI coordinate -30 52 38, p = 0.025). The second cluster of 279 voxels was located in the right inferior frontal gyrus and the right superior temporal gyrus, pars opercularis (MNI coordinate 63 20 11, p = 0.004). The third cluster of 299 voxels encompassed the right middle and superior frontal gyrus (MNI coordinate 30 62 29, p = 0.003). And a fourth large clusters of 13088 voxels was located in both cerebellar hemispheres, the left and right striatum, the right occipital gyrus, the left and right supramarginal gyrus, the left postcentral and the right precentral gyrus, the right SMA, the left and right cingulate gyrus, the left hippocampus, the left thalamus and the left and right superior temporal and superior frontal gyrus (MNI coordinate -42 -82 -13, p < 0.001). For a detailed overview over all clusters see table 8 below and fig. 8, p. 45. The analysis yielded no significant clusters when comparing healthy controls to PD patients or healthy controls to the prodromal group.

Table 8: Increased functional connectivity of the right putamen in the prodromal group when compared to patients

Cluster	p-value	MNI coordinates (mm)	Anatomical area
177	0.025	-30 52 38	l. middle frontal gyrus l. superior frontal gyrus
279	0.004	63 20 11	r. inferior frontal gyrus r. superior temporal gyrus
299	0.003	30 62 29	r. middle frontal gyrus r. superior frontal gyrus
13088	< 0.001	-42 -82 -13	l. and r. cerebellar hemispheres l. and r. striatum r. occipital gyrus l. and r. supramarginal gyrus r. SMA l. and r. cingulate gyrus l. hippocampus

			l. thalamus l. and r. superior temporal gyrus l. and r. superior frontal gyrus

MNI coordinates, Montreal neurological institute coordinates; SMA, supplementary motor area.

Figure 8: All clusters with the right putamen as ROI

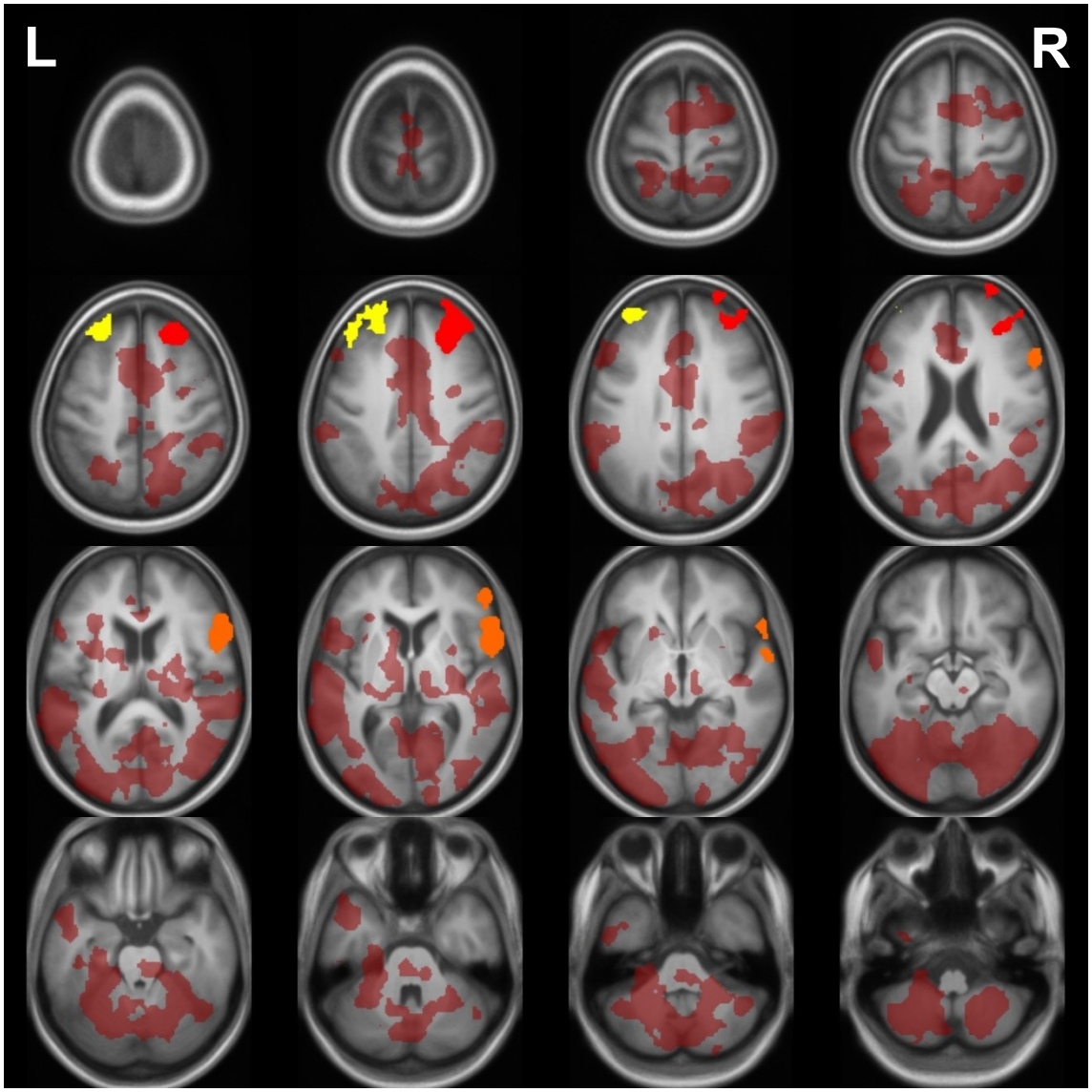

Increased Functional connectivity of the right putamen in the prodromal group compared to PD patients overlaid on a mean anatomical image of all participants. Color mapping for each cluster: 13088 voxels, dark red; 279 voxels, orange; 177 voxels, yellow; 299 voxels, red. L, left side; R, right side.

3.2.3 Comparison of mean functional connectivity in all clusters across groups

As neither the ANOVA with the correlation maps of the left putamen, nor the ANOVA with the correlation maps of the right putamen yielded significant findings when comparing healthy controls to PD patients the mean z-scores in every identified cluster was extracted for every group. This showed a stable TREND throughout all clusters: mean z-scores were highest in the Prodromal group and lowest in the PD group, while the connectivity of the healthy controls was found right in the middle (see fig. 9, p. 47).

Figure 9: Grouped boxplot of the mean z-scores of every group extracted from all significant clusters

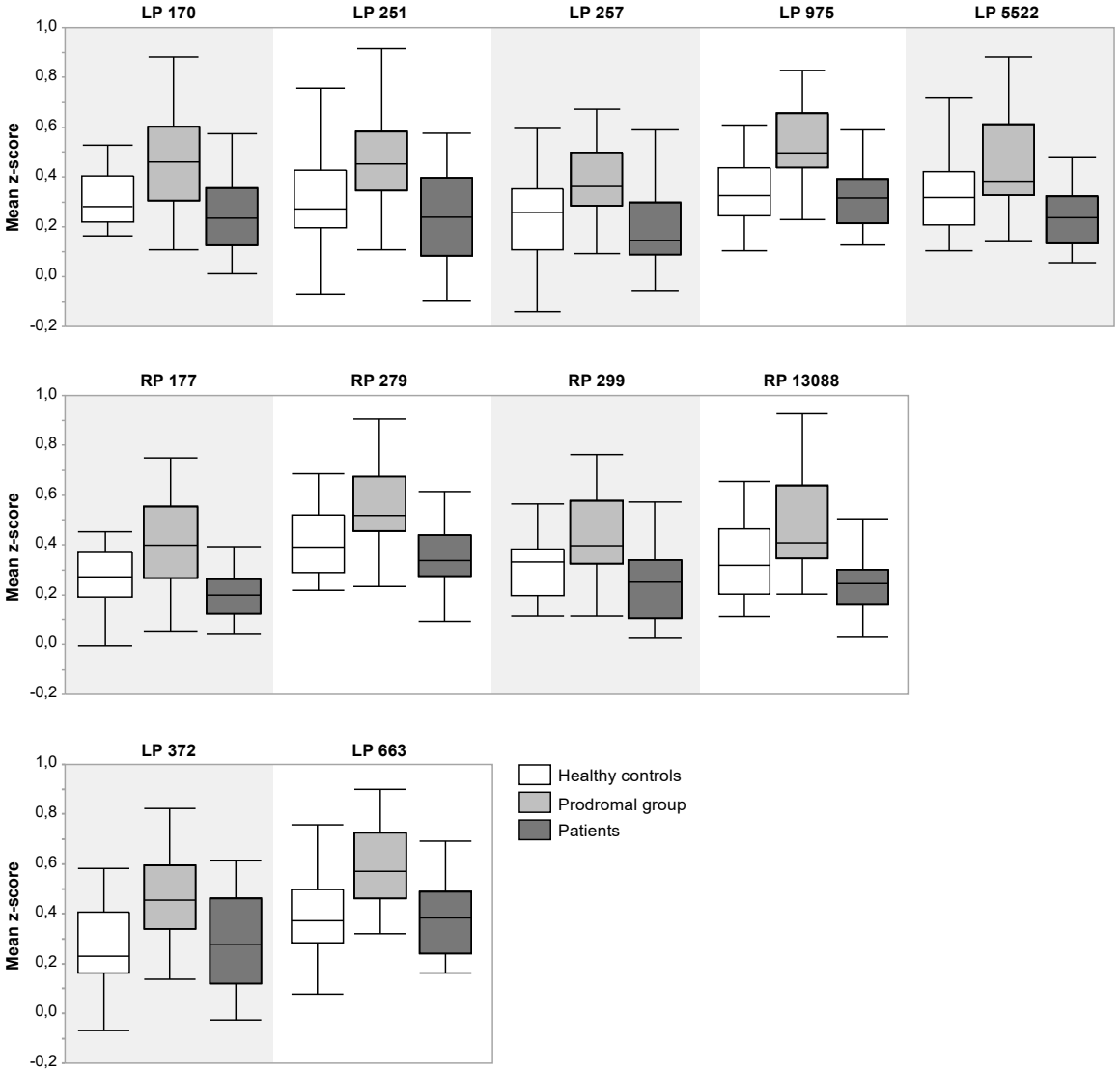

Grouped boxplots of the mean z-scores of each group in every cluster. White boxes represent healthy controls, light grey boxes the prodromal group and dark grey boxes the PD patients. Above each group of boxplots an abbreviation identifies the cluster, e.g. LP 170 (seed left putamen, cluster of 170 voxels). In all clusters, the prodromal group shows highest mean z-scores, whereas the patient group mostly shows lowest mean z-scores without ever differing significantly from the healthy controls.

3.4 Subgroup analysis

As described above a subgroup analysis was conducted excluding all left-handed participants, all patients with tremor-dominant subtype as well as patients which were later diagnosed with atypical PD (see p. 37). The set-up mostly did not change: two one-way between subject ANOVAs with correlation maps of the left and the right putamen and determination of differences between groups using T-contrasts. The chosen significance level was higher: p-values < 0.05 after family-wise error correction (FWE) and a minimum cluster size of 60 voxels were defined as significant.

3.4.1 Demographic and clinical characteristics of the subgroup

Within the subgroup no significant differences regarding age, gender and movement were found. As to be expected, a significant difference was found for MDS-UPDRS III scores, with higher values in PD patients. For details, see table 9 below.

Table 9: Demographic and clinical data of the subgroup

	HC (n=20)	PROD (n=20)	PD (n=16)	Statistics
Age (years)	67.4 ± 6.1	65.3 ± 7.0	65.9 ± 8.1	0.6
Men/Women (female %)	10/10 (50)	8/12 (60)	12/4 (25)	0.10
STS > 0,5 mm	8.4 ± 11.3	6.2 ± 10.5	6.6 ± 7.3	0. 7
UPDRS III [0-132]	2 ± 2 *	4 ± 4 *	23 ± 10	<0.0001
Disease duration (years)	-	-	1.5 ± 0.7 (0.5-2)	-
Hoehn & Yahr stage [0-5]	-	-	1.6 ± 0.5 (1-2.5)	-
Most effected side (l/r/u)	-	-	9/5/2	-
Disease subtype (AR/EQ/TD)	-	-	11/5/0	-
Levodopa equivalent dose (mg)	-	-	340 (100-640)	-
DEP + HYP (%)	-	9 (45)	-	-
DEP + RBD (%)	-	8 (40)	-	-
HYP + RBD (%)	-	1 (5)	-	-
DEP + HYP + RBD (%)	-	2 (10)	-	-

Data are presented with mean and standard deviation. AR, akinetic-rigid subtype; DEP, depression; EQ, equivalent subtype; HC, healthy controls; HYP, hyposmia; l, left; PD, Parkinson's disease patients; PROD, prodromal group; r, right; RBD, REM sleep behavior disorder; STS, Scan to scan deviation; TD, tremor-dominant; u, unknown; UPDRS III, Unified Parkinson's disease Rating Scale part III.

3.4.2 Findings for the left putamen within the subgroup

The ANOVA of the left putamen yielded four significant clusters with increased functional connectivity in the prodromal group when compared to the PD patients. One big mostly symmetric cluster of 2886 voxels comprised of the cerebellum, the precuneus, the inferior and middle occipital lobe and the inferior and middle temporal lobe (MNI coordinate -42 -82 -13, $p < 0.00001$). A left hemispheric cluster of 187 voxels comprised of the middle and superior temporal lobe and the supramarginal gyrus (MNI coordinate -63 -43 17, $p < 0.00001$). A third, again symmetric, cluster of 243 voxels contained the cingulum and the SMA (MNI coordinate 3 26 35, $p < 0.00001$). The smallest cluster (78 voxels) encompassed the bilateral precuneus and cuneus, as well as the superior occipital lobe (MNI coordinates 9 -85 47, $p = 0.00002$).

Comparing the left putamen functional connectivity of the prodromal group to healthy controls, four significant clusters showed increased functional connectivity in the prodromal group. A symmetric cluster of 251 voxels was located in the vermis and the crus cerebelli (MNI coordinate 6 -73 -37, $p < 0.00001$). Another cluster of 271 voxels comprised of the left and right cingulum, the left and right SMA and the left superior medial frontal gyrus (MNI coordinate 0 29 32, $p < 0.00001$). A third right hemispheric cluster of 119 voxels covered the inferior temporal and occipital gyrus as well as the fusiform gyrus (MNI coordinates 48 -58 -197, $p = 0.00002$). The last cluster of 73 voxels involved the left and right paracentral lobule, the right precentral gyrus, the right SMA and the left precuneus (MNI coordinate -6 -31 77, $p = 0.0005$).
The comparison of healthy controls and PD patients yielded no significant differences in both directions. All findings are summarized and illustrated in table 10 and 11 as well as fig. 10, p. 50/51. Further illustrations for each cluster can be found in the appendix (p. 97-100).

Table 10: Increased functional connectivity of the left putamen in the prodromal group when compared to healthy controls (subgroup)

Cluster	p-value	MNI coordinates (mm)	Anatomical area
251	< 0.00001	6 -73 -37	l. and r. cerebellum vermis l. and r. crus cerebellum
271	< 0.00001	0 29 32	l. and r. middle and anterior cingulum l. and r. SMA l. superior medial frontal gyrus
119	0.00002	48 -58 -19	r. inferior temporal gyrus r. inferior occipital gyrus r. fusiform gyrus
73	0.0005	-6 -31 77	l. and r. paracentral lobule r. precentral lobule r. SMA l. precuneus

MNI coordinates, Montreal neurological institute coordinates; SMA, supplementary motor area.

Table 11: Increased functional connectivity of the left putamen in the prodromal group when compared to the patients (subgroup)

Cluster	p-value	MNI coordinates (mm)	Anatomical area
2886	< 0.00001	-42 -82 -13	l. and r. cerebellum l. and r. lingual gyrus l. and r. inferior occipital lobe l. and r. fusiform gyrus vermis l. and r. inferior temporal lobe l. and r. calcarine gyrus l. and r. middle occipital lobe l. and r. precuneus r. middle temporal lobe r. cuneus l. and r. crus cerebelli
187	< 0.00001	-63 -43 17	l. middle and superior temporal lobe l. supramarginal gyrus
243	< 0.00001	3 26 35	l. and r. middle cingulum l. and r. SMA l. and r. anterior cingulum l. and r. medial superior frontal lobe
78	0.00002	9 -85 47	l. and r. cuneus l. and r. precuneus r. superior occipital lobe r. superior parietal lobe

MNI coordinates, Montreal neurological institute coordinates; SMA, supplementary motor area.

Figure 10: Clusters with the left putamen as ROI in the subgroup

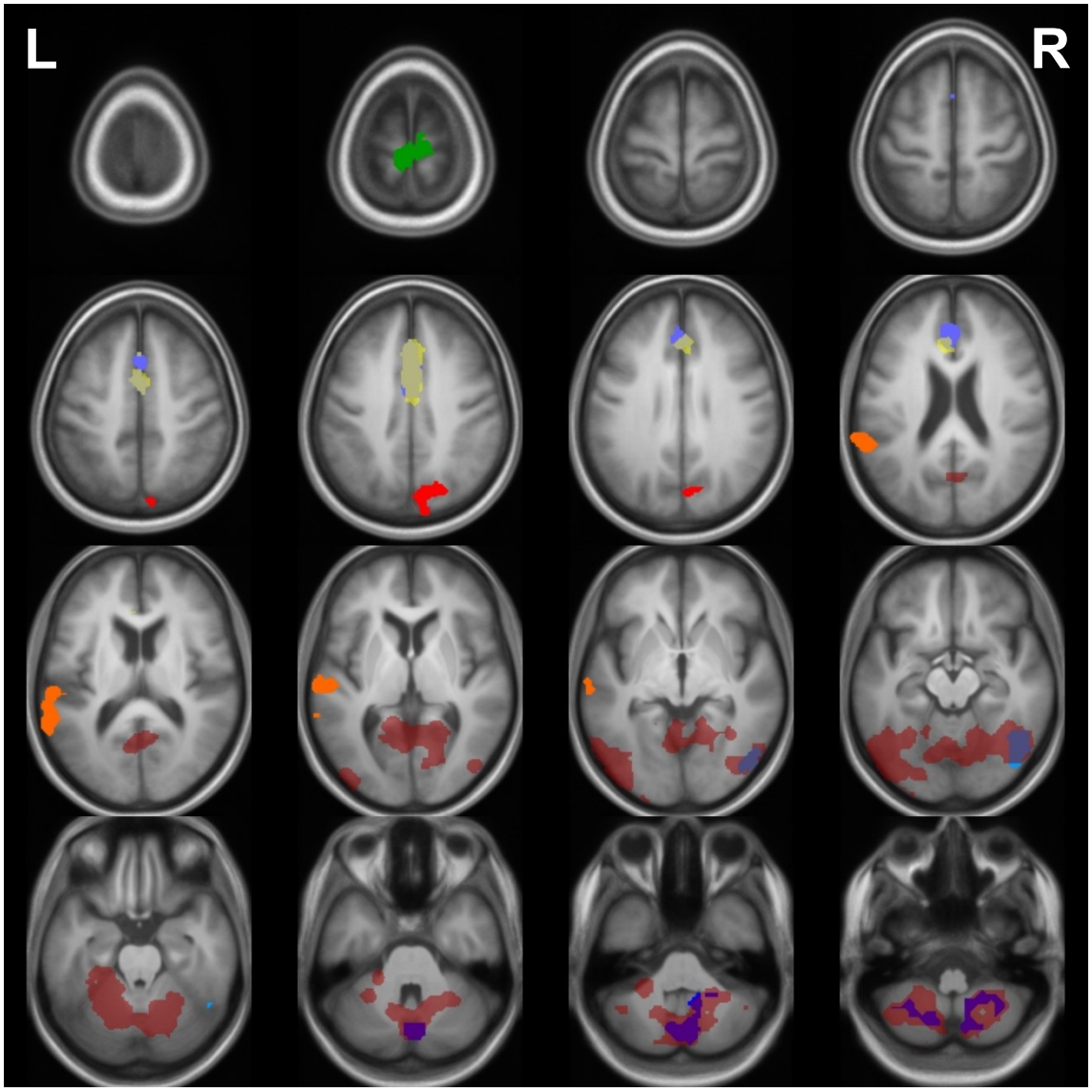

The clusters are overlaid on a mean anatomical image of all participants. All clusters shown indicate increased functional connectivity in the prodromal group. Clusters with increased functional connectivity compared to PD patients are displayed with warm colors. Clusters with increased functional connectivity compared to healthy controls are shown in cold colors. Color mapping for each cluster: 2886 voxels, dark red; 187 voxels, orange; 78 voxels, red; 243 voxels, yellow; 251 voxels, dark blue; 119 voxels, light blue; 73 voxels, green, 271 voxels, lilac. L, left side; R, right side.

3.4.3 Findings for the right putamen within the subgroup

The ANOVA of the right putamen yielded seven clusters with significantly increased functional connectivity in the prodromal group when compared to PD patients. A mostly symmetric cluster of 4184 voxels comprised of the cerebellum, the majority of the occipital and temporal lobe, the vermis and the precuneus (MNI coordinate -42 -82 -13, $p < 0.00001$). A left hemispheric cluster of 418 voxels was located in the middle and superior temporal lobe and the inferior frontal lobe pars opercularis (MNI coordinate -63 -43 17, $p < 0.00001$). A right hemispheric cluster of 119 voxels involved the inferior frontal lobe pars opercularis and pars orbitalis (MNI coordinate 60 14 -4, $p < 0.00001$). A symmetric cluster of 233 voxels encompassed the cingulum, the SMA and the superior medial frontal lobe (MNI coordinate 3 26 17, $p < 0.00001$). A cluster of 160 voxels was located in the right temporal lobe (MNI coordinates 66 -37 11, $p < 0.00001$). A sixth cluster of 78 voxels was located in the right supramarginal gyrus (MNI coordinate 60 -34 35, $p = 0.00002$). The last cluster of 106 voxels comprised of the left and right precuneus and paracentral lobule (MNI coordinate 3 -55 56, $p < 0.00001$).

Comparing the right putamen functional connectivity of the prodromal group to healthy controls, we found three significant clusters with increased functional connectivity in the prodromal group. The first cluster of 176 voxels sat in the right cerebellar hemisphere and the right fusiform gyrus (MNI coordinate 24 -52 -49, $p < 0.00001$). A second cluster of 366 voxels comprised of both cerebellar hemispheres, the vermis, the crus cerebelli as well as the left fusiform and parahippocampal gyrus (MNI coordinates 6 -73 -37, $p < 0.00001$). A third cluster of 85 voxels was located in the right inferior temporal and occipital lobe (MNI coordinate 51 -70 -10, $p = 0.00001$). The comparison of healthy controls and PD patients yielded no significant differences in both directions. All findings are illustrated in table 12 and 13, p. 53/54 as well as fig. 11, p. 55. Further illustrations for each cluster can be found in the appendix (p. 101-105).

Table 12: Increased functional connectivity of the right putamen in the prodromal group when compared to healthy controls (subgroup)

Cluster	p-value	MNI coordinates (mm)	Anatomical area
176	< 0.00001	24 -52 -49	r. cerebellum r. fusiform gyrus
366	< 0.00001	6 -73 -37	l. and r. cerebellum and vermis l. and r. crus cerebelli l. fusiform gyrus l. parahippocampal gyrus
85	< 0.00001	51 -70 -10	r. inferior temporal lobe r. inferior occipital lobe r. fusiform gyrus

MNI coordinates, Montreal neurological institute coordinates.

Table 13: Increased functional connectivity of the right putamen in the prodromal group when compared to patients (subgroup)

Cluster	p-value	MNI coordinates (mm)	Anatomical area
4184	< 0.00001	-42 -82 -13	l. and r. cerebellum l. inferior occipital lobe l. and r. fusiform gyrus l. and r. cuneus l. and r. calcarine gyrus l. and r. middle occipital lobe r. inferior occipital lobe l. and r. superior occipital lobe l. and r. middle temporal lobe l. and r. inferior temporal lobe vermis l. and r. crus cerebelli l. and r. lingual gyrus l. and r. precuneus r. superior parietal lobe
418	< 0.00001	-63 -43 17	l. middle and superior temporal lobe l. supramarginal gyrus l. superior temporal pole l. inferior frontal lobe pars opercularis l. rolandic operculum
119	< 0.00001	60 14 -4	r. inferior frontal operculum r. superior temporal pole r. inferior frontal gyrus (pars triangularis) r. rolandic operculum r. frontal inferior pars orbitalis

233	< 0.00001	3 26 17	l. and r. middle cingulum l. and r. anterior cingulum l. and r. SMA l. and r. superior medial frontal lobe
160	< 0.00001	66 -37 11	r. superior and middle temporal lobe r. heschl's gyrus r. rolandic operculum
78	0.00002	60 -34 35	r. supramarginal gyrus
106	0.00001	3 -55 56	l. and r. precuneus l. and r. paracentral lobule

MNI coordinates, Montreal neurological institute coordinates; SMA, supplementary motor area.

Figure 11: Clusters with the right putamen as ROI in the subgroup

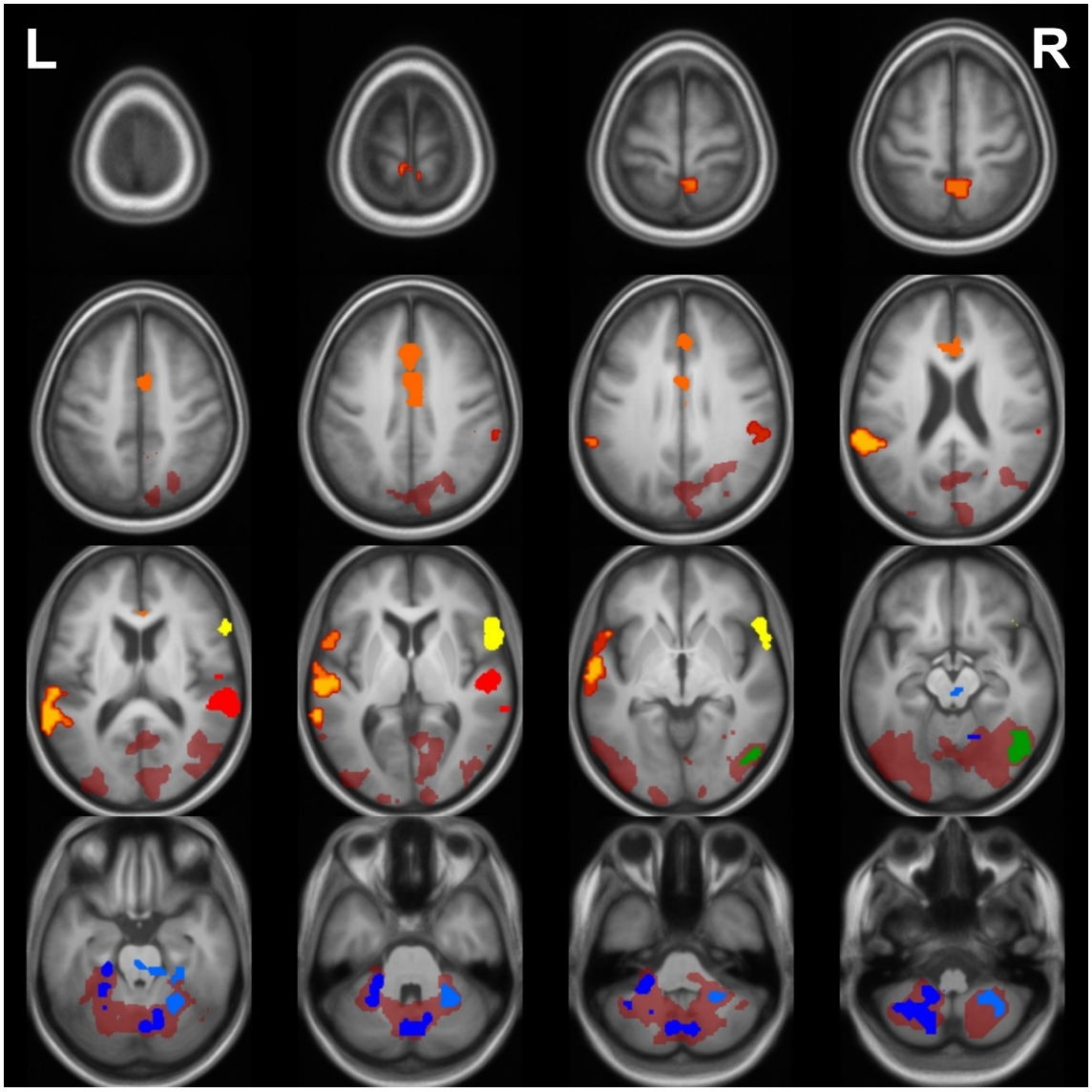

The clusters are overlaid on a mean anatomical image of all participants. All clusters shown here indicate increased functional connectivity in the prodromal group. Clusters with increased functional connectivity compared to PD patients are displayed with warm colors. Clusters with increased functional connectivity compared to healthy controls are shown in cold colors. Color mapping for each cluster: 4184 voxels, dark red; 160 voxels, red; 418 voxels, red-yellow; 119 voxels, yellow; 233 voxels, orange; 78 voxels, red; 106 voxels, orange-red; 366 voxels, dark blue; 176 voxels, blue; 85 voxels, green. L, left side; R, right side.

3.4.4 Comparison of mean functional connectivity in all clusters across the subgroup

The mean z-scores were extracted from all significant clusters and graphically plotted against each other. This revealed a consistent trend throughout all clusters: mean z-scores were highest in the prodromal group and similar in healthy control group compared to PD patients. The distribution of the mean z-scores is illustrated in a grouped boxplot chart in fig. 10 below.

Figure 12: Grouped boxplots with the mean z-scores of all subgroups in all significant clusters

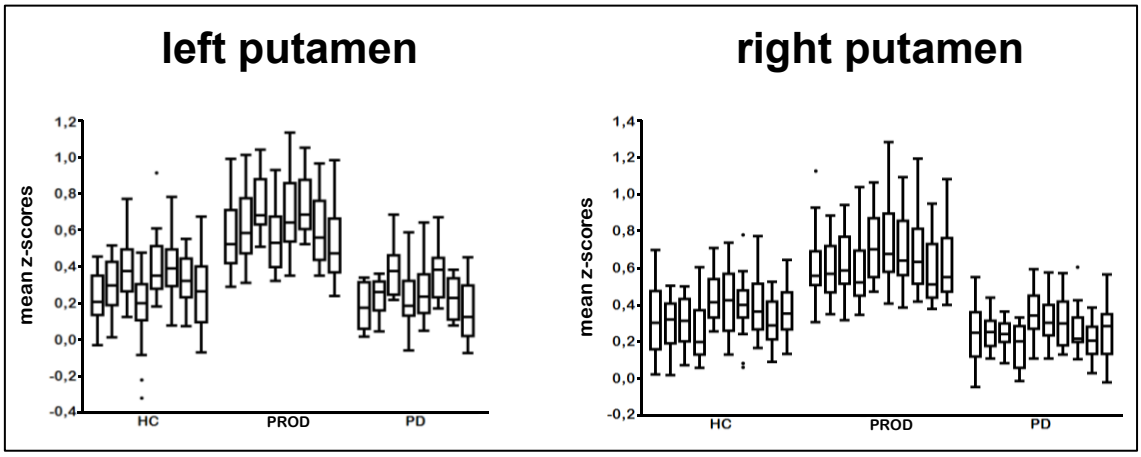

Grouped boxplots with the mean z-scores of all groups in all significant clusters. Mean z-scores were highest in the prodromal group and similar in the healthy control group compared to patients, resembling an inversed U-shaped curve. HC, healthy controls; PROD, prodromal group; PD, Parkinson's disease patients.

4. Discussion

This study aimed to compare the functional connectivity in rs-fMRI of 21 PD patients, 24 healthy controls and a group of 22 participants with an increased risk of developing PD (prodromal group), who had at least two out of three risk factors for PD. We hypothesized that rs-fMRI would reveal a pathophysiological correlate of a premotor phase of PD. We hoped to find differences in functional connectivity between healthy controls and the prodromal group that might enable us to detect PD in its early state by the use of fMRI.

In a seed-based approach we measured the functional connectivity of the left and the right putamen to the rest of the brain. Using a voxel-wise analysis of variance and T-contrasts we then searched for significant differences in correlation of the putamen to the rest of the brain between our three groups ($p < 0.001$ uncorrected, minimum cluster size 60 voxels).

The prodromal group showed increased functional connectivity of the left putamen to the right precuneus, the left and right posterior cingulate gyrus, the superior parietal lobule, the left middle frontal gyrus as well as the right visual cortex and the whole cerebellum (vermis and hemispheres) when compared to patients. When compared to healthy controls, again the prodromal group showed increased functional connectivity of the left putamen to the left and right pre- and postcentral gyrus, the right SMA as well as the medial left and right middle frontal gyrus. In comparison, functional connectivity of the right putamen was increased in the prodromal group when compared to patients in the left and right posterior cingulate gyrus, the left and right visual cortex and the cerebellum (both hemispheres and vermis). Interestingly, no significant differences in functional connectivity of the left or the right putamen where found between patients and healthy controls. But there was a stable trend throughout all significant clusters: the extracted mean z-score was lowest in PD patients and highest in the prodromal group while the healthy controls sat right in the middle. A result which at first glance seems surprising. Expected would be

highest functional connectivity in the healthy, lowest in the PD patients with the prodromal group sitting in the middle, portraying an attenuated version of PD patients.

We think these results could depict a compensatory mechanism which contributes to the long prodromal phase of PD. A state of disease, in which the brain increases connectivity of brain regions responsible for the execution and planning of motion to enable normal movement as long as possible. Fitting this paradigm, the prodromal group showed increased functional connectivity of the putamen to the visual cortex, the pre- and postcentral gyrus, the supplementary motor area and the cerebellum – areas of the brain involved in the execution of motion (Bagesteiro et al., 2006; Lemon, 2008; Manto et al., 2015; Nachev et al., 2008; Proske & Gandevia, 2012; Sarlegna & Sainburg, 2009). Furthermore, functional connectivity was increased in the bilateral posterior cingulate gyrus, the medial middle frontal gyrus and the right precuneus – brain regions belonging to the DMN. Among the RSNs, the DMN is unique as it reduces its activity during cognitive challenges and is thought to aid in planning future actions and behavior while resting, like the planning of movement (Rosazza & Minati, 2011). Failing of those compensatory mechanisms could equal lower functional connectivity in those brain regions and PD becoming clinically visible. Respectively, functional connectivity is lowest in our patient group.

While functional connectivity of the healthy controls was always higher than in the patient group, this difference never surpassed the threshold to significance. This is most likely due to the conscious decision to measure the patients on medication expecting to minimize movement in the scanner and stress for the patients. Nonetheless, it is well established that the administration of Levodopa restores normal functional connectivity in the basal ganglia network, thus explaining the failure of this study to find significant differences between the healthy controls and the patients (Bezard et al., 2003; Buhmann et al., 2003; Delaveau et al., 2010).

4.1 Comparison with findings of other studies investigating prodromal Parkinson's disease

Although there are several study groups investigating prodromal PD, so far (time of writing the doctoral thesis) only three studies have been published using fMRI as a mean to detect differences in brain activity in a group of individuals with risk factors for developing PD.

Ellmore ea investigated functional connectivity in the resting-state in a group of ten patients with RBD, age and gender matched with eleven patients and ten healthy controls (Ellmore et al., 2013). They used a seed-based approach, but chose the substantia nigra as ROI. They reported a decrease in functional connectivity of the left substantia nigra to the left putamen, and of the right sustantia nigra to the right superior occipital gyrus in the prodromal group when compared to healthy controls, while the lowest connectivity was found in patients. Respectively, the RBD patients showed an attenuated version of the decrease in functional connectivity found in PD patients in these clusters. However, there was one exception. The right precuneus showed increased functional connectivity to the right putamen in the RBD group, while connectivity in the PD group was lowest with the healthy controls sitting in the middle.

Rolinski ea performed rs-fMRI and functional connectivity analysis on a group of 26 patients with RBD, comparing them to 23 healthy controls and 48 PD patients (Rolinski et al., 2016). Different to our study, they chose with the ICA a data driven approach and found reduced functional connectivity within the basal ganglia network (putamen, caudate, pallidum) as well as in the cingulate, the paracingulate and the orbital and middle frontal gyrus when comparing PD and RBD patients to healthy controls. The changes in functional connectivity in PD patients mirrored those of the RBD patients, thus consolidating the findings of Ellmore ea.

Dayan and Browner used a ROI-to-ROI analysis with the caudate nucleus, the putamen and the thalamus as well as a seed-based approach with both putamina in a group of 15 participants suffering from RBD and/or hyposmia, comparing them to 17 matched healthy controls (Dayan & Browner, 2017). Considering the ROI-to-ROI analysis, they found a decrease in functional connectivity in their prodromal group, concerning interhemispheric connectivity as well as connectivity within the basal ganglia and the striato-thalamo-pallidal loop. These findings repeated themselves regarding the seed-based voxel-wise approach with both putamina as ROI, which from a methodology standpoint resembles our study. Again, they found decreased functional connectivity of the left putamen to the right basal ganglia and vice versa.

In reporting exclusively increased functional connectivity in our prodromal group, our study stands in contrast with these three studies, whose lowest common factor is a decrease in basal ganglia connectivity in their prodromal groups. The exact reason for this is uncertain and presumably multifaceted.

One part of the explanation could be that all studies tried to investigate a dynamic progress, the neurodegeneration preceding PD, cross-sectionally. Consequently, it could have happened, that the same condition was documented at different time points and thus results differ. Supporting this assumption, Ellmore ea also found a cluster in the right precuneus with increased functional connectivity to the right putamen in the prodromal group. For this cluster, the distribution of groups resembled all of our findings. Also, the two other studies failed to find any increase in functional connectivity of the basal ganglia to cortical brain regions, which is well-documented for PD patients (Baudrexel et al., 2011; Helmich et al., 2015; Kwak et al., 2010).

This effect could be further amplified by using different methodology and different attributes to define the prodromal group, as it is the case with the above-mentioned studies. Also, it is possible that different prodromal markers are accompanied by specific changes in functional connectivity and that a

certain combination of markers can augment or negate each other. To circumvent this issue and make results comparable a more detailed definition of the prodromal phase of PD would be necessary.

4.2 Comparison with findings of other studies investigating resting-state functional MRI in Parkinson's disease

In contrary to prior studies that also used a seed-based approach to investigate functional connectivity in PD we did not find any significant differences between patients and healthy controls. This is most likely due to the short disease duration of our patients (2.3 years, see table 5, p. 40) when compared to other studies (see table 1, p. 14), and our choice of measuring patients on medication (which is discussed in further detail below). Only one other study by Kwak ea used a seed-based approach and measured patients on medication. They found similar results, showing decreased functional connectivity of the striatum to the precentral gyrus, the supplementary motor cortex and the prefrontal cortex (Kwak et al., 2010). However, this decrease in functional connectivity existed in comparison to healthy controls, not to a prodromal group, as it is the case for our study. Taking a different approach, Wu ea used graph theory to compare functional connectivity within the motor network in patients on and off medication and healthy controls, also finding a decrease in functional connectivity of the SMA to the putamen in patients in the ON-state (Wu et al., 2009).

4.3 Limitations

Several limitations of this study must be taken into account.

4.3.1 Limitations of the groups

While we were able to achieve a sufficient match of age and gender in our groups, we failed at matching the groups regarding handedness. Usually,

studies investigating brain function only assess individuals with the same handedness, as difference in handedness implicates differences in brain morphology - e.g. in left-handers, the right central sulcus is deeper than in right-handers and vice versa (Amunts et al., 1996) - as well as in activation patterns (Hammond, 2002). In the case of fMRI studies investigating rather complex neuronal networks, Pool ea showed that the influence one brain area exerts over another is differentially modulated in right- and left-handers. Using dynamic causal modeling they showed that the interhemispheric coupling of the SMA, the primary motor cortex and the putamen was significantly stronger in right- than in left-handers (Pool et al., 2014). Of special interest for our study are the results of another study of Pool ea, which, using a seed based approach, showed that the resting-state movement network has increased functional connectivity of the left primary motor cortex to the right dorsolateral premotor cortex in right-handers, while functional connectivity was decreased in left-handers (Pool et al., 2015). These results implicate, that our failure to only measure individuals with the same handedness may have confounded the analysis and might have influenced the results.

We also failed at achieving sufficient homogeneity in our PD group regarding subtype of disease and affected side. A recent study by Zhang ea reports substantial differences in functional connectivity among different PD subtypes. Zhang ea performed a ReHo analysis in 27 patients with akinetic-rigid subtype and 20 patients with tremor-dominant subtype. Comparing these groups to healthy controls they found that the two PD subtypes are distinguishable from each other in terms of functional connectivity changes. Patients with the akinetic-rigid subtype exhibited a more substantial change in neural activity in the mesolimbic cortex, while in patients with tremor-dominant subtype the activation of the cerebellar regions increased (Zhang et al., 2015).

Also, in difference to the common practice of measuring PD patients for fMRI studies after 12 hours of withdrawal from medication in a clinically defined OFF-state, we decided to measure our patients on medication. We anticipated that

the suppression of involuntary movement in the ON-state would yield better results by minimizing the noise in the data. Furthermore, we were reluctant to submit our patients to the stress of the OFF-state during a full day of multiple assessments. Nonetheless, it has been shown that levodopa administration in PD patients restores functional connectivity in the basal ganglia, even to normal levels (Buhmann et al., 2003; Delaveau et al., 2010; Esposito et al., 2013; Haslinger et al., 2001; Palmer et al., 2009). Thus, our failure to find significant differences in functional connectivity between healthy controls and patients is most likely due to our decision to measure patients in the ON-state. Nevertheless, when comparing mean correlation of all three groups in all significant clusters, the extracted mean z-scores of the patient group, while failing to reach significance level in comparison to the healthy group, always were the lowest.

4.3.2 Limitations of measurements

The main confounder in fMRI studies is the exact measurement of the BOLD signal. A variety of different factors can cause unwanted changes in signal intensity, ranging from inhomogeneity of the magnetic field produced by the scanner to bodily functions that influence blood flow, like breathing and pulse rate. Especially detrimental to the BOLD signal is the movement of the subject. We took important steps on different levels of the measurement to compensate for that. During the measurement, the room between coil and subject's head was stuffed with soft foam to minimize involuntary movement. Also, a conscious decision was made to measure PD patients on medication. We excluded eight datasets due to excessive movement during scanning, in the remaining datasets all the motion influenced images were discarded and replaced by a mean image of the two neighboring scans. In the course of the data analysis we added a Volterra transformation of the realignment parameters as covariates of no interest. Furthermore, we recorded the subjects pulse rate during the measurement and added the pulse's time course as another covariate of no

interest. We did not, however, take respiration as possible confounder into account.

Next to its susceptibility to noise, significance of the bold signal is also limited by a poor spatial resolution. This is on one hand due to technical limitations. When recording the BOLD signal, spatial resolution is sacrificed in favor of temporal resolution. And on the other hand, due to the signal's character. Engel ea (Engel et al., 1997) estimated that focal brain activation leads to changes in bold signal intensity that spread up to 3.5mm around the actual center of activation, with peak values not in the active brain region but in the blood vessel supplying the region. As a consequence, when identifying the anatomic regions comprising our significant clusters, we did concentrate on the regions in the center of the clusters, while ignoring those regions barely touched by it and avoided making assumptions concerning spatially small anatomical areas (Boubela et al., 2015).

4.3.3 Consequences of the limitations

On the level of the fMRI measurement we took all necessary precautions, except monitoring breathing, to achieve the best signal quality possible, and therefore fall in line with the current standard of practice, as does our preprocessing pipeline and the data analysis.

Despite of our best efforts to create well matched groups, our study suffers from inhomogeneity of the groups, regarding handedness, affected side in patients and from disregarding subtype of disease and measuring patients on medication. These factors confound our study.

4.4. Subgroup analysis

Taking the shortcomings of the original study protocol into account a sub study was conducted excluding all left-handed participants, all patients with tremor

dominant subtype as well as two patients who had been diagnosed with atypical PD in the meantime. The remaining groups comprised of 20 healthy controls, 16 patients and 20 participants of the prodromal group. The data analysis for this subgroup was exactly the same as for the main group. It yielded more results (18 clusters above the threshold), with a substantially higher significance level (see chapter 3.4, p. 48). Interestingly, the significant clusters mostly contained similar brain regions as the results of the original study. Also, the hierarchy of functional connectivity in the clusters did not change: highest connectivity was always found in the prodromal group, lowest in the patient group with the healthy controls sitting in the middle. Again, no significant differences in functional connectivity between the medicated patient group and the healthy controls could be found due to the reasons discussed in detail above.
The brain regions with significantly higher functional connectivity to the putamina in the prodromal group again concerned the conscious and subconscious execution of motion (cerebellum, vermis, pre- and postcentral gyrus, the SMA, the cuneus) as well as the planning of motion and behavior (the middle frontal gyrus, the precuneus, the temporal lobe). Interestingly, while not being directly congruent, the clusters of the left and the right putamen shared some brain regions.

To summarize, the gain of this subgroup analysis mostly consists of reaching more results at a higher significance level. The grand scheme of the results does not diverge from the original study. This implicates that the original findings must portray a real difference in functional connectivity between our groups, which persisted although important confounders of functional imaging studies were ignored. A paper with the results of the subgroup analysis is submitted, the release is pending.

4.5 Outlook

This study was able to show that a group of highly preselected individuals, who might be in the prodromal phase of PD, has increased functional connectivity in

multiple brain areas, when compared to healthy controls and PD patients. This increase in functional connectivity might be the equivalent of a compensatory mechanism, which counteracts the neurodegeneration through an increase in activity, and connectivity. Thus, these changes in BOLD signal intensity might help to detect individuals in the prodromal stage of PD in the future, which finally may contribute to earlier treatment strategies.
Unfortunately, our understanding of the physiological meaning of the BOLD signal is up to this date very basic, achieving a reliable image quality is difficult, and the possibilities of statistical analysis are diverse. For now, all these factors diminish the usability and the validity of rs-fMRI, and sometimes reduce our interpretation of its results to speculations. However, in the future it might be possible to profit from technological advancements in neuroimaging, such as better temporal and spatial resolution through scanners which deploy stronger magnetic fields, and studies further defining the characteristics of the BOLD signal. A possibility of confirming our results would be a comparison with well-established forms of brain functional imaging like a PET scan (Positron emission tomography) – a study with this purpose is conducted right now (2020) at the University Hospital of Tuebingen.

5. Summary

This study aimed to compare the functional connectivity in rs-fMRI of PD patients, healthy controls and a highly preselected group of participants with an increased risk of developing PD (prodromal group). All participants included in the prodromal group had at least two out of the three following prodromal markers for PD: hyposmia, depression and RBD. We hypothesized that the rs-fMRI would reveal a pathophysiological correlate of the premotor phase of PD. We especially hoped to find differences in functional connectivity between healthy controls and the prodromal group that might enable us to detect PD in its early state by the use of functional MRI.

The study population was selected from participants of the TREND study, as well as PD patients from the ward and the outpatient clinic of the Neurodegenerative Department of the Center of Neurology, University Hospital Tuebingen. 53 healthy controls, 133 individuals for the prodromal group and 53 patients were contacted. 25 healthy controls, 55 participants for the prodromal group and 25 patients were invited for testing and scanning. The assessments made were identical for all participants: an MDS-UPDRS III test was performed by experienced practitioners, open eye rs-fMRI was recorded for ten minutes using EPI, while taking maximum precautions to minimize head movement and recording the pulse rate with an MRI save pulsometer. Three healthy controls and two patients did not complete the measurement due to technical difficulties, falling asleep or claustrophobia. The datasets of five healthy controls, two patients and eight participants of the prodromal group had to be excluded due to excessive movement, flawed physiological data and flawed datasets. The remaining datasets went through the established preprocessing steps using SPM12. Particular care was taken to compensate for motion by analyzing the datasets with the motion finger print toolbox by Marco Wilke, and excluding data with STS displacement > 0.5 mm in more than 20% of the images. Two seed-based analyses were performed using the REST toolbox V.1.8., one analysis with the left putamen, the other one with the right putamen as seed region. Noise originating from the pulse curve and motion were regressed out of the resulting correlation maps. The correlation maps were fed into two one-way between subject ANOVAs over the whole brain and T-contrasts were used to detect any significant differences in correlation between the three groups. Age and gender were added as covariates of no interest. As the first analysis did not yield any significant results, we reviewed our recruitment process. We found out, that the assignment of the participants to the groups was based on the baseline assessment of the TREND study, which dated back as much as six years for most participants and the number of prodromal markers had changed in the course of the follow-up examinations. We reorganized the groups based on the number of prodromal markers present at the follow-up closest to our rs-fMRI assessment. Consequently, we had to exclude 25 participants of the

prodromal group. Thus, the datasets of 24 healthy controls, 20 PD patients and 22 participants in the prodromal group were included in a second analysis. From the resulting significant clusters, we extracted the mean correlation to determine the exact order of functional connectivity of our three groups in each cluster.

Throughout all identified clusters, functional connectivity was highest in the prodromal group when compared to patients and healthy controls. As we measured the patients in the ON-state, no significant differences to healthy controls were found. However, the mean correlation extracted from all clusters was always lowest in PD patients. The identified clusters were primarily located in brain regions which are involved in the planning and execution of motion. It is intriguing to suggest, that the brain increases synchronous activation of different brain regions to enable smooth planning and execution of motion, despite degenerative processes within the basal ganglia, in the sense of a compensatory mechanism present in our prodromal group.

Based on the reorganized groups, we did a third analysis where we further eliminated possible confounding factors. We excluded all left-handed participants and all PD patients with tremor-dominant subtype, including 20 healthy controls, 20 participants of the prodromal group and 16 patients. Interestingly, the grand scheme of identified brain regions as well as the hierarchy of functional connectivity did not change, as the identified brain regions were tasked with motion and functional connectivity was highest in the prodromal group. The results did reach a higher significance level. A paper with these results is submitted, the release is pending.

In conclusion, there is hope that one day non-invasive imaging techniques might contribute to clinical observations and other biomarkers to detect PD before its motor symptoms allow clinical diagnosis, albeit there is a long road ahead.

6. Own contribution

I was involved in the recruitment, the clinical assessment and the conduction of the MRI measurements. I contacted potential participants, informed them on the study, checked for in- and exclusion criteria and organized the date of assessment. I accompanied the participants during the day of assessment, conducted the KVIQ (Kinesthetic and Visual Imagery Questionnaire) and two different motor tasks (balancing on thin lines and aiming at a target with a laser fixed on a balance board), which were used for another study investigating motor imagery in PD patients. I was present at the scanner during measurements to lead the participants through the different tasks and collect the data. I had input on the chosen form of analysis and proposed the new classification of cohorts. I conducted the statistical analysis and configured the presentation of the results.

D. Berg provided professional advice on hypothesis and study design and helped with the interpretation of the results. M. Wilke and T. Ethofer gave advice and practical help for the analysis of the data. M. Hobert and T. Klos helped recruit and assess the participants invited to this study. The UPDRS III scores were evaluated by D. Berg, W. Maetzler, M. Hobert and E. Schaefer, all neurologists of the Neurodegenerative Department of the Center of Neurology, University Hospital Tuebingen. Rs-fMRI measurements were also monitored by M. Hobert, T. Klos and E. Charyasz. In the analysis, the doctoral candidate used scripts provided by M. Wilke (mw_reducemask, mw_mfp, mw_getcorr, mw_combmov) and M. Erb (me_retriocor). M. Wilke also aided with the development of a fitting brain mask. The results of the extracted mean z-scores were graphically illustrated in a grouped boxplot put together by P. Weber.

7. References

Abbott, R. D., Petrovitch, H., White, L. R., Masaki, K. H., Tanner, C. M., Curb, J. D., Grandinetti, a, Blanchette, P. L., Popper, J. S., & Ross, G. W. (2001). Frequency of bowel movements and the future risk of Parkinson's disease. *Neurology*, *57*(3), 456–462. https://doi.org/10.1212/WNL.58.5.838-a

Ahlskog, J. . (2000). Diagnosis and differential diagnosis of Parkinson's disease and parkinsonism. *Parkinsonism & Related Disorders*, *7*(1), 63–70. https://doi.org/10.1016/S1353-8020(00)00047-X

Amunts, K., Schlaug, G., Schleicher, a, Steinmetz, H., Dabringhaus, a, Roland, P. E., & Zilles, K. (1996). Asymmetry in the human motor cortex and handedness. *NeuroImage*, *4*(3 Pt 1), 216–222. https://doi.org/10.1006/nimg.1996.0073

Ashburner, J., & Friston, K. (2003). Rigid Body Registration and Interpolation. *Human Brain Function: Second Edition*, 635–653. https://doi.org/10.1016/B978-012264841-0/50034-2

Ashburner, J., & Friston, K. J. (2005). Unified segmentation. *NeuroImage*, *26*(3), 839–851. https://doi.org/10.1016/j.neuroimage.2005.02.018

Bagesteiro, L. B., Sarlegna, F. R., & Sainburg, R. L. (2006). Differential influence of vision and proprioception on control of movement distance. *Experimental Brain Research*, *171*(3), 358–370. https://doi.org/10.1007/s00221-005-0272-y

Bandettini, P. a. (2009). Functional MRI Limitations and Aspirations. *Neural Correlates of Thinking*, 15–39. https://doi.org/10.1007/978-3-540-68044-4_2

Baudrexel, S., Witte, T., Seifried, C., von Wegner, F., Beissner, F., Klein, J. C., Steinmetz, H., Deichmann, R., Roeper, J., & Hilker, R. (2011). Resting state fMRI reveals increased subthalamic nucleus-motor cortex connectivity in Parkinson's disease. *NeuroImage*, *55*(4), 1728–1738. https://doi.org/10.1016/j.neuroimage.2011.01.017

Berg, D., Postuma, R. B., Adler, C. H., Bloem, B. R., Chan, P., Dubois, B., Gasser, T., Goetz, C. G., Halliday, G., Joseph, L., Lang, A. E., Liepelt-Scarfone, I., Litvan, I., Marek, K., Obeso, J., Oertel, W., Olanow, C. W., Poewe, W., Stern, M., & Deuschl, G. (2015). MDS research criteria for prodromal Parkinson's disease. *Movement Disorders*, *30*(12), 1600–1611. https://doi.org/10.1002/mds.26431

Bezard, E., Gross, C. E., & Brotchie, J. M. (2003). Presymptomatic compensation in Parkinson's disease is not dopamine-mediated. *Trends in Neurosciences*, *26*(4), 215–221. https://doi.org/10.1016/S0166-2236(03)00038-9

Biswal, B., Yetkin, F. Z., Haughton, V. M., & Hyde, J. S. (1995). *Functional Connectivity in the Motor Cortex of Resting*. *9*, 537–541.

Bonavita, S., Sacco, R., Esposito, S., d'Ambrosio, A., Della Corte, M., Corbo, D., Docimo, R., Gallo, A., Lavorgna, L., Cirillo, M., Bisecco, A., Esposito, F., & Tedeschi, G. (2017). Default mode network changes in multiple sclerosis: a link between depression and cognitive impairment? *European Journal of Neurology*, *24*(1), 27–36. https://doi.org/10.1111/ene.13112

Boubela, R. N., Kalcher, K., Huf, W., Seidel, E.-M., Derntl, B., Pezawas, L., Našel, C., & Moser, E. (2015). fMRI measurements of amygdala activation are confounded by stimulus correlated signal fluctuation in nearby veins draining distant brain regions. *Scientific Reports*, *June 2014*, 1–15. https://doi.org/10.1038/srep10499

Brett, M., Anton, J.-L., Valabregue, R., & Poline, J.-B. (2002). Region of Interest Analysis Using an SPM Toolbox [Abstract]. *Neuroimage*, *16*.

Buhmann, C., Glauche, V., Sturenburg, H. J., Oechsner, M., Weiller, C., & Buchel, C. (2003). Pharmacologically modulated fMRI--cortical responsiveness to levodopa in drug-naive hemiparkinsonian patients. *Brain : A Journal of Neurology*, *126*(Pt 2), 451–461.

Camp, C. (1913). Paralysis Agitans, multiple sclerosis and their treatment. *Modern Treatment of Nervous and Mental Disease*, *2*, 651–667.

Choe, I.-H., Yeo, S., Chung, K.-C., Kim, S.-H., & Lim, S. (2013). Decreased and increased cerebral regional homogeneity in early Parkinson's disease. *Brain Research*, *1527*, 230–237. https://doi.org/10.1016/j.brainres.2013.06.027

Collignon, A., Maes, F., Delaere, D., Vandermeulen, D., Suetens, P., & Marchal, G. (1995). Automated Multi-Modality Image Registration Based on Information Theory. *Lect Notes Comput Sci*, *3*.

Dayan, E., & Browner, N. (2017). Alterations in striato-thalamo-pallidal intrinsic functional connectivity as a prodrome of Parkinson's disease. *NeuroImage: Clinical*, *16*(July), 313–318. https://doi.org/10.1016/j.nicl.2017.08.003

de Lau, L. M. L., & Breteler, M. M. B. (2006). Epidemiology of Parkinson's disease. *The Lancet. Neurology*, *5*(6), 525–535. https://doi.org/10.1016/S1474-4422(06)70471-9

De Lau, L. M. L., Koudstaal, P. J., Hofman, A., & Breteler, M. M. B. (2006). Subjective complaints precede Parkinson disease: The Rotterdam study. *Archives of Neurology*, *63*(3), 362–365. https://doi.org/10.1001/archneur.63.3.noc50312

Delaveau, P., Salgado-Pineda, P., Fossati, P., Witjas, T., Azulay, J. P., & Blin, O. (2010). Dopaminergic modulation of the default mode network in Parkinson's disease. *European Neuropsychopharmacology*, *20*(11), 784–792. https://doi.org/10.1016/j.euroneuro.2010.07.001

Eggert, K., Oertel, W., & Reichmann, H. (2012). S2 Leitlinie Parkinson-Syndrom - Diagnostik und Therapie. *Deutesche Gesellschaft Für Neurologie*, 1–48. https://doi.org/10.1007/978-3-540-48351-9_1

Ellmore, T. M., Castriotta, R. J., Hendley, K. L., Aalbers, B. M., Furr-Stimming, E., Hood, A. J., Suescun, J., Beurlot, M. R., Hendley, R. T., & Schiess, M. C. (2013). Altered nigrostriatal and nigrocortical functional connectivity in rapid eye movement sleep behavior disorder. *Sleep*, *36*(12), 1885–1892. https://doi.org/10.5665/sleep.3222

Engel, S. A., Glover, G. H., & Wandell, B. A. (1997). Retinotopic organization in human visual cortex and the spatial precision of functional MRI. *Cerebral Cortex (New York, N.Y. : 1991)*, *7*(2), 181–192.

Esposito, F., Tessitore, A., Giordano, A., De Micco, R., Paccone, A., Conforti, R., Pignataro, G., Annunziato, L., & Tedeschi, G. (2013). Rhythm-specific modulation of the sensorimotor network in drug-na??ve patients with

Parkinson's disease by levodopa. *Brain*, *136*(3), 710–725. https://doi.org/10.1093/brain/awt007
Faro, Scott H.; Mohamed, F. B. (2006). *Functional MRI*. Springer.
Fearnley, J. M., & Lees, a J. (1991). Ageing and Parkinson's disease: substantia nigra regional selectivity. *Brain : A Journal of Neurology*, *114 (Pt 5*, 2283–2301. https://doi.org/10.1093/brain/114.5.2283
Fox, M. D., & Raichle, M. E. (2007). Spontaneous fluctuations in brain activity observed with functional magnetic resonance imaging. *Nat Rev Neurosci*, *8*(9), 700–711. https://doi.org/nrn2201 [pii]\n10.1038/nrn2201
Fox, P. T., & Raichle, M. E. (1986). Focal physiological uncoupling of cerebral blood flow and oxidative metabolism during somatosensory stimulation in human subjects. *Proceedings of the National Academy of Sciences of the United States of America*, *83*(4), 1140–1144. https://doi.org/10.1073/pnas.83.4.1140
Friston, K. J. (2011). Functional and Effective Connectivity: A Review. *Brain Connectivity*, *1*(1), 13–36. https://doi.org/10.1089/brain.2011.0008
Friston, K. J., Williams, S., Howard, R., Frackowiak, R. S. J., & Turner, R. (1996). Movement-related effects in fMRI time-series. *Magnetic Resonance in Medicine*, *35*(3), 346–355. https://doi.org/10.1002/mrm.1910350312
Gaenslen, A., Wurster, I., Brockmann, K., Huber, H., Godau, J., Faust, B., Lerche, S., Eschweiler, G. W., Maetzler, W., & Berg, D. (2014). Prodromal features for Parkinson's disease - baseline data from the TREND study. *European Journal of Neurology*, *21*(5), 766–772. https://doi.org/10.1111/ene.12382
Gaenslen, Alexandra, Swid, I., Liepelt-Scarfone, I., Godau, J., & Berg, D. (2011). The patients' perception of prodromal symptoms before the initial diagnosis of Parkinson's disease. *Movement Disorders*, *26*(4), 653–658. https://doi.org/10.1002/mds.23499
Galluzzi, S., Beltramello, A., Filippi, M., & Frisoni, G. B. (2008). Aging. *Neurological Sciences*, *29*(S3), 296–300. https://doi.org/10.1007/s10072-008-1002-6
Gibb, W. R., & Lees, a J. (1988). The relevance of the Lewy body to the pathogenesis of idiopathic Parkinson's disease. *Journal of Neurology, Neurosurgery, and Psychiatry*, *51*(6), 745–752. https://doi.org/10.1136/jnnp.51.6.745
Glover, G. H., Li, T. Q., & Ress, D. (2000). Image-based method for retrospective correction of physiological motion effects in fMRI: RETROICOR. *Magnetic Resonance in Medicine*, *44*(1), 162–167. https://doi.org/10.1002/1522-2594(200007)44:1<162::AID-MRM23>3.0.CO;2-E
Goedert, M., & Spillantini, M. G. (2012). 100 years of Lewy pathology. *Nature Reviews Neurology*, *9*(1), 13–24. https://doi.org/10.1038/nrneurol.2012.242
Grieder, M., Wang, D. J. J., Dierks, T., Wahlund, L.-O., & Jann, K. (2018). Default Mode Network Complexity and Cognitive Decline in Mild Alzheimer's Disease. *Frontiers in Neuroscience*, *12*(October), 1–9. https://doi.org/10.3389/fnins.2018.00770
Hacker, C. D., Perlmutter, J. S., Criswell, S. R., Ances, B. M., & Snyder, A. Z. (2012). Resting state functional connectivity of the striatum in Parkinson's

disease. *Brain*, *135*(12), 3699–3711. https://doi.org/10.1093/brain/aws281
Hammers, A., Allom, R., Koepp, M. J., Free, S. L., Myers, R., Lemieux, L., Mitchell, T. N., Brooks, D. J., & Duncan, J. S. (2003). Three-dimensional maximum probability atlas of the human brain, with particular reference to the temporal lobe. *Human Brain Mapping*, *19*(4), 224–247. https://doi.org/10.1002/hbm.10123
Hammond, G. (2002). Correlates of human handedness in primary motor cortex: A review and hypothesis. *Neuroscience and Biobehavioral Reviews*, *26*(3), 285–292. https://doi.org/10.1016/S0149-7634(02)00003-9
Haslinger, B., Erhard, P., Kampfe, N., Boecker, H., Rummeny, E., Schwaiger, M., Conrad, B., & Ceballos-Baumann, A. O. (2001). Event-related functional magnetic resonance imaging in Parkinson's disease before and after levodopa. *Brain : A Journal of Neurology*, *124*(Pt 3), 558–570.
Helmich, R. C., Derikx, L. C., Bakker, M., Scheeringa, R., Bloem, B. R., & Toni, I. (2010). Spatial remapping of cortico-striatal connectivity in parkinson's disease. *Cerebral Cortex*, *20*(5), 1175–1186. https://doi.org/10.1093/cercor/bhp178
Helmich, R. C., Thaler, A., Van Nuenen, B. F. L., Gurevich, T., Mirelman, A., Marder, K. S., Bressman, S., Orr-Urtreger, A., Giladi, N., Bloem, B. R., & Toni, I. (2015). Reorganization of corticostriatal circuits in healthy G2019S LRRK2 carriers. *Neurology*, *84*(4), 399–406. https://doi.org/10.1212/WNL.0000000000001189
Hughes, A. J., Daniel, S. E., Kilford, L., & Lees, A. J. (1992). *Accuracy of clinical diagnosis of idiopathic Parkinson ' s disease : a clinico-pathological study of 100 cases*. 181–184. https://doi.org/10.1136/jnnp.55.3.181
Ishihara, L., & Brayne, C. (2006). A systematic review of depression and mental illness preceding Parkinson's disease. *Acta Neurologica Scandinavica*, *113*(4), 211–220. https://doi.org/10.1111/j.1600-0404.2006.00579.x
Jezzard, P., & Balaban, R. S. (1995). *Correction for Geometric Distortion in Echo Planar Images from B , Field Variations*. 65–73.
Jiang, T., He, Y., Zang, Y., & Weng, X. (2004). *Modulation of Functional Connectivity During the Resting State and the Motor Task*. *1*. https://doi.org/10.1002/hbm.20012
Kasper, L., Bollmann, S., Diaconescu, A. O., Hutton, C., Heinzle, J., Iglesias, S., Hauser, T. U., Sebold, M., Manjaly, Z. M., Pruessmann, K. P., & Stephan, K. E. (2017). The PhysIO Toolbox for Modeling Physiological Noise in fMRI Data. *Journal of Neuroscience Methods*, *276*, 56–72. https://doi.org/10.1016/j.jneumeth.2016.10.019
Kish, S. J., Shannak, K., & Hornykiewicz, O. (1988). Uneven Pattern of Dopamine Loss in the Striatum of Patients with Idiopathic Parkinson's Disease. *New England Journal of Medicine*, *318*(14), 876–880. https://doi.org/10.1056/NEJM198804073181402
Krajcovicova, L., Mikl, M., Marecek, R., & Rektorova, I. (2012). The default mode network integrity in patients with Parkinson's disease is levodopa equivalent dose-dependent. *Journal of Neural Transmission*, *119*(4), 443–454. https://doi.org/10.1007/s00702-011-0723-5
Kwak, Y., Peltier, S., Bohnen, N. I., Müller, M. L. T. M., Dayalu, P., & Seidler, R. D. (2010). Altered resting state cortico-striatal connectivity in mild to

moderate stage Parkinson's disease. *Frontiers in Systems Neuroscience*, *4*(September), 143. https://doi.org/10.3389/fnsys.2010.00143
Lemieux, L., Salek-Haddadi, A., Lund, T. E., Laufs, H., & Carmichael, D. (2007). Modelling large motion events in fMRI studies of patients with epilepsy. *Magnetic Resonance Imaging*, *25*(6), 894–901. https://doi.org/10.1016/j.mri.2007.03.009
Lemon, R. N. (2008). Descending Pathways in Motor Control. *Annual Review of Neuroscience*, *31*(1), 195–218. https://doi.org/10.1146/annurev.neuro.31.060407.125547
Liu, H., Kale Edmiston, E., Fan, G., Xu, K., Zhao, B., Shang, X., & Wang, F. (2013). Altered resting-state functional connectivity of the dentate nucleus in Parkinson's disease. *Psychiatry Research - Neuroimaging*, *211*(1), 64–71. https://doi.org/10.1016/j.pscychresns.2012.10.007
Logothetis, N. K., Pauls, J., Augath, M., Trinath, T., & Oeltermann, A. (2001). *Neurophysiological investigation of the basis of the fMRI signal*.
Luo, C., Song, W., Chen, Q., Zheng, Z., Chen, K., Cao, B., Yang, J., Li, J., Huang, X., Gong, Q., & Shang, H. F. (2014). Reduced functional connectivity in early-stage drug-naive Parkinson's disease: A resting-state fMRI study. *Neurobiology of Aging*, *35*(2), 431–441. https://doi.org/10.1016/j.neurobiolaging.2013.08.018
Maetzler, W., & Hausdorff, J. M. (2012). Motor signs in the prodromal phase of Parkinson's disease. *Movement Disorders*, *27*(5), 627–633. https://doi.org/10.1002/mds.24973
Maetzler, W., Mancini, M., Liepelt-Scarfone, I., Müller, K., Becker, C., van Lummel, R. C., Ainsworth, E., Hobert, M., Streffer, J., Berg, D., & Chiari, L. (2012). Impaired Trunk Stability in Individuals at High Risk for Parkinson's Disease. *PLoS ONE*, *7*(3), e32240. https://doi.org/10.1371/journal.pone.0032240
Manto, M., Bower, J. M., Gerwig, M., & Neuropsychology, I. (2015). Cerebellarfuncandcognition. *Pmc*, *11*(2), 457–487. https://doi.org/10.1007/s12311-011-0331-9.Consensus
Marek, K., & Jennings, D. (2009). Can we image premotor Parkinson disease? [Article]. *Neurology Premotor Parkinson Disease*, *72*(7), S21–S26. https://doi.org/10.1212/WNL.0b013e318198df97
Müller, B., Larsen, J. P., Wentzel-Larsen, T., Skeie, G. O., & Tysnes, O.-B. (2011). Autonomic and sensory symptoms and signs in incident, untreated Parkinson's disease: Frequent but mild. *Movement Disorders*, *26*(1), 65–72. https://doi.org/10.1002/mds.23387
Nachev, P., Kennard, C., & Husain, M. (2008). Functional role of the supplementary and pre-supplementary motor areas. *Nature Reviews Neuroscience*, *9*(11), 856–869. https://doi.org/10.1038/nrn2478
Ogawa, S., Lee, T. M., Kay, a R., & Tank, D. W. (1990). Brain magnetic resonance imaging with contrast dependent on blood oxygenation. In *Proceedings of the National Academy of Sciences of the United States of America* (Vol. 87, Issue 24, pp. 9868–9872). https://doi.org/10.1073/pnas.87.24.9868
Pakkenberg, B., Møller, a, Gundersen, H. J., Mouritzen Dam, a, & Pakkenberg, H. (1991). The absolute number of nerve cells in substantia

nigra in normal subjects and in patients with Parkinson's disease estimated with an unbiased stereological method. *Journal of Neurology, Neurosurgery, and Psychiatry*, *54*(1), 30–33. https://doi.org/10.1136/jnnp.54.1.30

Palmer, S. J., Eigenraam, L., Hoque, T., McCaig, R. G., Troiano, A., & McKeown, M. J. (2009). Levodopa-sensitive, dynamic changes in effective connectivity during simultaneous movements in Parkinson's disease. *Neuroscience*, *158*(2), 693–704. https://doi.org/http://dx.doi.org/10.1016/j.neuroscience.2008.06.053

Parkinson, J. (2002). An essay on the shaking palsy. 1817. *The Journal of Neuropsychiatry and Clinical Neurosciences*, *14*(2), 223–236; discussion 222. https://doi.org/10.1176/jnp.14.2.223

Pauling, L. (1935). The Oxygen Equilibrium of Hemoglobin and Its Structural Interpretation. *Proceedings of the National Academy of Sciences of the United States of America*, *21*(4), 186–191. https://doi.org/10.1073/pnas.21.4.186

Penny, W., Friston, K., Ashburner, J., Kiebel, S., & Nichols, T. (2006). *Statistical Parametric Mapping: The Analysis of Functional Brain Images*. Elsevier.

Pool, E. M., Rehme, A. K., Eickhoff, S. B., Fink, G. R., & Grefkes, C. (2015). Functional resting-state connectivity of the human motor network: Differences between right- and left-handers. *NeuroImage*, *109*, 298–306. https://doi.org/10.1016/j.neuroimage.2015.01.034

Pool, E. M., Rehme, A. K., Fink, G. R., Eickhoff, S. B., & Grefkes, C. (2014). Handedness and effective connectivity of the motor system. *NeuroImage*, *99*, 451–460. https://doi.org/10.1016/j.neuroimage.2014.05.048

Postuma, R. B., Gagnon, J. F., Vendette, M., Fantini, M. L., Massicotte-Marquez, J., & Montplaisir, J. (2009). Quantifying the risk of neurodegenerative disease in idiopathic REM sleep behavior disorder. *Neurology*, *72*, 1296–1300. https://doi.org/10.1212/WNL.0b013e3181a52fbe

Postuma, R. B., Lang, a. E., Gagnon, J. F., Pelletier, a., & Montplaisir, J. Y. (2012). How does parkinsonism start? Prodromal parkinsonism motor changes in idiopathic REM sleep behaviour disorder. *Brain*, *135*(6), 1860–1870. https://doi.org/10.1093/brain/aws093

Postuma, Ronald B., & Berg, D. (2016). Advances in markers of prodromal Parkinson disease. *Nature Reviews Neurology*, *12*(11), 622–634. https://doi.org/10.1038/nrneurol.2016.152

Postuma, Ronald B., Berg, D., Stern, M., Poewe, W., Olanow, C. W., Oertel, W., Obeso, J., Marek, K., Litvan, I., Lang, A. E., Halliday, G., Goetz, C. G., Gasser, T., Dubois, B., Chan, P., Bloem, B. R., Adler, C. H., & Deuschl, G. (2015). MDS clinical diagnostic criteria for Parkinson's disease. *Movement Disorders*, *30*(12), 1591–1601. https://doi.org/10.1002/mds.26424

Postuma, Ronald B, Gagnon, J.-F., Bertrand, J.-A., Génier Marchand, D., & Montplaisir, J. Y. (2015). Parkinson risk in idiopathic REM sleep behavior disorder. *Neurology*, *84*(11), 1104 LP – 1113. http://n.neurology.org/content/84/11/1104.abstract

Power, J. D., Barnes, K. a., Snyder, A. Z., Schlaggar, B. L., & Petersen, S. E. (2012). Spurious but systematic correlations in functional connectivity MRI

networks arise from subject motion. *NeuroImage*, *59*(3), 2142–2154. https://doi.org/10.1016/j.neuroimage.2011.10.018
Pringsheim, T., Jette, N., Frolkis, A., & Steeves, T. D. L. (2014). The prevalence of Parkinson's disease: A systematic review and meta-analysis. *Movement Disorders*, *29*(13), 1583–1590. https://doi.org/10.1002/mds.25945
Prodoehl, J., Burciu, R. G., & Vaillancourt, D. E. (2014). Resting state functional magnetic resonance imaging in Parkinson's disease. *Current Neurology and Neuroscience Reports*, *14*(6), 448. https://doi.org/10.1007/s11910-014-0448-6
Proske, U., & Gandevia, S. C. (2012). The proprioceptive senses: Their roles in signaling body shape, body position and movement, and muscle force. *Physiological Reviews*, *92*(4), 1651–1697. https://doi.org/10.1152/physrev.00048.2011
Rolinski, M., Griffanti, L., Piccini, P., Roussakis, A. A., Szewczyk-Krolikowski, K., Menke, R. A., Quinnell, T., Zaiwalla, Z., Klein, J. C., Mackay, C. E., & Hu, M. T. M. (2016). *Basal ganglia dysfunction in idiopathic REM sleep behaviour disorder parallels that in early Parkinson's disease*. 2224–2234. https://doi.org/10.1093/brain/aww124
Rosazza, C., & Minati, L. (2011). Resting-state brain networks: Literature review and clinical applications. *Neurological Sciences*, *32*(5), 773–785. https://doi.org/10.1007/s10072-011-0636-y
Ross, G. W., Abbott, R. D., Petrovitch, H., Tanner, C. M., & White, L. R. (2012). Pre-motor features of Parkinson's disease: the Honolulu-Asia Aging Study experience. *Parkinsonism & Related Disorders*, *18*, S199–S202. https://doi.org/10.1016/S1353-8020(11)70062-1
Roy, C. S., & Sherrington, C. S. (1890). On the Regulation of the Blood-supply of the Brain. *The Journal of Physiology*, *11*(1–2), 85-158.17. https://doi.org/10.1152/japplphysiol.00257.2010
Sala-Llonch, R., Bartrés-Faz, D., & Junqué, C. (2015). Reorganization of brain networks in aging: a review of functional connectivity studies. *Frontiers in Psychology*, *6*(May), 1–11. https://doi.org/10.3389/fpsyg.2015.00663
Sarlegna, R. F., & Sainburg, L. R. (2009). The Roles of Vision and Proprioception in the Planning of Reaching Movements. *Adv Exp Med Biol.*, *585*, 317–335. https://doi.org/10.1007/978-0-387-77064-2
Schenck, C. H., Bundlie, S. R., Ettinger, M. G., & Mahowald, M. W. (1986). Chronic behavioral disorders of human REM sleep: a new category of parasomnia. *Sleep*, *9*(2), 293–308.
Schild, H. H. (1990). *MRI made easy*. Schering AG Berlin/Bergkamen.
Sharman, M., Valabregue, R., Perlbarg, V., Marrakchi-Kacem, L., Vidailhet, M., Benali, H., Brice, A., & Lehéricy, S. (2013). Parkinson's disease patients show reduced cortical-subcortical sensorimotor connectivity. *Movement Disorders*, *28*(4), 447–454. https://doi.org/10.1002/mds.25255
Siderowf, A., Jennings, D., Eberly, S., Oakes, D., Hawkins, K. a., Ascherio, A., Stern, M. B., & Marek, K. (2012). Impaired olfaction and other prodromal features in the Parkinson At-Risk Syndrome study. *Movement Disorders*, *27*(3), 406–412. https://doi.org/10.1002/mds.24892
Singleton, A. B., Farrer, M. J., & Bonifati, V. (2013). The genetics of Parkinson's disease: progress and therapeutic implications. *Movement Disorders :*

Official Journal of the Movement Disorder Society, *28*(1), 14–23. https://doi.org/10.1002/mds.25249
Song, X.-W., Dong, Z.-Y., Long, X.-Y., Li, S.-F., Zuo, X.-N., Zhu, C.-Z., He, Y., Yan, C.-G., & Zang, Y.-F. (2011). REST: A Toolkit for Resting-State Functional Magnetic Resonance Imaging Data Processing. *PLoS ONE*, *6*(9), e25031. https://doi.org/10.1371/journal.pone.0025031
Szewczyk-Krolikowski, K., Menke, R. a L., Rolinski, M., Duff, E., Salimi-Khorshidi, G., Filippini, N., Zamboni, G., Hu, M. T. M., & Mackay, C. E. (2014). Functional connectivity in the basal ganglia network differentiates PD patients from controls. *Neurology*, *83*(3), 208–214. https://doi.org/10.1212/WNL.0000000000000592
Tessitore, A., Amboni, M., Esposito, F., Russo, A., Picillo, M., Marcuccio, L., Pellecchia, M. T., Vitale, C., Cirillo, M., Tedeschi, G., & Barone, P. (2012). Resting-state brain connectivity in patients with Parkinson's disease and freezing of gait. *Parkinsonism & Related Disorders*, *18*(6), 781–787. https://doi.org/10.1016/j.parkreldis.2012.03.018
Tessitore, A., Esposito, F., Vitale, C., Santangelo, G., Amboni, M., Russo, A., Corbo, D., Cirillo, G., Barone, P., & Tedeschi, G. (2013). Default-mode network connectivity in cognitively unimpaired patients with Parkinson disease. *Neurology*, *81*(23), e172-5. https://doi.org/10.1212/01.wnl.0000436943.62904.09
Tolosa, E., Wenning, G., & Poewe, W. (2006). The diagnosis of Parkinson's disease. *Lancet Neurology*, *5*(1), 75–86. https://doi.org/10.1016/S1474-4422(05)70285-4
Trepel, M. (2008). Neuroanatomie, Struktur und Funktion. In *Neuroanatomie, Struktur und Funktion* (pp. 220–230). Elsevier.
Tzourio-Mazoyer, N., Landeau, B., Papathanassiou, D., Crivello, F., Etard, O., Delcroix, N., Mazoyer, B., & Joliot, M. (2002). Automated anatomical labeling of activations in SPM using a macroscopic anatomical parcellation of the MNI MRI single-subject brain. *NeuroImage*, *15*(1), 273–289. https://doi.org/10.1006/nimg.2001.0978
Wilke, M. (2012). An alternative approach towards assessing and accounting for individual motion in fMRI timeseries. *NeuroImage*, *59*(3), 2062–2072. https://doi.org/10.1016/j.neuroimage.2011.10.043
Wu, T., Long, X., Wang, L., Hallett, M., Zang, Y., Li, K., & Chan, P. (2011). Functional connectivity of cortical motor areas in the resting state in Parkinson's disease. *Human Brain Mapping*, *32*(9), 1443–1457. https://doi.org/10.1002/hbm.21118
Wu, T., Wang, L., Chen, Y., Zhao, C., Li, K., & Chan, P. (2009). Changes of functional connectivity of the motor network in the resting state in Parkinson's disease. *Neuroscience Letters*, *460*(1), 6–10. https://doi.org/10.1016/j.neulet.2009.05.046
Yang, H., Zhou, X. J., Zhang, M.-M., Zheng, X.-N., Zhao, Y.-L., & Wang, J. (2013). Changes in spontaneous brain activity in early Parkinson's disease. *Neuroscience Letters*, *549*, 24–28. https://doi.org/10.1016/j.neulet.2013.05.080
Yu, R., Liu, B., Wang, L., Chen, J., & Liu, X. (2013). Enhanced Functional Connectivity between Putamen and Supplementary Motor Area in

Parkinson's Disease Patients. *PLoS ONE*, *8*(3). https://doi.org/10.1371/journal.pone.0059717

Zhang, J., Wei, L., Hu, X., Xie, B., Zhang, Y., Wu, G.-R., & Wang, J. (2015). Akinetic-rigid and tremor-dominant Parkinson's disease patients show different patterns of intrinsic brain activity. *Parkinsonism & Related Disorders*, *21*(1), 23–30. https://doi.org/10.1016/j.parkreldis.2014.10.017

8. Appendix

8.1 Fact sheet sent to participants

Universitätsklinikum Tübingen
Hertie-Institut für Klinische Hirnforschung
Hoppe-Seyler-Str. 3
72076 Tübingen
Ansprechpartner: Markus Hobert, Prof. Dr. D. Berg, PD Dr. T. Ethofer, Prof. Dr. W. Maetzler
Tel.: 07071/2983621
markus.hobert@med.uni-tuebingen.de

Allgemeines Informationsblatt für Teilnehmer/innen der Studie:

Pathophysiologische Aspekte von Gang und Gleichgewicht bei Personen mit erhöhtem Risiko für eine Parkinson-Erkrankung: eine fMRT-Studie

Sehr geehrte/r Interessent/in an dieser Studie,
Sie sind Teilnehmer/in der TREND-Studie (Longitudinalstudie zur Früherkennung von Neurodegeneration), oder aber leiden an einer Parkinsonerkrankung. Sie wurden angesprochen bzw. angeschrieben, ob Sie an der hier beschriebenen Studie teilnehmen wollen. Nachfolgend werden die Ziele, der Ablauf und die einzelnen Untersuchungen der Studie dargestellt, und welche möglichen Risiken und Nebenwirkungen die Untersuchungen aufweisen.

Hintergrund
Die Parkinsonerkrankung ist eine der häufigsten neurologischen Erkrankungen, deren Häufigkeit ab dem 50. Lebensjahr stark zunimmt. Es besteht jedoch berechtigte Hoffnung, dass bald Medikamente zum Einsatz kommen könnten, die evtl. das Potential haben die Krankheit zu verlangsamen oder das Auftreten zu verhindern. Dafür ist es aber wichtig, diejenigen Personen zu finden, die ein deutlich erhöhtes Erkrankungsrisiko aufweisen. In diese Studie werden daher Probanden eingeschlossen, die Risikofaktoren (Riechstörung, Depression, REM-Schlafstörung) für die Parkinsonkrankheit haben *und* sich in den letzten Jahren in der Bewegungsmessung im Rahmen der TREND-Studie verändert haben. Außerdem werden Probanden eingeschlossen bei denen diese Veränderungen nicht vorliegen, sowie Patienten die bereits an einer Parkinsonerkrankung leiden. Diese letzten beiden Gruppen stellen die Kontrollgruppen dar.

Ziel der Studie
Diese Studie hat das Ziel, die Steuerung von Bewegungen wie Gehen und Gleichgewicht bei Risikopersonen für die Parkinsonerkrankung besser zu verstehen. Dies wird im Prinzip nicht „live", sondern während der Vorstellung von einer Gang- bzw. Gleichgewichtsübung („Imagination") in liegender Position mittels funktioneller Kernspintomographie (fMRT) gemessen, Insgesamt werden 120 Personen in die Studie eingeschlossen.

Ablauf im Überblick
Diese Studie wird in Kooperation mit der Radboud Universitätsklinik Nijmegen durchgeführt, welche das identische Studienprotokoll bereits anwendet, und damit Parkinsonpatienten und Kontrollpersonen untersucht. Alle Untersuchungen der hier vorgestellten Studie finden in

Tübingen statt. Die gesamte Untersuchungsdauer beträgt ca. 6 Stunden und wird an zwei aufeinanderfolgenden Tagen stattfinden. Es ist auch möglich die ganze Untersuchung an einem Tag durchzuführen. Die Untersuchungen von Tag 1 werden dann am Vormittag, die Untersuchungen von Tag 2 am Nachmittag durchgeführt. Die gesamte Untersuchung läuft folgendermaßen ab:

Kontaktaufnahme, Aufklärung und Einwilligung (A oder B):

A) Nach Erhalt eines Briefes, und den für die Studie erforderlichen Aufklärungstexten und Einwilligungserklärungen können Sie bei Interesse entweder bei uns anrufen (Markus Hobert oder Vertretung, Tel 07071/2983621), oder wir werden sie etwa 2 Wochen nach Verschicken der Unterlagen telefonisch kontaktieren. Wir werden zu Beginn des Telefonats natürlich fragen, ob Sie für ein Gespräch bereit sind Wenn Sie zum Gespräch einwilligen, werden wir ein standardisiertes Interview mit Ihnen durchführen und damit prüfen ob Sie die Ein- oder Ausschlusskriterien der Studie erfüllen. Dies werden wir dokumentieren und in einem Ordner bis zum Ende der Studie aufbewahren. Der Ordner ist nur der Studienleitung zugänglich. Falls Sie nach Prüfung der Ein- und Ausschlusskriterien prinzipiell für die Studie geeignet sind und Sie weiterhin Interesse haben, werden wir Ihnen den Ablauf der Studie auch mündlich ausführlich darlegen, und Ihre Fragen beantworten. Wenn Sie nicht teilnehmen wollen oder Bedenkzeit benötigen, können Sie dies jederzeit während des Gesprächs äußern.

Dauer: 30-40 Minuten

B) Sie werden im Rahmen eines Besuches in unserer Klinik (auf der Station, oder in der Ambulanz der Neurologischen Abteilung mit Schwerpunkt Neurodegenerative Erkrankungen) über die Möglichkeit informiert, an der Studie teilzunehmen. Es werden Ihnen bei Interesse und ausreichender Bedenkzeit die Aufklärungstexte und Einwilligungserklärungen ausgehändigt. Nach weiterer ausreichender Bedenkzeit erfolgt die mündliche Vorstellung der Studie, und die Prüfung der Ein- und Ausschlusskriterien. Dies kann auch in mehreren Kontakten durchgeführt werden.

(Dauer ca. 30-40 Minuten)

Studienablauf im engeren Sinn

Tag 1 (oder Vormittag):

1. **Einverständniserklärung (Dauer ca. 10min)**

- Aushändigen der Informationsunterlagen und der schriftlichen Einwilligung (in doppelter Ausführung, eine ist für Ihre Unterlagen)

(Dauer ca. 10min)

2. **Klinische Untersuchung (Dauer ca. 4 Stunden)**

- Befragung durch den/die Untersucher/in
  Erhebung der Krankengeschichte inkl. möglicher Gründe, die gegen die Kernspinuntersuchung sprechen, und der aktuellen Medikamenteneinnahme.

(Dauer ca. 35min)

- Klinisch-neurologische Untersuchung
  Semiquantitative Testung auf allgemeine neurologische und auf Parkinson-typische Symptome: UPDRS (Unified Parkinson Disease Rating Scale; Parkinson-spezifische klinische Testung die auf Vorhandensein und ggfs. Ausmaß von Steifigkeit, Zittern, Gangqualität, Gleichgewicht untersucht; Fragen nach Problemen beim Verrichten alltäglicher Dinge, Überbewegungen, etc.)

(Dauer ca. 15min)

- Fragebogen zur „Vorstellungskraft für Bewegung“
  KVIQ (The Kinesthetic and Visual Imagery Questionnaire, Deutsche Version). Dies ist ein Fragebogen zur Abschätzung des Vorstellungsvermögen von Bewegungsabläufen.

(Dauer ca. 20min)

- Durchführen der Gleichgewichtsaufgabe
  Sie werden gebeten auf einer Matte zu stehen, die einen halbkreisförmigen Boden hat und daher nach vorne und hinten kippen kann (siehe Bild). An dieser Matte ist vorne ein Laserpointer befestigt. Durch vorsichtiges Vor- und Zurücklehnen Ihres Körpers können Sie die Auslenkung des Laserstrahls steuern. Auf diese Weise sollen Sie auf vorgegebene Ziele zeigen (auf dem Bild z.B. auf den schwarzen, und dann auf den grauen Punkt). Der Test wird mehrmals mit kleinen Änderungen, z.B. veränderter Größe der Punkte, durchgeführt

(Dauer ca. 60min)

- Durchführung der Gangaufgabe
  Sie werden gebeten auf einem Weg, der auf dem Fußboden markiert ist, zu gehen ohne die Fläche daneben zu betreten. Der Gangtest wird mehrmals mit kleinen Änderungen, z.B. Veränderung der Breite und der Länge des Weges, durchgeführt.

(Dauer ca. 30min)

- Üben der Vorstellungsaufgaben
  Wir erklären Ihnen den Ablauf der Vorstellungsaufgaben und leiten Sie an, sich die zuvor praktisch durchgeführten Aufgaben sowie die Kontrollaufgaben vorzustellen. Sollten Sie dabei Schwierigkeiten haben, bekommen Sie von uns dazu Hilfestellung.
  Bei der Vorstellung der Gleichgewichtsaufgabe, sollen Sie sich vorstellen, dass Sie auf der Matte mit dem befestigten Laserpointer stehen und durch Vor- und Zurücklehnen den Laserstrahl steuern (siehe Bild 1). Zusätzlich wird es eine Kontrollbedingung geben, bei der Sie sich vorstellen sollen, dass sich der Laserstrahl ohne Ihr Zutun bewegt. Bei der Vorstellung der Gangaufgabe, sollen Sie sich vostellen auf einem Weg zu gehen, der auf dem Fußboden markiert ist. Bei der Kontrollbedingung sollen Sie sich vorstellen, dass sich ein Gegenstand ohne Ihr Zutun auf dem Weg bewegt (siehe Bild 2).

(Dauer ca. 30min)

- Durchführen der Vorstellungsaufgaben unter Versuchsbedingungen
  Um Sie an die Durchführung der Vorstellungsaufgaben im Kernspintomographen einfacher hinzuführen, bitten wir Sie, die zuvor geübten Aufgaben unter Versuchsbedingungen, aber außerhalb des Kernspintomographen durchzuführen. Dabei liegen Sie in einem Raum auf einer Liege und führen die Vorstellungsaufgaben genauso durch, wie Sie es später in der „richtigen“ Kernspintomographie machen werden. Wir kontrollieren Ihre „Vorstellungskraft“ mittels Zeitmesssung.

(Dauer ca. 40min)

Tag 2 (oder Nachmittag):

3. **Funktionelle Kernspintomographie (Dauer ca. 2 Stunden, dafür erhalten Sie einen gesonderten Aufklärungs- und Einwilligungsbogen)**

- Erneute Durchführung der Vorstellungsaufgaben
  Wir zeigen Ihnen vor der Durchführung der Kernspintomographie nochmal den Aufbau der Gleichgewichts- und Gangaufgabe und bitten Sie, die Aufgaben nochmal durchführen. Damit können Sie sich wieder gut daran erinnern und sich die Aufgaben gut vorstellen. Anschließend würden wir Sie auch bitten die Vorstellungsaufgaben nochmal durchzuführen.

  (Dauer ca. 30min)
- Vorbereitung der Kernspintomographie
  Anbringen der Elektroden zur Überwachung (EKG zur Kontrolle der Herzfrequenz, EMG zur Kontrolle der Muskelaktivität)

  (Dauer ca. 15min)
- Funktionelle Kernspintomographie (fMRT)
  Wir bitten Sie den separaten Informationsbogen zur funktionellen Kernspintomographie durchzulesen. Dieser erklärt die technische Durchführung der Untersuchung. Zusätzlich bitten wir Sie nun, die im Vorfeld eingeübten Vorstellungsaufgaben während der Kernspinuntersuchung erneut durchzuführen.

  (Dauer ca. 60-70min)

Risken und Nebenwirkungen
Alle geplanten Untersuchungen sind nicht invasiv, was eine schädigende Wirkung praktisch ausschließt, insbesondere werden keine Medikamente verabreicht oder belastende risikoreiche Eingriffe vorgenommen.

Weitergehende Aufklärung
Die Studienverantwortlichen und/oder Ihr behandelnder Arzt sind jederzeit bereit, alle die Untersuchung betreffenden Fragen im Detail zu erläutern. Bitte machen Sie davon Gebrauch, wenn Sie noch Fragen haben sollten.
Zufallsbefunde welche im Rahmen der Untersuchung auftreten und für Sie gesundheitsrelevant sind oder sein könnten, werden Ihnen umgehend mitgeteilt, und erste Schritte in der weiterführenden Abklärung oder Therapie in die Wege geleitet.
Sollte es bei der Kernspintompgraphie Zufallsbefunde geben, wird dies mit Ihnen unter Hinzuziehung eines Neuroradiologen besprochen. Falls Sie nicht über mögliche Zufallsbefunde informiert werden wollen, können wir Sie leider nicht in diese Studie einschließen.
Die Teilnahme an dieser Untersuchung ist vollkommen freiwillig.
Sie haben jederzeit das Recht, die Einwilligung zur Teilnahme an dieser Untersuchung ohne Angaben von Gründen zu verweigern oder zurückzuziehen, ohne dass Ihr Verhältnis zum behandelnden Arzt oder Ihre weitere Behandlung in irgendeiner Weise davon berührt wird. Die Studie ist rein wissenschaftlich angelegt. Es entsteht Ihnen daher weder direkter therapeutischer Nutzen noch erwachsen Ihnen durch die Studienteilnahme irgendwelche Nachteile.

Information zum Datenschutz

Alle im Rahmen der Studie anfallenden Daten von Ihnen werden vertraulich behandelt. Eine Weitergabe von persönlichen Daten an Dritte findet nicht statt. Die studienbedingt erhobenen Daten werden passwortgeschützt auf dem Computer (digitale Daten, Kernspindaten) oder im Arbeitszimmer von Markus Hobert (Ebene 1.2 der Kinderklinik, Tübingen; gesicherter Zugang

durch selbstschliessende Flurtür und abgeschlossene Bürotür) bzw. dessen Vertreter für die Dauer von 30 Jahren aufbewahrt. Zugang zu den Daten haben alle Personen die mit der Auswertung der Daten beauftragt sind (daher Mitarbeiter der Teams um Frau Prof. Berg, PD Dr. Ethofer, Prof. Maetzler und an der Etablierung und Durchführung beteiligte Mitarbeiter der Radboud Universitätsklinik Nijmegen, Niederlande). Alle unterliegen der Schweigepflicht.
Da die Studie nur diagnostische, nicht aber direkt therapeutische Relevanz hat, ist nicht vorgesehen, dass Sie über die Ergebnisse informiert werden.
Es ist möglich, dass die Ergebnisse der Untersuchung in einer komprimierten Form in einer Fachzeitschrift veröffentlicht werden. In diesem Fall ist es keinesfalls möglich, auf Ihre Person rückzuschließen.
Die Datenbank und die Codenummern werden getrennt aufbewahrt. Wenn Sie die Einwilligung zur Teilnahme an dieser Untersuchung zurückziehen, werden sowohl der Eintrag in der Datenbank gelöscht.

Versicherung

Es besteht eine Haftpflichtversicherung des Klinikums, die für den Fall, dass es einmal wider Erwarten zu fahrlässig verursachte Schäden in der Studie kommt, aufkommen wird. Es wurde keine Wegeunfallversicherung abgeschlossen.

Die Ethikkommission der Universität Tübingen hat diese Studie beraten.

Einwilligung zur Studie:

Pathophysiologische Aspekte von Gang und Gleichgewicht bei Personen mit erhöhtem Risiko für eine Parkinson-Erkrankung: eine fMRT-Studie

Name des/der Teilnehmers/in:_____

Ich erkläre mich bereit, an der oben genannten Studie teilzunehmen.

Ich bin durch _____

in verständlicher und ausreichender Form über Wesen, Bedeutung, Tragweite und Risiken meiner Studienteilnahme ausführlich und in mir verständlicher Form aufgeklärt worden. Ich hatte ausreichend Zeit, meine Studienteilnahme anhand des Informationsschreibens zu überdenken und ich hatte ausreichend Gelegenheit, zusätzliche Fragen zu stellen.

Ich willige in die Durchführung der im Informationsblatt genannten Untersuchungen (Telefonische Befragung, Eignungsuntersuchung, Erhebung der Krankengeschichte, Neurologische Untersuchung mittels Parkinson-spezifischer Skalen, Fragebögen, Bewegungsaufgaben, Vorstellungsaufgaben, funktionelle Kernspintomographie (siehe auch separaten Aufklärungsbogen) mit Durchführung der Vorstellungsaufgaben) ein.

Erklärung zum Datenschutz: Ich erkläre mich damit einverstanden, dass im Rahmen dieser Studie erhobene Daten / Krankheitsdaten auf Fragebögen und elektronischen Datenträgern aufgezeichnet und ohne Namensnennung weitergegeben werden. Außerdem erkläre ich mich damit einverstanden, dass die im Rahmen dieser Studie erhobenen Daten wissenschaftlich ausgewertet werden und evtl., ohne Namensnennung, veröffentlicht werden. Ich bin darüber informiert, dass die Teilnahme an der Studie vollkommen freiwillig ist und dass ich mein Einverständnis jederzeit formlos und ohne Angabe von Gründen widerrufen kann. Aus einem Abbruch der Studie wird mir kein Nachteil entstehen. Ich kann jederzeit meine Daten beim Studienleiter einsehen.

_____ _____

(Ort/Datum) Unterschrift Proband(in)

_____ _____

(Ort/Datum) Unterschrift Arzt/Ärztin

8.2 Written informed consent for functional MRI measurement

Pathophysiologische Aspekte von Gang und Gleichgewicht bei Personen mit erhöhtem Risiko für eine Parkinson-Erkrankung: eine fMRT-Studie

Allgemeine Aufklärung zur Magnetresonanztomographie

Universitätsklinikum Tübingen
Abteilung Neurodegenerative Erkrankungen und Hertie-Institut für Klinische Hirnforschung
Abteilung Biomedizinische Magnetresonanz
Department für Radiologie Tübingen

Information zur funktionellen Kernspintomographie

Diese Untersuchung wird mittels **funktioneller Kernspintomographie** durchgeführt. Die Kernspintomographie verwendet **keine Röntgenstrahlen, Kontrastmittel oder radioaktive Stoffe**, sondern ein kurzzeitig aufgebautes Magnetfeld, das uns in ähnlicher Form auch im Alltag permanent umgibt. Wie man im Alltag, z.B. Rundfunk- und Radiowellen nicht spürt, so sind auch das Magnetfeld und die vom Körper abgegebenen Echosignale nicht wahrnehmbar.
Das kurzzeitig von Ihrem Körper zurückgesendete Signal wird von empfindlichen Spulen aufgefangen und in einem leistungsfähigen Computer in ein Bild umgerechnet (siehe rechts). Da das Echosignal aus Ihrem Körper außerordentlich gering ist, wird es von empfindlichen Spulen aufgefangen, die sehr groß sind und im Tomographen Ihren ganzen Körper umgeben. Deshalb wird die Untersuchung auch in einem speziellen Raum durchgeführt, der von äußeren Störeinflüssen abgeschirmt ist. Bei der Untersuchung liegen Sie auf einer beweglichen Liege, die sich langsam in die ca. ein Meter große Öffnung des Gerätes bewegt. Die während den Messungen auftretenden lauten Klopfgeräusche sind auf Schaltungen im Kernspintomographen zurückzuführen und brauchen Sie nicht zu beunruhigen.

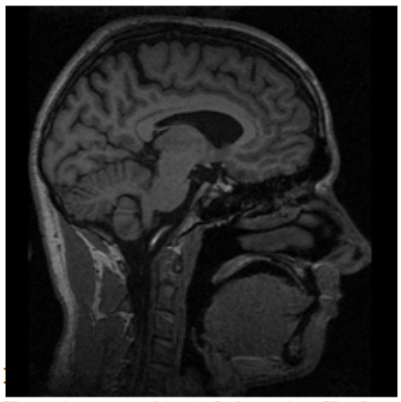

Kernspintomographie-Aufnahme eines Kopfes. Anatomisches Bild, sagittale Schichtführung

Da diese Situation nicht alltäglich ist, können zu Beginn der Untersuchung Engegefühle auftreten, die ganz normal sind und erfahrungsgemäß nach wenigen Sekunden bis Minuten abklingen. Sie erhalten außerdem einen Gummiball, mit dem Sie im Überwachungsraum ein Notsignal auslösen können. Darüber hinaus besteht die Möglichkeit zum Gesprächskontakt über Lautsprecher und Mikrophon.

Ist Kernspintomographie gefährlich?

Die Kernspintomographie ist ein modernes Untersuchungsverfahren, das weltweit in vielen Krankenhäusern eingesetzt wird. Bei sachgemäßer Durchführung sind von diesem etablierten Untersuchungsverfahren mit sehr hoher Wahrscheinlichkeit **keine gesundheitlichen Gefahren oder Risiken** zu erwarten. Die sachgemäße Durchführung der Untersuchung wird durch einen speziell ausgebildeten Arzt gewährleistet. Erfahrungsgemäß scheint das Engegefühl im Tomographen, das allerdings relativ rasch abklingt, für einige Menschen am unangenehmsten zu sein. Die Messgeräusche können theoretisch zu vorübergehenden Ohrgeräuschen (Tinnitus) führen. Es wird jedoch ein spezielles Kopfhörersystem verwendet, um mögliche Lärmbelästigungen zu minimieren. Während der Messung können in seltenen Fällen Muskel- und Nervenerregungen auftreten, die eventuell unangenehm, aber harmlos sind.
Im Untersuchungsraum herrscht während der Messung ein Magnetfeld. Metallteile können, wenn sie in das Magnetfeld kommen, Unfälle verursachen - einfache Zahnplomben sind allerdings ohne Belang. Bitte legen Sie deshalb vor Betreten des Untersuchungsraumes alle Metallgegenstände ab. Außerdem müssen wir prüfen, ob sich irgendwelche Metallteile an oder in Ihrem Körper befinden oder andere Gegenanzeigen

bestehen, die eine Kernspinuntersuchung bei Ihnen nicht zulassen. Lesen Sie deshalb die folgenden Hinweise aufmerksam durch und beantworten Sie die Fragen sorgfältig.

Bitte beantworten Sie diese Fragen in Anwesenheit und Rücksprache mit dem zuständigen Arzt vor Durchführung der Untersuchung:

Ist jemals durch einen Unfall oder eine Verletzung Metall in Ihren Körper gekommen?
(zum Beispiel durch eine Schussverletzung, durch Granatsplitter oder durch einen Berufsunfall)

○ **Nein** ○ **Ja**

Befinden sich seit einer Operation Metallteile oder Prothesen in Ihrem Körper?
(zum Beispiel ein Herzschrittmacher, künstliche Herzklappen, Gefäße oder Katheter, oder orthopädische oder chirurgische Metallteile wie künstliche Gelenke, Platten, Nägel, Drähte oder Klammern, Zahnplomben sind ohne Belang)

○ **Nein** ○ **Ja**

Hatten Sie je eine Operation am Kopf oder am Herzen?

○ **Nein** ○ **Ja**

Leiden Sie an einer chronischen Krankheit?
(zum Beispiel Bluthochdruck, Nierenerkrankung, Lungenerkrankung, Herzerkrankung)

○ **Nein** ○ **Ja**

Haben Sie in letzter Zeit wegen eines körperlichen Problems einen Arzt aufgesucht?

○ **Nein** ○ **Ja**

Nehmen Sie zur Zeit Medikamente?

○ **Nein** ○ **Ja**

Leiden Sie unter Platzangst?

○ **Nein** ○ **Ja**

Bei Frauen: Könnten Sie schwanger sein?

○ **Nein** ○ **Ja**

Sind Sie tätowiert oder gepierct? Verwenden Sie metallhaltige Kosmetik (Lidschatten)?
(Metallhaltige Tätowierungen oder Kosmetik können zu Wärmeempfindungen bis hin zu Verbrennungen führen!)

○ **Nein** ○ **Ja**

Zufallsbefunde:

Die im Rahmen der Studie angefertigten Kernspin-Aufnahmen werden im Regelfall nicht durch einen klinischen Neuroradiologen befundet. Auch sind die verwendeten Sequenzen für eine klinische Diagnostik nur sehr eingeschränkt zu verwenden.
Dennoch werden in **extrem seltenen** Fällen an klinisch gesunden Probanden während einer Kernspinuntersuchung klinisch relevante und gegebenenfalls behandlungsbedürftige Befunde (z.B. krankhafte Gefäßerweiterung, Gewebsentzündung, Gewebsneubildung) erhoben. Im Hinblick auf den aktuellen Stand der ethischen Diskussion ist es damit erforderlich, vor Beginn der Untersuchung gewisse Informationen von dem/der Probanden/Probandin einzuholen, die es erlauben dessen/deren Autonomie zu wahren, ohne die ärztliche Fürsorgepflicht zu verletzen. Beantworten sie deshalb die folgenden Fragen:

Sollte im Rahmen der folgenden Untersuchung ein Zufallsbefund auftreten, so möchte ich darüber in Kenntnis gesetzt werden.

○ **Nein** ○ **Ja**

Im Fall eines Zufallsbefundes, wünsche ich die weitere Abklärung durch einen Neuroradiologen.

○ **Nein** ○ **Ja**

Aktuell befinde ich mich in einem Verfahren, das mich zu Auskünften über meinen Gesundheitszustand verpflichtet.
(z.B. Abschluss einer privaten Krankenversicherung oder Lebensversicherung)

○ **Nein** ○ **Ja**

(Sollten sie diese Frage mit ja beantworten, wird Ihnen der aufklärende Arzt die Bedeutung dieses Sachverhalts näher erläutern. Bei Verneinung ist die Frage für die folgende Untersuchung irrelevant.)

Metallteile müssen abgelegt werden!

Metallteile können, wenn sie in das Magnetfeld kommen, Unfälle verursachen.
Bitte helfen Sie Unfälle zu vermeiden!

Legen Sie deshalb bitte vor Betreten des Untersuchungsraumes die folgenden Gegenstände ab:

- Uhr, Brille, Hörgerät
- Scheckkarten und andere Karten mit Magnetstreifen
- Metallteile an der Kleidung (z.B. Gürtelschnallen, BH-Bügel, Metallknöpfe)
- Geldmünzen, Kleingeld, Kugelschreiber, Schlüssel und andere Metallteile in den Taschen
- Schmuck (Ringe, Halsketten, Ohrringe etc.)
- Taschenmesser, Sicherheitsnadeln, Geldbörse, Haarklammern und -nadeln, Büroklammern
- evtl. vorhandene Prothesen soweit möglich (z.B. Zahnersatz), auch Haarteile u. -klammern
- sonstige Gegenstände aus Metall, die Sie bei sich tragen

Bitte kontrollieren Sie noch mal ***alle*** Taschen (auch die Gesäßtaschen der Hose) und vergewissern Sie sich, daß Sie **keine metallischen Gegenstände** mehr bei sich haben, bevor Sie den Untersuchungsraum betreten.

Sie können die abgelegten Sachen vor dem Untersuchungsraum in Schließfächern deponieren. Ein Raum zum Umziehen ist ebenfalls vorhanden. Brille, Schließfachschlüssel und Schuhe können im Untersuchungsraum abgelegt werden.

Einverständniserklärung

Ich bestätige hiermit, daß ich den Aufklärungsbogen gründlich gelesen und alle Fragen gewissenhaft beantwortet habe. Ich wurde von _____ über den Untersuchungshergang und die Durchführung der Kernspintomographie informiert. Ich hatte ausreichend Gelegenheit alle in diesem Zusammenhang aufgetretenen Fragen zu stellen. Ich habe momentan keine weiteren Fragen und bin mit der Durchführung der funktionellen Kernspintomographie-Untersuchung einverstanden.

Tübingen,_____ _____
Ort, Datum Unterschrift des Probanden

Bei der Überprüfung der Ein- und Ausschlußkriterien ergab sich kein Ausschlußgrund für die Durchführung der kernspintomographischen Untersuchung

_____ _____
Datum Unterschrift des Arzt

Patient name TREND_7216_LE **Date of birth 01/01/43** **Patient ID TREND_7216_LE**
Study description MPI Standard Ethofer **Study date 07/10/13**

Series No	Series Description	Series Date and Time	Instances	Work Status	Protocol Name
1	localizer	07/10/13 15:30:09	3	/com/ / /E/ /	localizer
2	MPRAGE GRAPPA2	07/10/13 15:36:58	176	/com/ / /E/ /	MPRAGE GRAPPA2
3	gre_field_mapping	07/10/13 15:39:02	72	/com/ / /E/ /	gre_field_mapping
4	gre_field_mapping	07/10/13 15:39:02	36	/com/ / /E/ /	gre_field_mapping
5	ep2d_bold_rest	07/10/13 15:47:57	179	/com/ / /E/ /	ep2d_bold_rest
6	ep2d_bold_rest_1	07/10/13 15:55:18	300	/com/ / /E/ /	ep2d_bold_rest_1
7	ep2d_bold_fMRI_BVI	07/10/13 16:09:29	240	/com/ / /E/ /	ep2d_bold_fMRI_BVI
8	ep2d_bold_fMRI_BMI	07/10/13 16:21:57	240	/com/ / /E/ /	ep2d_bold_fMRI_BMI
9	ep2d_bold_fMRI_GVI	07/10/13 16:32:38	240	/com/ / /E/ /	ep2d_bold_fMRI_GVI
10	ep2d_bold_fMRI_GMI	07/10/13 16:43:29	240	/com/ / /E/ /	ep2d_bold_fMRI_GMI
11	ep2d_diff_mddw_30_p2	07/10/13 16:55:18	72	/com/ / /E/ /	ep2d_diff_mddw_30_p2
12	ep2d_diff_mddw_30_p2_ADC	07/10/13 17:00:25	50	/com/ / /E/ /	ep2d_diff_mddw_30_p2
13	ep2d_diff_mddw_30_p2_TRACEW	07/10/13 17:00:25	50	/com/ / /E/ /	ep2d_diff_mddw_30_p2
14	ep2d_diff_mddw_30_p2_FA	07/10/13 17:00:25	50	/com/ / /E/ /	ep2d_diff_mddw_30_p2
15	ep2d_diff_mddw_30_p2_ColFA	07/10/13 17:00:25	50	/com/ / /E/ /	ep2d_diff_mddw_30_p2
16	ep2d_diff_mddw_30_p2_TENSOR	07/10/13 17:00:26	1	/com/ / /E/ /	ep2d_diff_mddw_30_p2

SIEMENS MAGNETOM Prisma_fit syngo MR D13D

\\USER\MPI Standard\Ethofer\TREND\ep2d_diff_mddw_30_p2

TA:7:32 PAT:2 Voxel size:1.7×1.7×2.0 mm Rel. SNR:1.00 :epse

Mosaic	On
Tensor	On
Distortion Corr.	Off
b-Value >=	0 s/mm²
Exponential ADC Maps	Off
Invert Gray Scale	Off
Calculated Image	Off

SIEMENS MAGNETOM Prisma_fit syngo MR D13D

\\USER\MPI Standard\Ethofer\TREND\ep2d_diff_mddw_30_p2

TA:7:32 PAT:2 Voxel size:1.7×1.7×2.0 mm Rel. SNR:1.00 :epse

Eigenschaften	
Prio Recon	Off
Load to viewer	On
Inline movie	Off
Auto store images	On
Load to stamp segments	Off
Load images to graphic segments	Off
Auto open inline display	Off
Wait for user to start	Off
Start measurements	single
Routine	
Nr. of slice groups	1
Slices	50
Dist. factor	25 %
Position	Isocenter
Orientation	Transversal
Phase enc. dir.	A >> P
AutoAlign	---
Phase oversampling	0 %
FoV read	220 mm
FoV phase	100,0 %
Slice thickness	2,0 mm
TR	6000 ms
TE	69,0 ms
Concatenations	1
Filter	None
Coil elements	HE1-4
Kontrast	
MTC	Off
Magn. preparation	None
Fat suppr.	Fat sat.
Fat sat. mode	Strong
Averaging mode	Long term
Measurements	1
Delay in TR	0 ms
Reconstruction	Magnitude
Multiple series	Off
Auflösung	
Base resolution	128
Phase resolution	100 %
Phase partial Fourier	6/8
Interpolation	Off
PAT mode	GRAPPA
Accel. factor PE	2
Ref. lines PE	38
Reference scan mode	Separate
Distortion Corr.	Off
Prescan Normalize	Off
Raw filter	Off
Elliptical filter	Off
Dynamic Field Corr.	Off
Geometrie	
Nr. of slice groups	1
Slices	50
Dist. factor	25 %
Position	Isocenter
Phase enc. dir.	A >> P
Phase oversampling	0 %
Multi-slice mode	Interleaved
Series	Interleaved
Nr. of sat. regions	0
Position mode	L-P-H
Fat suppr.	Fat sat.
Special sat.	None
Fat sat. mode	Strong
Special sat.	None
Table position	P
System	
Body	Off
HE1	On
HE3	On
NE1	Off
HE2	On
HE4	On
NE2	Off
Position mode	L-P-H
Positioning mode	REF
Table position	H
Table position	0 mm
MSMA	S - C - T
Sagittal	R >> L
Coronal	A >> P
Transversal	F >> H
Coil Combine Mode	Adaptive Combine
AutoAlign	---
Coil Select Mode	Off - AutoCoilSelect
B0 Shim mode	Standard
Adjust with body coil	Off
Confirm freq. adjustment	Off
Assume Dominant Fat	Off
Assume Silicone	Off
Adjustment Tolerance	Auto
? Ref. amplitude 1H	0,000 V
Position	Isocenter
Rotation	0,00 deg
R >> L	220 mm
A >> P	220 mm
F >> H	125 mm
Frequency 1H	123,255892 MHz
Correction factor	1
AddCSaCSatNS 1H	65,325 V
Gain	High
Table position	0 mm
Img. Scale. Cor.	1,000
Physio	
1st Signal/Mode	None
Magn. preparation	None
Resp. control	Off
Inline	
Distortion correction	Off
Sequenz	
Introduction	On
Averaging mode	Long term
Multi-slice mode	Interleaved
Bandwidth	1954 Hz/Px
Optimization	None
Free echo spacing	Off
Echo spacing	0,6 ms
EPI factor	128
RF pulse type	Normal
Gradient mode	Performance
Excitation	Standard
TX/RX delta frequency	0 Hz
TX Nucleus	None
TX delta frequency	0 Hz
Coil elements	HE1-4
Acquisition duration	0 ms
BOLD	
Delay in TR	0 ms
Diffusion mode	MDDW
Diff. weightings	2
b-value 1	0 s/mm²
Diff. weighted images	On
Trace weighted images	On
ADC maps	On
FA maps	On

SIEMENS MAGNETOM Prisma_fit syngo MR D13D

\\USER\MPI Standard\Ethofer\TREND\ep2d_bold_fMRI

TA:10:05 PAT:Off Voxel size:3.0×3.0×3.2 mm Rel. SNR:1.00 :epfid

Eigenschaften	
Prio Recon	Off
Load to viewer	On
Inline movie	Off
Auto store images	On
Load to stamp segments	Off
Load images to graphic segments	Off
Auto open inline display	Off
Wait for user to start	On
Start measurements	single
Routine	
Nr. of slice groups	1
Slices	36
Dist. factor	25 %
Position	R1.2 A13.6 F0.6 mm
Orientation	Transversal
Phase enc. dir.	A >> P
AutoAlign	---
Phase oversampling	0 %
FoV read	192 mm
FoV phase	100,0 %
Slice thickness	3,2 mm
TR	2500 ms
TE	35,0 ms
Averages	1
Concatenations	1
Filter	Prescan Normalize
Coil elements	HE1-4
Kontrast	
MTC	Off
Flip angle	90 deg
Fat suppr.	Fat sat.
Averaging mode	Long term
Measurements	240
Delay in TR	0 ms
Reconstruction	Magnitude
Multiple series	Off
Auflösung	
Base resolution	64
Phase resolution	100 %
Phase partial Fourier	Off
Interpolation	Off
PAT mode	None
Distortion Corr.	Off
Hamming	Off
Prescan Normalize	On
Raw filter	Off
Elliptical filter	Off
Geometrie	
Nr. of slice groups	1
Slices	36
Dist. factor	25 %
Position	R1.2 A13.6 F0.6 mm
Phase enc. dir.	A >> P
Phase oversampling	0 %
Multi-slice mode	Interleaved
Series	Ascending
Nr. of sat. regions	0
Position mode	L-P-H
Fat suppr.	Fat sat.
Special sat.	None
Special sat.	None
Table position	P
System	
Body	Off
HE1	On
HE3	On
NE1	Off
HE2	On
HE4	On
NE2	Off
Position mode	L-P-H
Positioning mode	REF
Table position	H
Table position	0 mm
MSMA	S - C - T
Sagittal	R >> L
Coronal	A >> P
Transversal	F >> H
Coil Combine Mode	Sum of Squares
AutoAlign	---
Coil Select Mode	Default
B0 Shim mode	Standard
Adjust with body coil	Off
Confirm freq. adjustment	Off
Assume Dominant Fat	Off
Assume Silicone	Off
Adjustment Tolerance	Auto
? Ref. amplitude 1H	0,000 V
Position	R1.2 A13.6 F0.6 mm
Rotation	0,00 deg
R >> L	192 mm
A >> P	192 mm
F >> H	144 mm
Frequency 1H	123,255892 MHz
Correction factor	1
SincRFPulse 1H	269,076 V
Gain	High
Table position	0 mm
Img. Scale. Cor.	1,000
Physio	
1st Signal/Mode	None
Inline	
Distortion correction	Off
Sequenz	
Introduction	Off
Averaging mode	Long term
Multi-slice mode	Interleaved
Bandwidth	2232 Hz/Px
Free echo spacing	Off
Echo spacing	0,51 ms
EPI factor	64
RF pulse type	Normal
Gradient mode	Fast
Excitation	Standard
TX/RX delta frequency	0 Hz
TX Nucleus	None
TX delta frequency	0 Hz
Coil elements	HE1-4
Acquisition duration	0 ms
BOLD	
GLM Statistics	Off
Dynamic t-maps	On
Ignore meas. at start	0
Ignore after transition	0
Model transition states	On
Temp. highpass filter	On
Threshold	4,00
Paradigm size	20
Motion correction	Off
Spatial filter	Off
Delay in TR	0 ms
Distortion Corr.	Off

SIEMENS MAGNETOM Prisma_fit syngo MR D13D

\\USER\MPI Standard\Ethofer\TREND\ep2d_bold_rest

TA:10:06 PAT:2 Voxel size:3.0×3.0×3.2 mm Rel. SNR:1.00 :epfid

Eigenschaften	
Prio Recon	Off
Load to viewer	On
Inline movie	Off
Auto store images	On
Load to stamp segments	Off
Load images to graphic segments	Off
Auto open inline display	Off
Wait for user to start	On
Start measurements	single
Routine	
Nr. of slice groups	1
Slices	36
Dist. factor	25 %
Position	R1.2 A13.6 F0.6 mm
Orientation	Transversal
Phase enc. dir.	A >> P
AutoAlign	---
Phase oversampling	0 %
FoV read	192 mm
FoV phase	100,0 %
Slice thickness	3,2 mm
TR	2000 ms
TE	31,0 ms
Averages	1
Concatenations	1
Filter	Prescan Normalize
Coil elements	HE1-4
Kontrast	
MTC	Off
Flip angle	90 deg
Fat suppr.	Fat sat.
Averaging mode	Long term
Measurements	300
Delay in TR	0 ms
Reconstruction	Magnitude
Multiple series	Off
Auflösung	
Base resolution	64
Phase resolution	100 %
Phase partial Fourier	Off
Interpolation	Off
PAT mode	GRAPPA
Accel. factor PE	2
Ref. lines PE	32
Reference scan mode	Separate
Distortion Corr.	Off
Hamming	Off
Prescan Normalize	On
Raw filter	Off
Elliptical filter	Off
Geometrie	
Nr. of slice groups	1
Slices	36
Dist. factor	25 %
Position	R1.2 A13.6 F0.6 mm
Phase enc. dir.	A >> P
Phase oversampling	0 %
Multi-slice mode	Interleaved
Series	Ascending
Nr. of sat. regions	0
Position mode	L-P-H
Fat suppr.	Fat sat.
Special sat.	None
Special sat.	None
Table position	P
System	
Body	Off
HE1	On
HE3	On
NE1	Off
HE2	On
HE4	On
NE2	Off
Position mode	L-P-H
Positioning mode	REF
Table position	H
Table position	0 mm
MSMA	S - C - T
Sagittal	R >> L
Coronal	A >> P
Transversal	F >> H
Coil Combine Mode	Sum of Squares
AutoAlign	---
Coil Select Mode	Default
B0 Shim mode	Standard
Adjust with body coil	Off
Confirm freq. adjustment	Off
Assume Dominant Fat	Off
Assume Silicone	Off
Adjustment Tolerance	Auto
? Ref. amplitude 1H	0,000 V
Position	R1.2 A13.6 F0.6 mm
Rotation	0,00 deg
R >> L	192 mm
A >> P	192 mm
F >> H	144 mm
Frequency 1H	123,255892 MHz
Correction factor	1
SincRFPulse 1H	269,076 V
Gain	High
Table position	0 mm
Img. Scale. Cor.	1,000
Physio	
1st Signal/Mode	None
Inline	
Distortion correction	Off
Sequenz	
Introduction	Off
Averaging mode	Long term
Multi-slice mode	Interleaved
Bandwidth	2232 Hz/Px
Free echo spacing	Off
Echo spacing	0,53 ms
EPI factor	64
RF pulse type	Normal
Gradient mode	Fast
Excitation	Standard
TX/RX delta frequency	0 Hz
TX Nucleus	None
TX delta frequency	0 Hz
Coil elements	HE1-4
Acquisition duration	0 ms
BOLD	
GLM Statistics	Off
Dynamic t-maps	On
Ignore meas. at start	0
Ignore after transition	0
Model transition states	On
Temp. highpass filter	On
Threshold	4,00
Paradigm size	20
Motion correction	Off
Spatial filter	Off
Delay in TR	0 ms
Distortion Corr.	Off

SIEMENS MAGNETOM Prisma_fit syngo MR D13D

\\USER\MPI Standard\Ethofer\TREND\gre_field_mapping

TA:0:54 Voxel size:3.0×3.0×3.2 mm Rel. SNR:1.00 :fm_r

Eigenschaften	
Prio Recon	Off
Load to viewer	On
Inline movie	Off
Auto store images	On
Load to stamp segments	Off
Load images to graphic segments	Off
Auto open inline display	Off
Wait for user to start	Off
Start measurements	single
Routine	
Nr. of slice groups	1
Slices	36
Dist. factor	25 %
Position	Isocenter
Orientation	Transversal
Phase enc. dir.	R >> L
AutoAlign	---
Phase oversampling	0 %
FoV read	192 mm
FoV phase	100,0 %
Slice thickness	3,2 mm
TR	400,0 ms
TE 1	4,92 ms
Averages	1
Concatenations	1
Filter	None
Coil elements	HE1-4
Kontrast	
MTC	Off
Flip angle	60 deg
Fat suppr.	None
Averaging mode	Long term
Measurements	1
Reconstruction	Magn./Phase
Multiple series	Off
Auflösung	
Base resolution	64
Phase resolution	100 %
Phase partial Fourier	Off
Interpolation	Off
Image Filter	Off
Distortion Corr.	Off
Prescan Normalize	Off
Normalize	Off
B1 filter	Off
Raw filter	Off
Elliptical filter	Off
Geometrie	
Nr. of slice groups	1
Slices	36
Dist. factor	25 %
Position	Isocenter
Phase enc. dir.	R >> L
Phase oversampling	0 %
Multi-slice mode	Interleaved
Series	Interleaved
Nr. of sat. regions	0
Position mode	L-P-H
Fat suppr.	None
Special sat.	None
Special sat.	None
Table position	P
System	
Body	Off
HE1	On
HE3	On
NE1	Off
HE2	On
HE4	On
NE2	Off
Position mode	L-P-H
Positioning mode	REF
Table position	H
Table position	0 mm
MSMA	S - C - T
Sagittal	R >> L
Coronal	A >> P
Transversal	F >> H
Save uncombined	Off
Coil Combine Mode	Sum of Squares
AutoAlign	---
Coil Select Mode	Off - AutoCoilSelect
B0 Shim mode	Standard
Adjust with body coil	Off
Confirm freq. adjustment	Off
Assume Dominant Fat	Off
Assume Silicone	Off
Adjustment Tolerance	Auto
? Ref. amplitude 1H	0,000 V
Position	Isocenter
Rotation	90,00 deg
A >> P	192 mm
R >> L	192 mm
F >> H	144 mm
Frequency 1H	123,255892 MHz
Correction factor	1
01GreFCE 1H	126,052 V
Gain	High
Table position	0 mm
Img. Scale. Cor.	1,000
Physio	
Inline	
Distortion correction	Off
Sequenz	
Introduction	On
Dimension	2D
Averaging mode	Long term
Multi-slice mode	Interleaved
Asymmetric echo	Off
Contrasts	2
Bandwidth	290 Hz/Px
Flow comp.	Yes
RF pulse type	Normal
Gradient mode	Fast
RF spoiling	On
TX/RX delta frequency	0 Hz
TX Nucleus	None
TX delta frequency	0 Hz
Coil elements	HE1-4
Acquisition duration	0 ms
Mode	Off
BOLD	
Distortion Corr.	Off
Contrasts	2

SIEMENS MAGNETOM Prisma_fit syngo MR D13D

\\USER\MPI Standard\Ethofer\TREND\MPRAGE GRAPPA2

TA:5:30 PAT:2 Voxel size:1.0×1.0×1.0 mm Rel. SNR:1.00 :tfl

Eigenschaften	
Prio Recon	Off
Load to viewer	On
Inline movie	Off
Auto store images	On
Load to stamp segments	Off
Load images to graphic segments	Off
Auto open inline display	Off
Wait for user to start	Off
Start measurements	single
Routine	
Nr. of slab groups	1
Slabs	1
Dist. factor	50 %
Position	Isocenter
Orientation	Sagittal
Phase enc. dir.	A >> P
AutoAlign	Head > Basis
Phase oversampling	0 %
Slice oversampling	0,0 %
FoV read	256 mm
FoV phase	100,0 %
Slice thickness	1,00 mm
TR	2300,0 ms
TE	4,18 ms
Averages	1
Concatenations	1
Filter	Normalize
Coil elements	HE1-4
Kontrast	
Magn. preparation	Non-sel. IR
TI	900 ms
Flip angle	9 deg
Fat suppr.	None
Water suppr.	None
Averaging mode	Long term
Measurements	1
Reconstruction	Magnitude
Multiple series	Off
Auflösung	
Base resolution	256
Phase resolution	100 %
Phase partial Fourier	Off
Interpolation	Off
PAT mode	GRAPPA
Accel. factor PE	2
Ref. lines PE	32
Reference scan mode	Integrated
Image Filter	Off
Distortion Corr.	Off
Accel. factor 3D	1
Prescan Normalize	Off
Normalize	On
B1 filter	Off
Raw filter	Off
Elliptical filter	Off
Slice resolution	100 %
Slice partial Fourier	Off
Geometrie	
Nr. of slab groups	1
Slabs	1
Dist. factor	50 %
Position	Isocenter
Phase enc. dir.	A >> P
Phase oversampling	0 %
Slice oversampling	0,0 %
Slices per slab	176
Multi-slice mode	Single shot
Series	Interleaved
Nr. of sat. regions	0
Position mode	L-P-H
Fat suppr.	None
Water suppr.	None
Special sat.	None
Table position	P
System	
Body	Off
HE1	On
HE3	On
NE1	Off
HE2	On
HE4	On
NE2	Off
Position mode	L-P-H
Positioning mode	REF
Table position	H
Table position	0 mm
MSMA	S - C - T
Sagittal	R >> L
Coronal	A >> P
Transversal	F >> H
Save uncombined	Off
Coil Combine Mode	Adaptive Combine
AutoAlign	Head > Basis
Coil Select Mode	Off - AutoCoilSelect
B0 Shim mode	Standard
Adjust with body coil	Off
Confirm freq. adjustment	Off
Assume Dominant Fat	Off
Assume Silicone	Off
Adjustment Tolerance	Auto
? Ref. amplitude 1H	0,000 V
Position	Isocenter
Rotation	0,00 deg
F >> H	256 mm
A >> P	256 mm
R >> L	176 mm
Frequency 1H	123,255892 MHz
Correction factor	1
SLoopIRns1 1H	397,009 V
Gain	Low
Table position	0 mm
Img. Scale. Cor.	1,000
Physio	
1st Signal/Mode	None
Magn. preparation	Non-sel. IR
TI	900 ms
Dark blood	Off
Resp. control	Off
Inline	
Distortion correction	Off
Sequenz	
Introduction	On
Dimension	3D
Elliptical scanning	Off
Averaging mode	Long term
Multi-slice mode	Single shot
Reordering	Linear
Asymmetric echo	Off
Bandwidth	150 Hz/Px
Flow comp.	No
Echo spacing	9,6 ms
Turbo factor	176
RF pulse type	Fast
Gradient mode	Normal
Excitation	Non-sel.

SIEMENS MAGNETOM Prisma_fit syngo MR D13D

\\USER\MPI Standard\Ethofer\TREND\MPRAGE GRAPPA2

TA:5:30 PAT:2 Voxel size:1.0×1.0×1.0 mm Rel. SNR:1.00 :tfl

RF spoiling	On
TX/RX delta frequency	0 Hz
TX Nucleus	None
TX delta frequency	0 Hz
Coil elements	HE1-4
Acquisition duration	0 ms
Mode	Off
BOLD	
Subtract	Off
StdDev	Off
MIP-Sag	Off
MIP-Cor	Off
MIP-Tra	Off
MIP-Time	Off
Save original images	On
Distortion Corr.	Off
Save original images	On

8.4. Additional figures of the results of the subgroup analysis

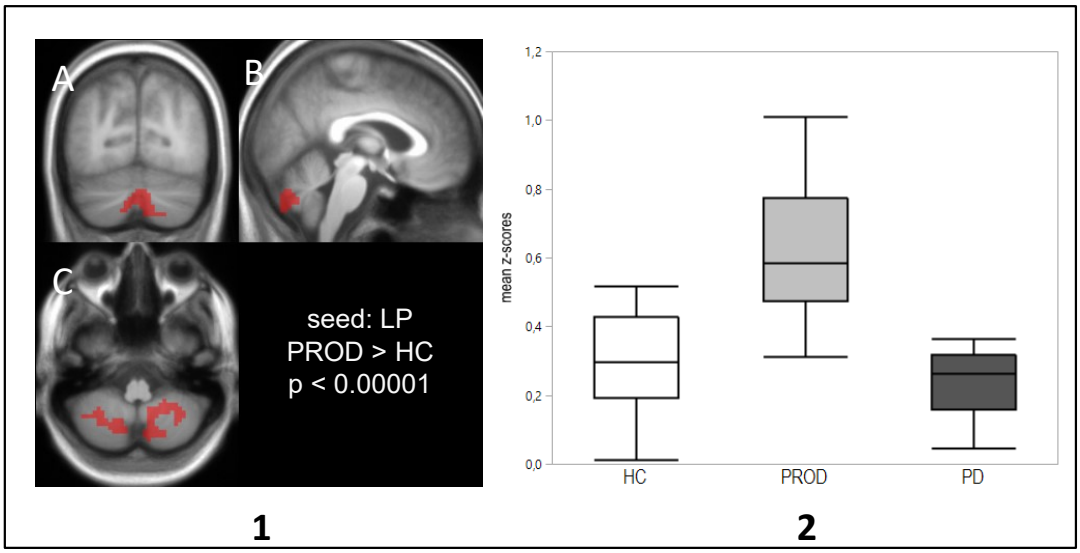

1: Cluster (red) resulting from an ANOVA of the left putamen correlation maps overlaid on a mean anatomical image of all participants. The cluster contains 251 voxels is mainly located in the cerebellum and the vermis. P-value (cluster level, FWE corr.) < 0.00001. **2:** Boxplot showing the extracted mean correlation of each cohort in the cluster displayed in (1). White box, healthy controls; light grey box, prodromal group; dark grey box, patients. A, coronal view; B, sagittal view; C, axial view; LP, left putamen; PD, patients; PROD, prodromal group.

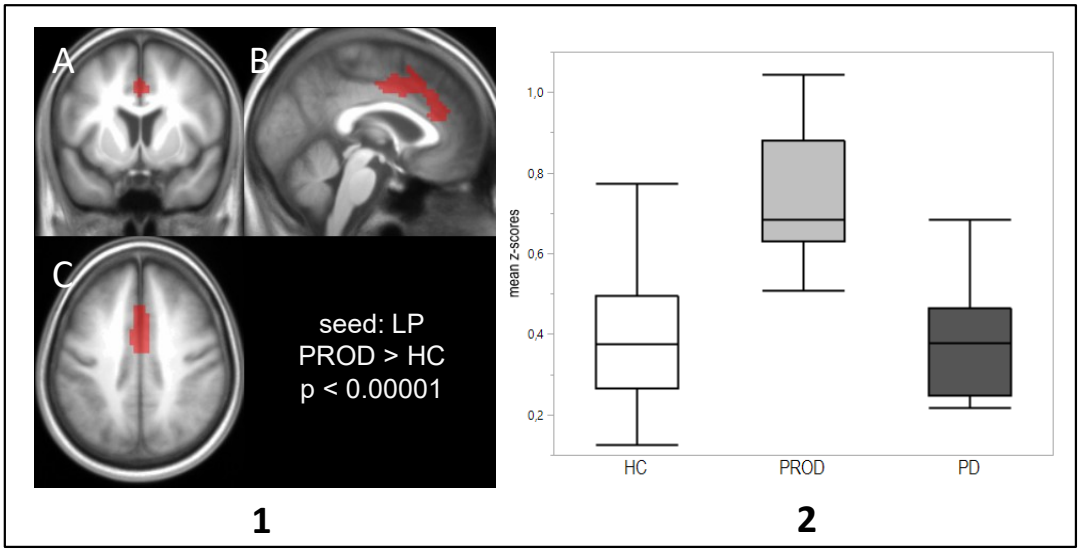

1: Cluster (red) resulting from an ANOVA of the left putamen correlation maps overlaid on a mean anatomical image of all participants. It contains 271 voxels and is mainly located in the bilateral cingulate gyrus, the SMA and the l. superior medial frontal gyrus. P-value (cluster level, FWE corr.) < 0.00001. **2:** Boxplot showing the extracted mean correlation of each cohort in the cluster displayed in (1). White box, healthy controls; light grey box, prodromal group; dark grey box, patients. A, coronal view; B, sagittal view; C, axial view; LP, left putamen; PD, patients; PROD, prodromal group; SMA, supplementary motor area.

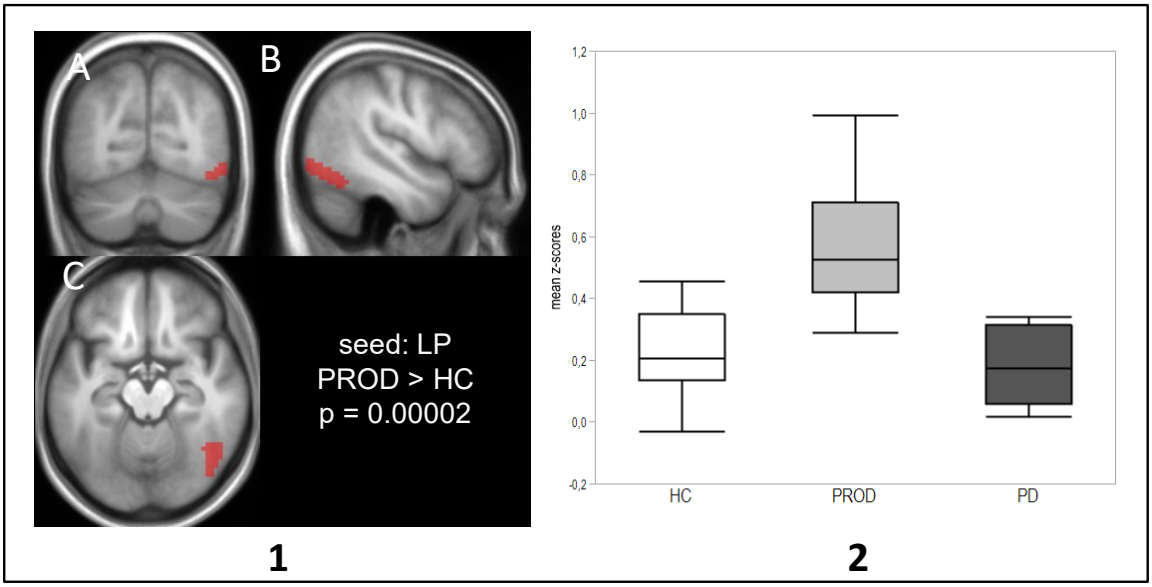

1: Cluster (red) resulting from an ANOVA of the left putamen correlation maps overlaid on a mean anatomical image of all participants. It contains 119 voxels and is mainly located in the right temporal and occipital gyrus. P-value (cluster level, FWE corr.) 0.00002. **2:** Boxplot showing the extracted mean correlation of each cohort in the cluster displayed in (1). White box, healthy controls; light grey box, prodromal group; dark grey box, patients. A, coronal view; B, sagittal view; C, axial view; LP, left putamen; PD, patients; PROD, prodromal group.

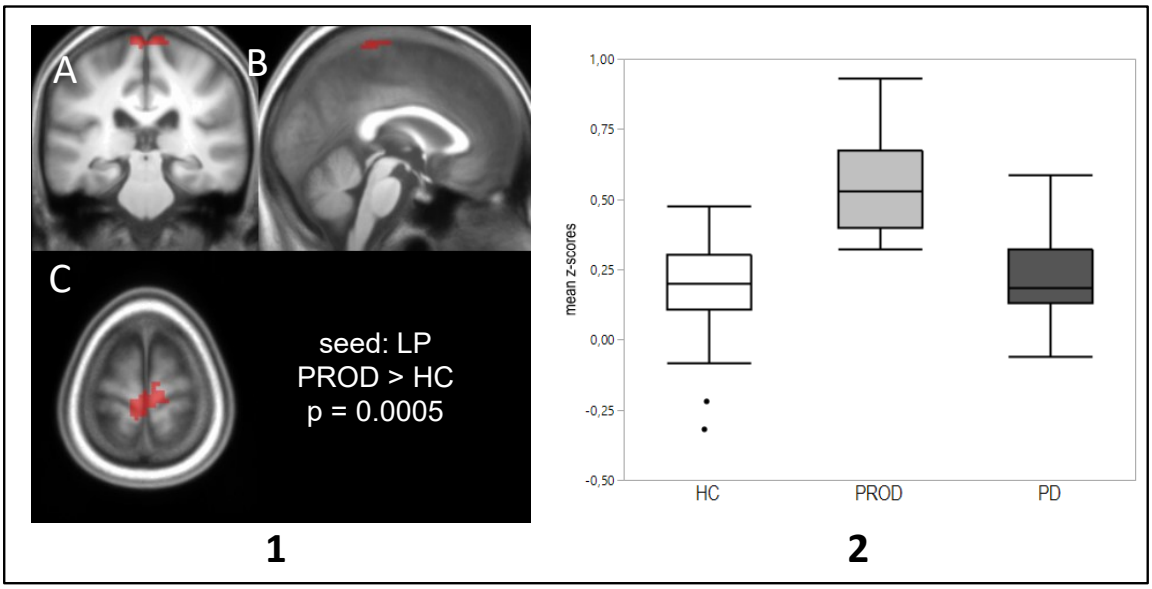

1: Cluster (red) resulting from an ANOVA of the left putamen correlation maps overlaid on a mean anatomical image of all participants. The cluster contains 73 voxels is mainly located in the paracentral lobule, the r. precentral gyrus and the r. SMA. P-value (cluster level, FWE corr.) 0.0005. **2:** Boxplot showing the extracted mean correlation of each cohort in the cluster displayed in (1). White box, healthy controls; light grey box, prodromal group; dark grey box, patients. A, coronal view; B, sagittal view; C, axial view; LP, left putamen; PD, patients; PROD, prodromal group; SMA, supplementary motor area.

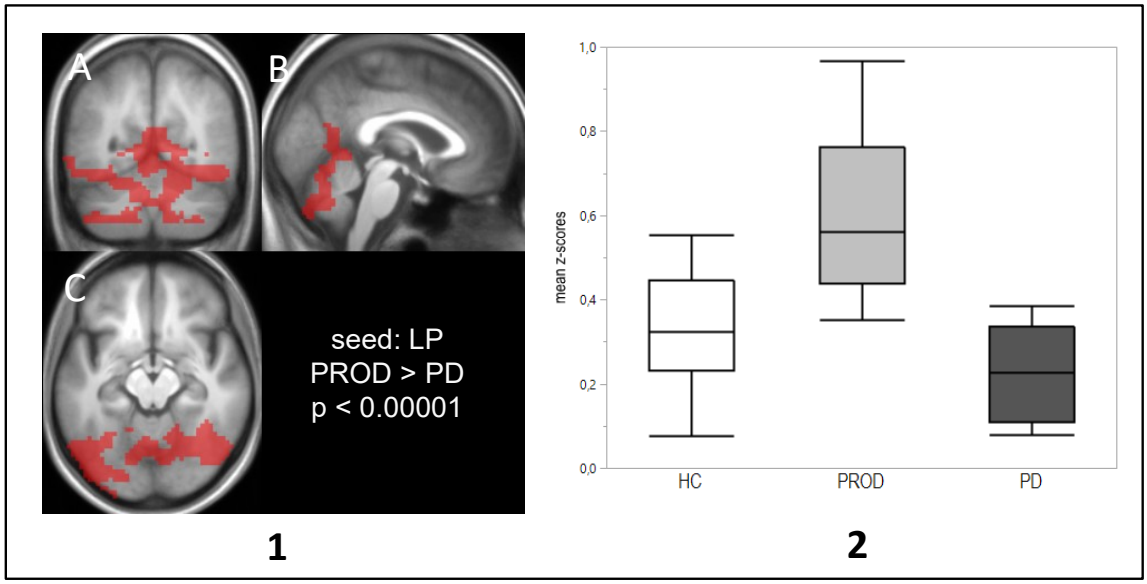

1: Cluster (red) resulting from an ANOVA of the left putamen correlation maps overlaid on a mean anatomical image of all participants. The cluster contains 2886 voxels and is mainly in the cerebellum, the temporal and the occipital lobe. P-value (cluster level, FWE corr.) < 0.00001. **2:** Boxplot showing the extracted mean correlation of each cohort in the cluster displayed in (1). White box, healthy controls; light grey box, prodromal group; dark grey box, patients. A, coronal view; B, sagittal view; C, axial view; LP, left putamen; PD, patients; PROD, prodromal group.

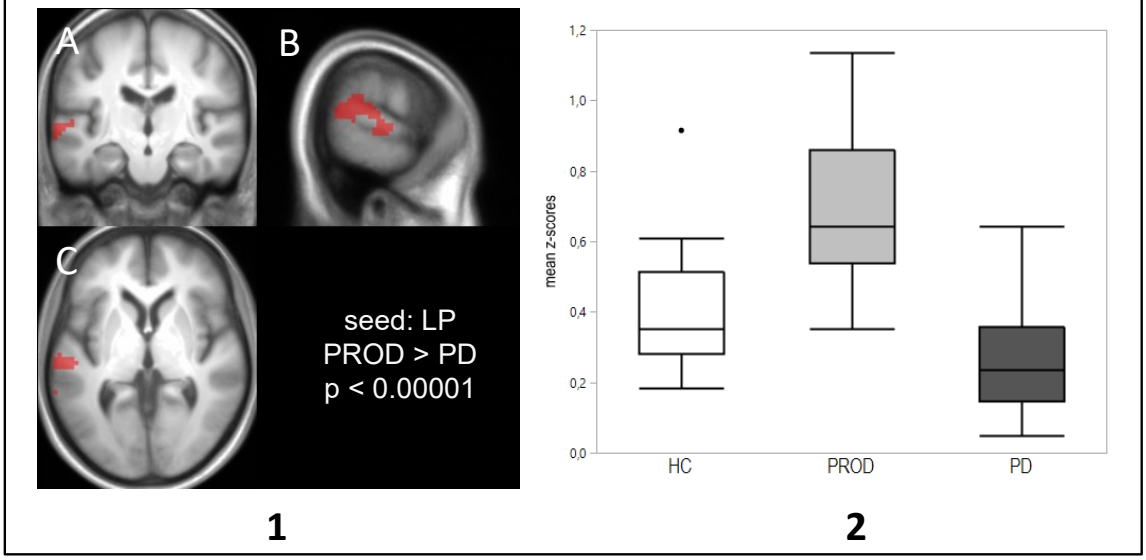

1: Cluster (red) resulting from an ANOVA of the left putamen correlation maps overlaid on a mean anatomical image of all participants. It contains 187 voxels and is mainly located in the l. temporal lobe and the l. supramarginal gyrus. P-value (cluster level, FWE corr.) < 0.00001. **2:** Boxplot showing the extracted mean correlation of each cohort in the cluster displayed in (1). White box, healthy controls; light grey box, prodromal group; dark grey box, patients. A, coronal view; B, sagittal view; C, axial view; LP, left putamen; PD, patients; PROD, prodromal group.

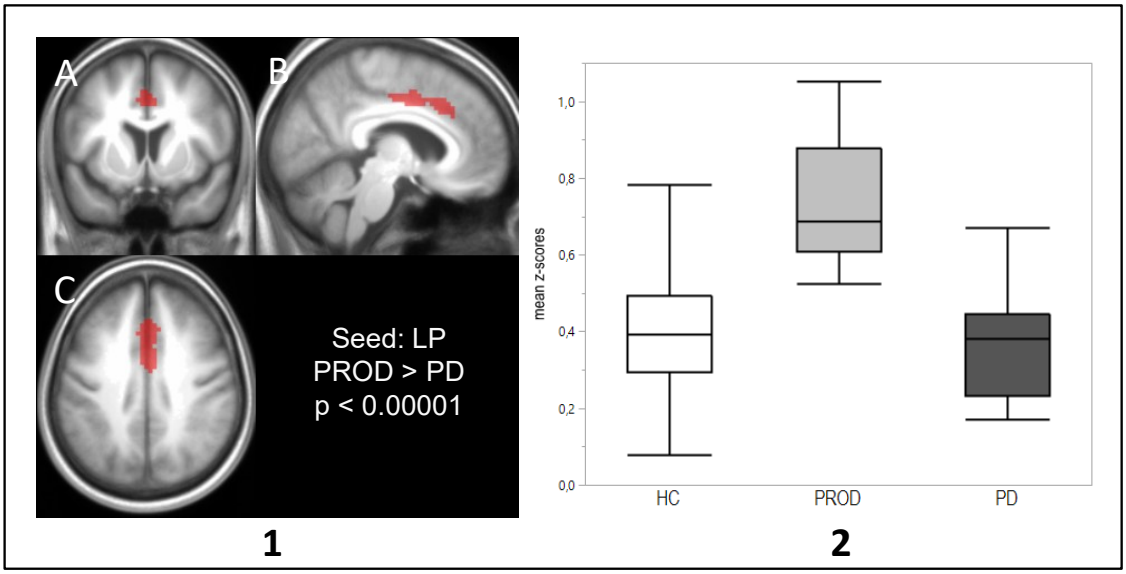

1: Cluster (red) resulting from an ANOVA of the left putamen correlation maps overlaid on a mean anatomical image of all participants. It contains 243 voxels and is mainly located in the cingulum, the SMA and superior frontal lobe. P-value (cluster level, FWE corr.) < 0.00001. **2:** Boxplot showing the extracted mean correlation of each cohort in the cluster displayed in (1). White box, healthy controls; light grey box, prodromal group; dark grey box, patients. A, coronal view; B, sagittal view; C, axial view; LP, left putamen; PD, patients; PROD, prodromal group; SMA, supplementary motor area.

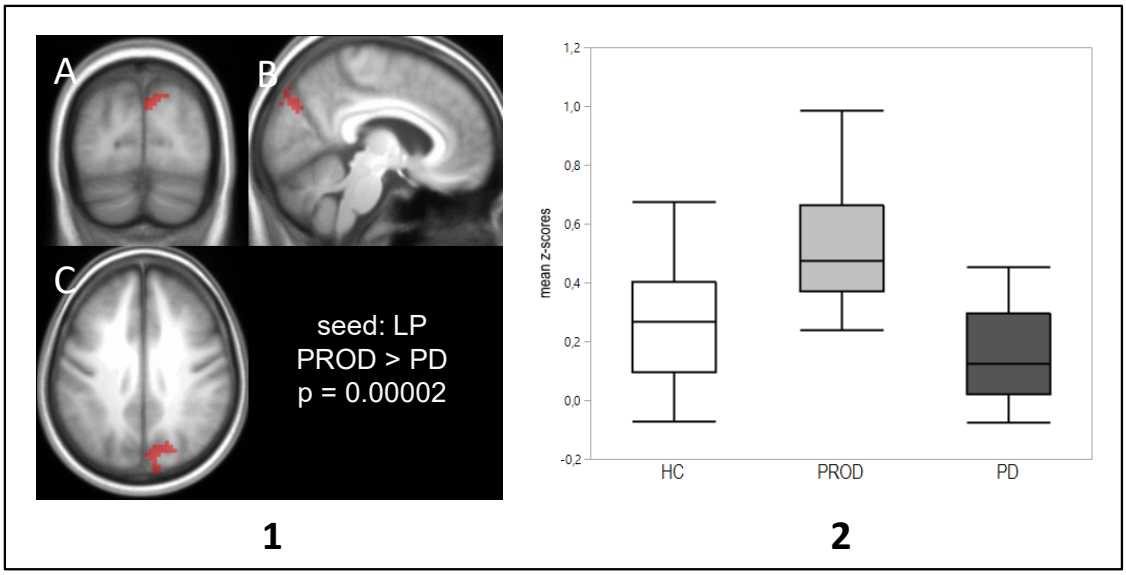

1: Cluster (red) resulting from an ANOVA of the left putamen correlation maps overlaid on a mean anatomical image of all participants. It contains 78 voxels (red) and is mainly located in the cuneus, the precuneus and the superior occipital lobe. P-value (cluster level, FWE corr.) 0.00002. **2:** Boxplot showing the extracted mean correlation of each cohort in the cluster displayed in (1). White box, healthy controls; light grey box, prodromal group; dark grey box, patients. A, coronal view; B, sagittal view; C, axial view; LP, left putamen; PD, patients; PROD, prodromal group.

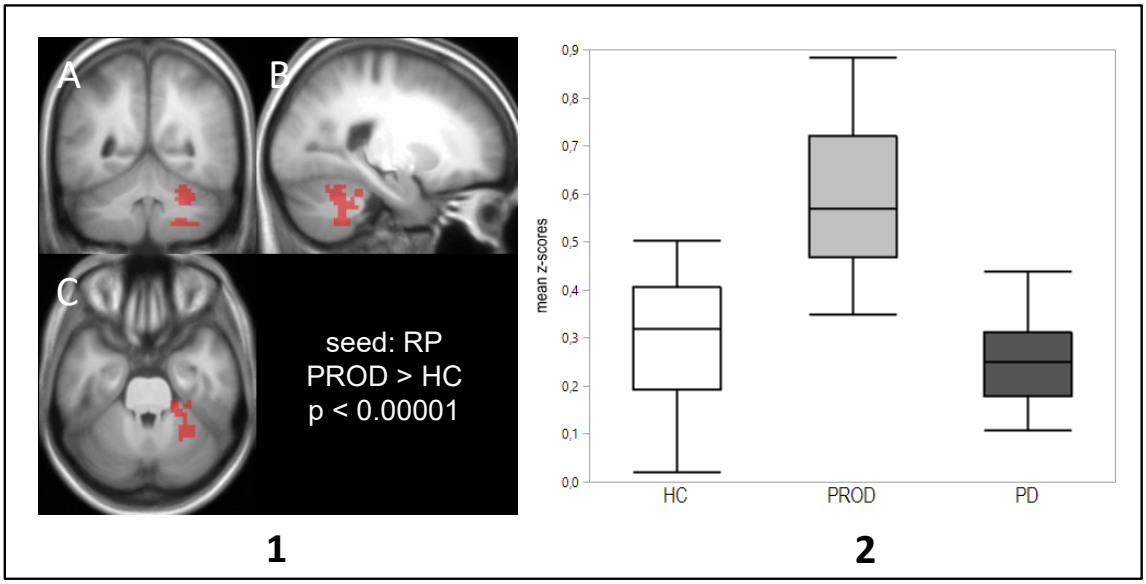

1: Cluster (red) resulting from an ANOVA of the right putamen correlation maps overlaid on a mean anatomical image of all participants. It contains176 voxels and is mainly located in the right cerebellum and the right fusiform gyrus. P-value (cluster level, FWE corr.) < 0.00001. **2:** Boxplot showing the extracted mean correlation of each cohort in the cluster displayed in (1). White box, healthy controls; light grey box, prodromal group; dark grey box, patients. A, coronal view; B, sagittal view; C, axial view; PD, patients; PROD, prodromal group; RP, right putamen.

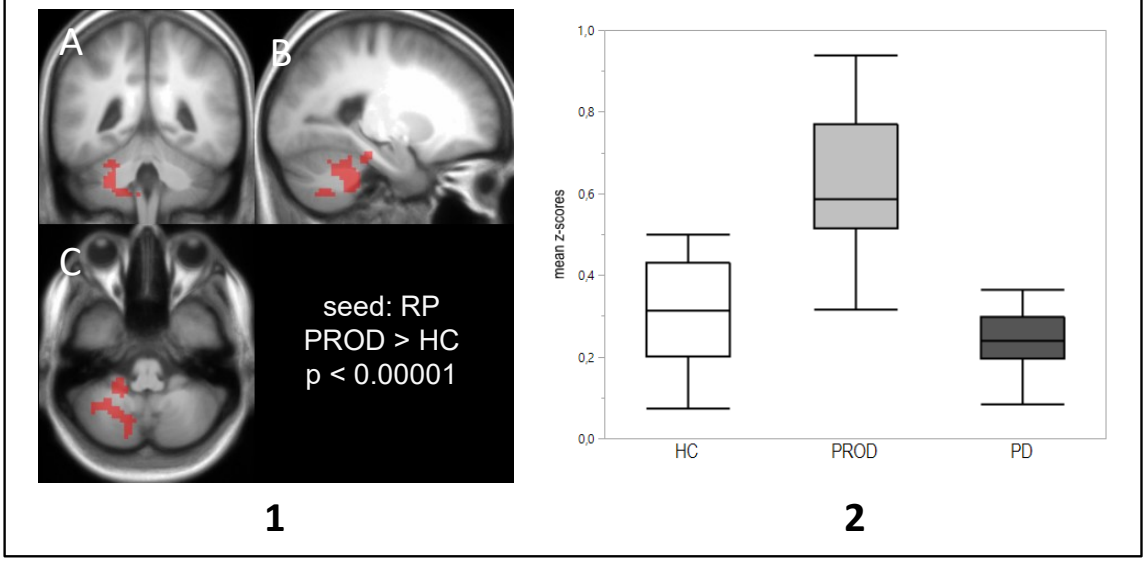

1: Cluster (red) resulting from an ANOVA of the right putamen correlation maps overlaid on a mean anatomical image of all participants. It contains 366 voxels and is mainly located in the cerebellum, the vermis, the left fusiform and the parahippocampal gyrus. P-value (cluster level, FWE corr.) < 0.00001. **2:** Boxplot showing the extracted mean correlation of each cohort in the cluster displayed in (1). White box, healthy controls; light grey box, prodromal group; dark grey box, patients. A, coronal view; B, sagittal view; C, axial view; PD, patients; PROD, prodromal group; RP, right putamen.

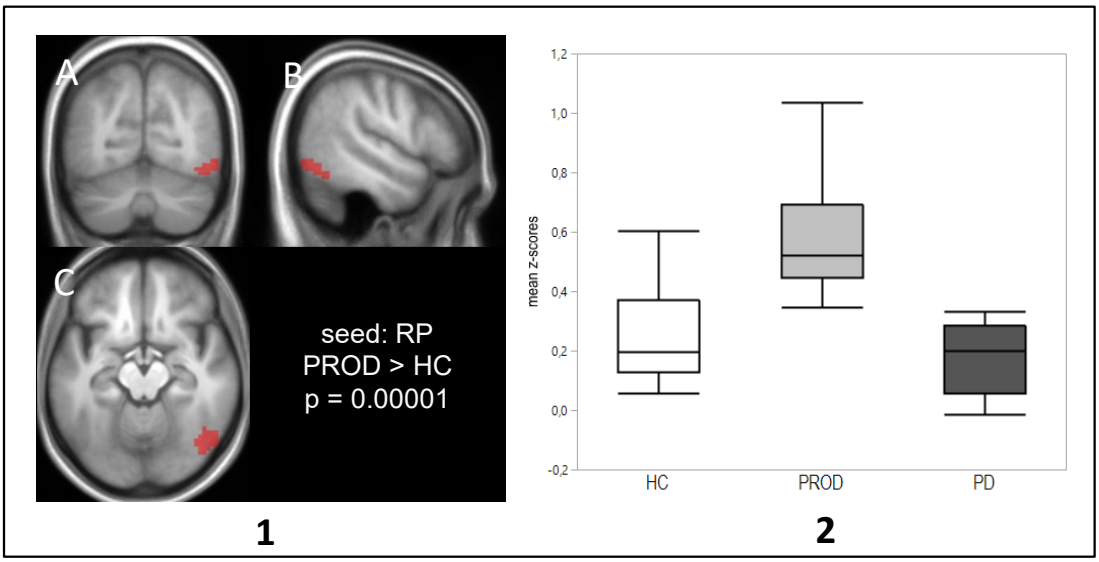

1: Cluster (red) resulting from an ANOVA of the right putamen correlation maps overlaid on a mean anatomical image of all participants. It contains 85 voxels and is mainly located in the right temporal and the occpital gyrus. P-value (cluster level, FWE corr.) is 0.00001. **2:** Boxplot showing the extracted mean correlation of each cohort in the cluster displayed in (1). White box, healthy controls; light grey box, prodromal group; dark grey box, patients. A, coronal view; B, sagittal view; C, axial view; PD, patients; PROD, prodromal group; RP, right putamen.

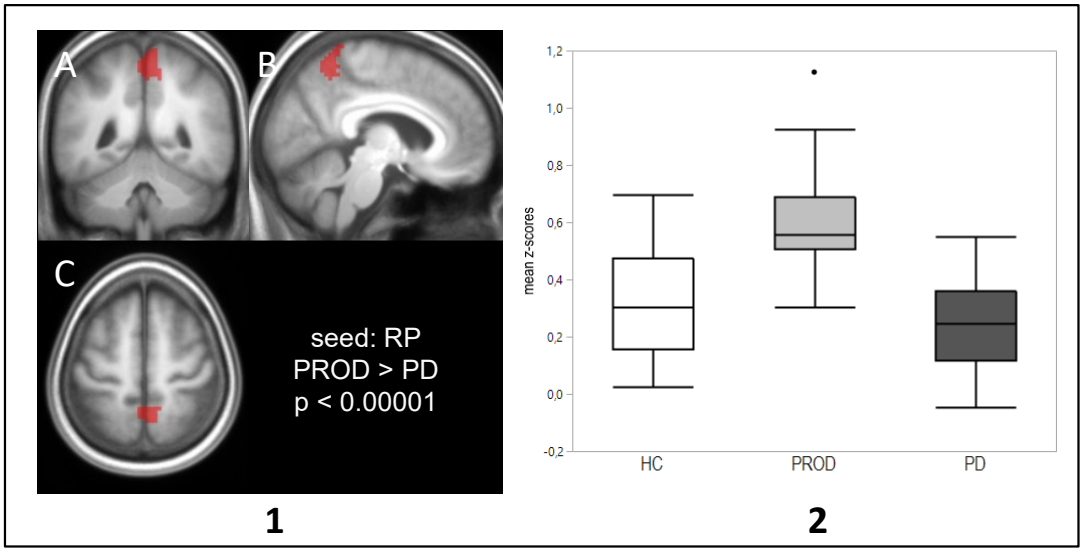

1: Cluster (red) resulting from an ANOVA of the right putamen correlation maps overlaid on a mean anatomical image of all participants. It contains 106 voxels and is mainly located in precuneus and the paracentral lobule. P-value (cluster level, FWE corr.) < 0.00001. **2:** Boxplot showing the extracted mean correlation of each cohort in the cluster displayed in (1). White box, healthy controls; light grey box, prodromal group; dark grey box, patients; A, coronal view; B, sagittal view; C, axial view; PD, patients; PROD, prodromal group; RP, right putamen.

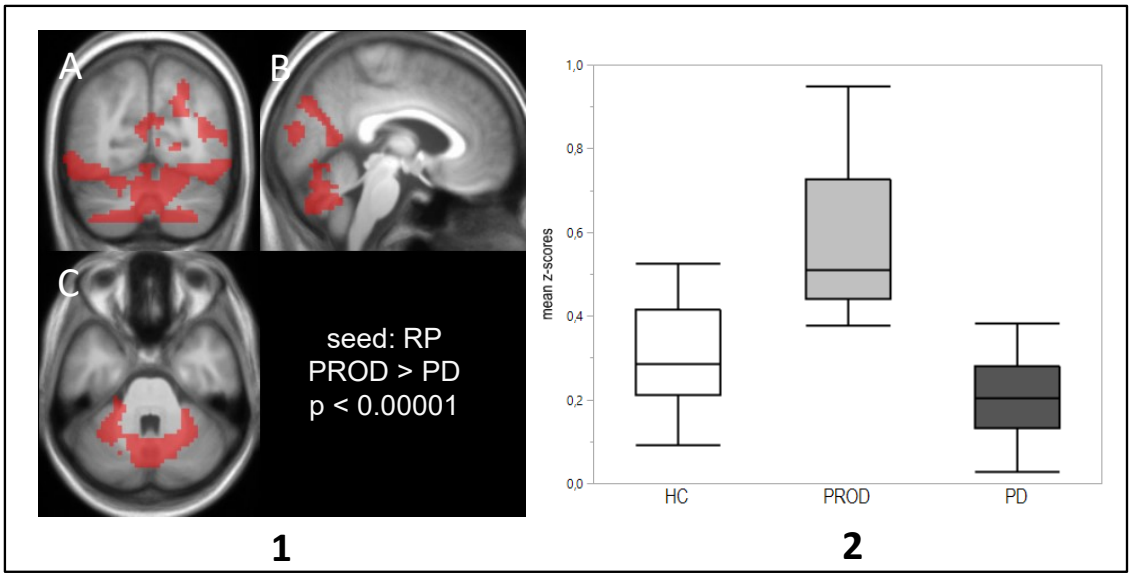

1: Cluster (red) resulting from an ANOVA of the right putamen correlation maps overlaid on a mean anatomical image of all participants. It contains 4184 voxels and is mainly located in the cerebellum, the occipital and the parietal lobe. P-value (cluster level, FWE corr.) < 0.00001. **2:** Boxplot showing the extracted mean correlation of each cohort in the cluster displayed in (1). White box, healthy controls; light grey box, prodromal group; dark grey box, patients. A, coronal view; B, sagittal view; C, axial view; PD, patients; PROD, prodromal group; RP, right putamen.

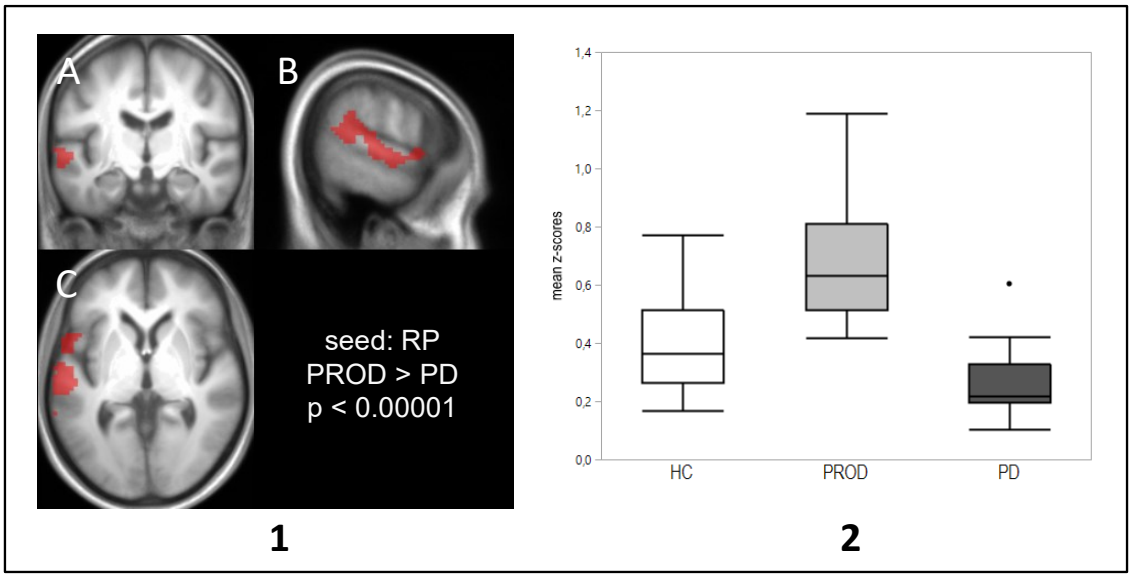

1: Cluster (red) resulting from an ANOVA of the right putamen correlation maps overlaid on a mean anatomical image of all participants. It contains 418 voxels and is mainly located in the l. temporal lobe, the l. supramarginal gyrus and the l. rolandic operculum. P-value (cluster level, FWE corr.) < 0.00001. **2:** Boxplot showing the extracted mean correlation of each cohort in the cluster displayed in (1). White box, healthy controls; light grey box, prodromal group; dark grey box, patients. A, coronal view; B, sagittal view; C, axial view; PD, patients; PROD, prodromal group; RP, right putamen.

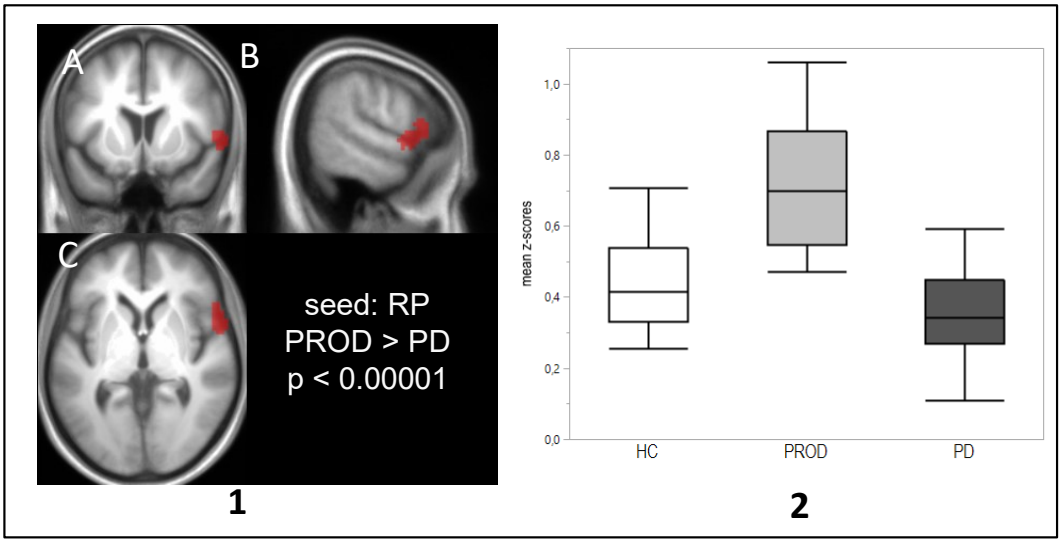

1: Cluster (red) resulting from an ANOVA of the right putamen correlation maps overlaid on a mean anatomical image of all participants. It contains 119 voxels (red) and is mainly located in the right inferior frontal lobe and the r. rolandic operculum. P-value (cluster level, FWE corr.) < 0.00001. **2:** Boxplot showing the extracted mean correlation of each cohort in the cluster displayed in (1). White box, healthy controls; light grey box, prodromal group; dark grey box, patients. A, coronal view; B, sagittal view; C, axial view, PD, patients; PROD, prodromal group; RP, right putamen.

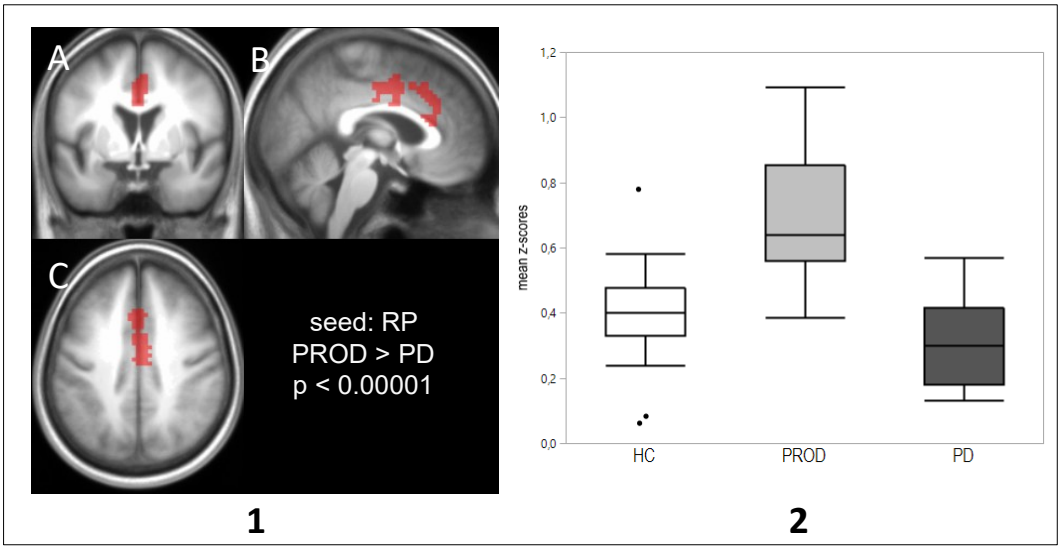

1: Cluster (red) resulting from an ANOVA of the right putamen correlation maps overlaid on a mean anatomical image of all participants. It contains 233 voxels and is mainly located in the cingulum, the SMA and the superior frontal gyrus. P-value (cluster level, FWE corr.) < 0.00001. **2:** Boxplot showing the extracted mean correlation of each cohort in the cluster displayed in (1). White box, healthy controls; light grey box, prodromal group; dark grey box, patients. A, coronal view; B, sagittal view; C, axial view; PD, patients; PROD, prodromal group; RP, right putamen; SMA, supplementary motor area.

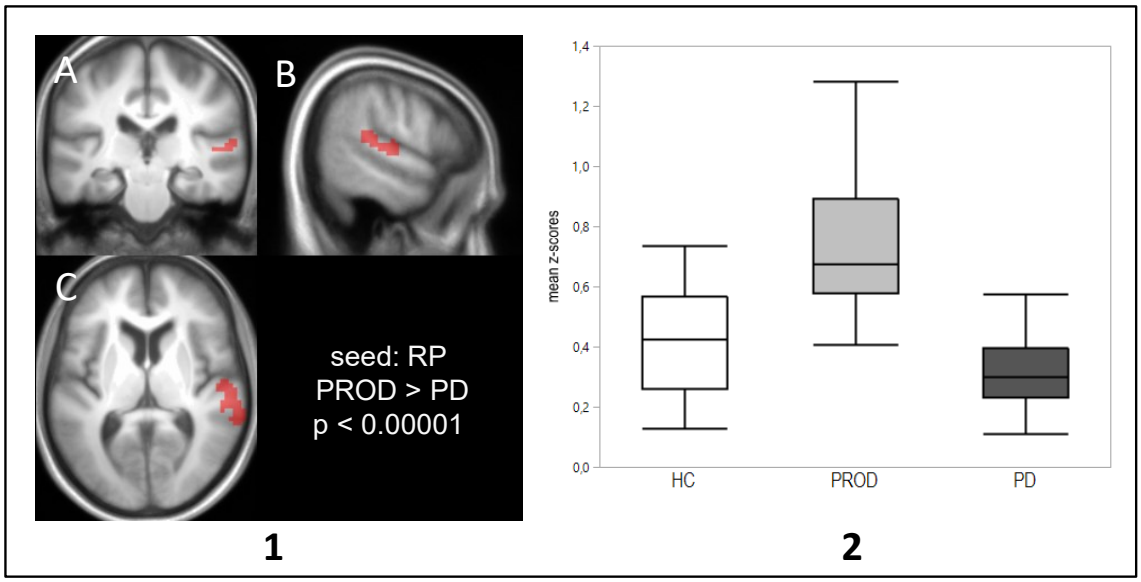

1: Cluster (red) resulting from an ANOVA of the right putamen correlation maps overlaid on a mean anatomical image of all participants. It contains 160 voxels and is mainly located in the r. superior and middle temporal lobe, the r. heschl's gyrus and the r. rolandic operculum. P-value (cluster level, FWE corr.) < 0.00001. **2:** Boxplot showing the extracted mean correlation of each cohort in the cluster displayed in (1). White box, healthy controls; light grey box, prodromal group; dark grey box, patients; A, coronal view; B, sagittal view; C, axial view; PD, patients; PROD, prodromal group; RP, right putamen.

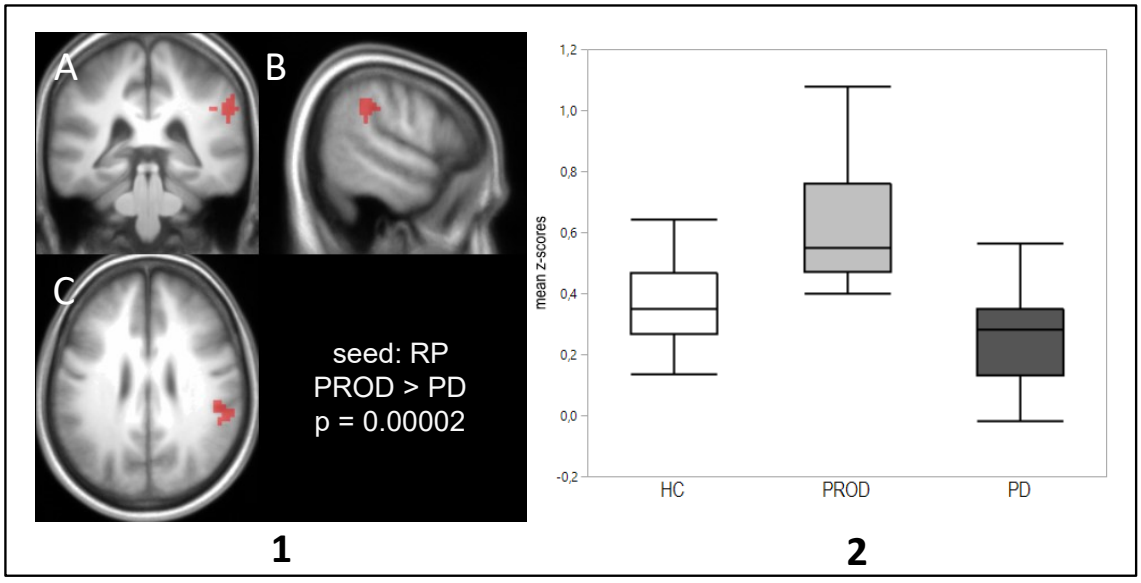

1: Cluster (red) resulting from an ANOVA of the right putamen correlation maps overlaid on a mean anatomical image of all participants. It contains 78 voxels and is mainly located in the right supramarginal gyrus. P-value (cluster level, FWE corr.) 0.00002. **2:** Boxplot showing the extracted mean correlation of each cohort in the cluster displayed in (1). White box, healthy controls; light grey box, prodromal group; dark grey box, patients; A, coronal view; B, sagittal view; C, axial view; PD, patients; PROD, prodromal group; RP, right putamen.